Ternary graphite intercalation compounds for the reversible storage of alkali ions in electrochemical cells

Ternäre Graphitinterkalationsverbindungen zur reversiblen Speicherung von Alkali-Ionen in elektrochemischen Zellen

dem Fachbereich Biologie und Chemie

der Justus-Liebig-Universität Giessen

vorgelegte Dissertation zur Erlangung des akademischen Grades

Doktor der Naturwissenschaften

- Dr. rer. nat.-

von

Birte Andrea Jache

geboren am 15. Mai 1985 in Büdingen

Gießen, November 2016

First referee: Professor Dr. Jürgen Janek

Second referee: Professor Dr. Philipp Adelhelm

Submission date: Gießen, _____ 2016

Statutory Declaration

"I declare that I have completed this dissertation single-handedly without the unauthorized help of a second party and only with the assistance acknowledged therein. I have appropriately acknowledged and cited all text passages that are derived verbatim from or are based on the content of published work of others, and all information relating to verbal communications. I consent to the use of an anti-plagiarism software to check my thesis. I have abided by the principles of good scientific conduct laid down in the charter of the Justus Liebig University Gießen 'Satzung der Justus-Liebig-Universität Gießen zur Sicherung guter wissenschaftlicher Praxis' in carrying out the investigations described in the dissertation."

Gießen, _____ 2016

_____

Birte Andrea Jache

Dedication

For my father
for being an example showing that it is never to late to learn something new.

"I may not have gone where I intended to go,
but I think I have ended up where I needed to be."

Douglas Adams, *The Long Dark Tea-Time of the Soul*

Acknowledgement

I would like to thank my two supervising professors, Prof. Jürgen Janek and Prof. Philipp Adelhelm, for the possibility to conduct this research project within their research groups, and for scientific discussions and guidance throughout the last years. Especially their optimistic view on complex problems eased up my fundamental pessimism significantly.

Furthermore I would like to thank my cooperation partners, Prof. Takeshi Abe and Prof. Shinichi Komaba. Prof. Abe offered generously lots of knowledge on the formation and structural characterization of ternary graphite intercalation compounds which lead to a shared publication within this research project. Prof. Komaba accepted me for an internship in his laboratories in Tokyo and made it possible to conduct first measurements on sodium-ion batteries based on the co-intercalation electrode reaction. To both a grateful *domo arigatou gozaimashita*.

I thank my co-authors Dr. Conrad Bender and Dr. Shyamal Das for the possibility to apply the here presented knowledge onto other research projects and the whole "sodium team" for a nice working atmosphere and an always tidy laboratory. Additionally, I thank my office colleagues for fun, coffee and cookies and the research groups from Gießen and Jena for a pleasant, and not too stern, working atmosphere.

Many thanks to my family, which was always supporting and reminded me that the best scientific results do not have any meaning if you cannot explain them and their benefit to somebody that is not into science. Thank you for keeping my feet firmly on the ground.

Last but not least, I thank Heiko with all my heart for being there, for taking care and for never giving up to reassure and support me. You are the best!

Contents

List of Figures

List of Tables

List of Abbreviations

1,5-DMP	1,5-Dimethoxy pentane
1G	Monoglyme, Dimethoxyethane
2G	Diglyme, Bis(2-methoxyethyl) ether
3G	Triglyme, Triethylene glycol dimethyl ether
4G	Tetraglyme, Tetraethylene glycol dimethyl ether
Li/O_2 (cells)	Lithium-oxygen (cells)
Na/O_2 (cells)	Sodium-oxygen (cells)
OTf^-	Triflate anion
$TFSI^-$	Trifluoro methane sulfonyl imide anion
b-GIC	Binary graphite intercalation compound
t-GIC	Ternary graphite intercalation compound
Butyl-2G	Bis(2-butoxyethyl) ether
CN	Coordination number
CV	Cyclic voltammetry
DEC	Dieethyl carbonate
DMC	Dimethyl carbonate
DME	Dimethyl ether
DMSO	Dimethyl sulfoxide
DPGDME	Bis(methoxypropyl) ether
EC	Ethylene carbonate
EMC	Ethyl methyl carbonate
FEC	Fluoroethylene carbonate
GIC	Graphite intercalation compound

Glymes	Ethylene glycol dimethyl ethers
LIBs	Lithium-ion batteries
Na-CMC	Sodium carboxymethyl cellulose
NIBs	Sodium-ion batteries
NMP	N-methyl-2-pyrrolidone
NNMO	P2 - $Na_{2/3}Ni_{1/3}Mn_{2/3}O_2$
OCV	Open circuit voltage
PC	Propylene carbonate
PVDF	Polyvinylidene fluoride
SEI	Solid electrolyte interphase
SFG-44	Synthetic graphite from *Imerys S.A.*
SHE	Standard hydrogen electrode
THF	Tetrahydrofuran
XRD	X-ray diffraction
ZEBRA cells	Zeolite Battery Research Africa cells, $Na-NiCl_2$

List of Publications

1. B. Jache, P. Adelhelm "Use of Graphite as a Highly Reversible Electrode with Superior Cycle Life for Sodium-Ion Batteries by Making Use of Co-Intercalation Phenomena" *Angewandte Chemie Int. Ed.* **2014**, *53*, 10169 - 10173

2. C. L. Bender, B. Jache, P. Adelhelm, J. Janek "Sodiated carbon: A reversible anode for the sodium-oxygen battery and route for the chemical synthesis of sodium superoxide (NaO_2)" *Journal of Material Chemistry A*, **2015**, *3*, 20633 - 20641

3. S. K. Das, B. Jache, H. Lahon , C. L. Bender , J. Janek, P. Adelhelm "Graphene mediated improved sodium storage in nanocrystalline anatase TiO_2 for sodium ion batteries with ether electrolyte" *Chemical Communications* **2016**, *52*, 1428 - 1431

4. B. Jache, J. O. Binder, T. Abe, P. Adelhelm "A comparative study on the impact of different glymes and its derivatives as electrolyte solvents for graphite co-intercalation electrodes in lithium-ion and sodium-ion batteries" *Physical Chemistry Chemical Physics*, **2016**, *18*, 14299 - 14316

Part of the experimental data and figures shown in sections 3.2 and 3.3 were published in *Angewandte Chemie International Edition* and were adapted from Ref. [1] for this work with permission from the *John Wiley and Sons*. The experimental data and figures in subsection 3.3.2 and in section 3.5 were published in *Physical Chemistry Chemical Physics*. Reproduced from Ref. [2] with permission from the PCCP Owner Societies.

1 Introduction

The decision of Germany and other EU countries with the turn of the millennium, to reorganize their energy sectors and switch to renewable energy sources (key words: "Energiewende", "Integriertes Energie und Klimaprogramm"), leads to an increase in demand for electrochemical energy storage devices for mobile and stationary applications. These devices are necessary to buffer the volatile, renewable energy sources to ensure grid stability.[3,4] In the course of these actions, the discussion on lithium as a critical resource lead to a renewed interest in sodium-ion batteries (NIBs) as complement to lithium-ion technology.[5–14] Due to the position of sodium in the periodic table, next to lithium, similar electrochemical properties are expected for its compounds. Furthermore, sodium would offer an even, worldwide distribution and a large variety of possible sources. While recently progress was made and described on the cathode side[15–18] almost no suitable anode materials for NIBs have been found since the 1980s,[14,19–22] when lithium-ion batteries (LIBs) were commercialised after establishing graphite as reliable, cost-effective anode material. This triggered the premature stop of research on NIBs.

This study is focused on graphite as anode material for NIBs. Graphite electrodes, prepared by lithium-ion technology standards, are implemented into sodium-ion cells without further structural modification, using a different kind of electrode reaction (co-intercalation) to store ions inside the graphite structure. These co-intercalation electrodes might be implemented into NIBs and allow the simple construction of reliable, low-cost NIBs that may be suitable for stationary applications, where the price is more relevant than energy density. These NIBs may thereby lower the demand and price of lithium compounds for LIBs for mobile applications.

1.1 Historical development

At a first glance a similar cell chemistry is expected for lithium and sodium compounds and their reactions due to their vicinity in the periodic table. The difference in the ionic radii between both alkali metal ions however leads to changes in the thermodynamic and kinetic properties which can be advantageous or disadvantageous for a reversible cell reaction. In the dawn of alkali battery research, lithium and sodium based systems were studied simultaneously. In the early 1980s the insertion materials were investigated in parallel for both alkali metals, such as Li_xTiS_2[23] and Na_xTiS_2[24] or layered transition metal oxides such as Li_xCoO_2[25] and Na_xCoO_2.[26–28] Due to a higher reactivity of the sodium metal electrode towards electrolyte solvents or solvent impurities and the larger ionic radius of the sodium ions, which leads to a lower energy density, sodium-ion batteries were soon marginalised.

When the research community focused on replacing the alkali metal electrode by another insertion electrode material for safety reasons (e.g. the prevention of dendrite formation) the interest in sodium cells further decreased. The successful implementation of graphite into lithium based systems, due to such beneficial properties as good kinetics inside the graphite host, the formation of a stable ion-conducting and electron-blocking surface film ("solid electrolyte interphase", SEI[29]), low operating voltages of 0.1V - 0.2V and a charge storage capability of one lithium ion per six carbon atoms, lead to the further neglect of sodium battery technology.[30] The incompatibility between the sodium ions and the graphite electrode, which is based on a mismatch between the size of sodium ion and the graphitic host structure, hindered further comparing research on lithium-ion and sodium-ion batteries.[31–34] While the research activities on lithium-ion batteries further rose, leading to the final commercialisation in the 1990s by Sony,[30] sodium-ion technology almost sank into oblivion. Only some special cases of sodium batteries were further investigated and commercialized, such as high temperature cells that work with a molten sodium electrode such as sodium/sulphur and ZEBRA cells (Zeolite Battery Research Africa cells, $Na-NiCl_2$) usually used for stationary applications.[6,12,35] Interestingly, while the

use of metallic sodium in rechargeable high-temperature batteries was quite successful, till today there is no competing high-temperature lithium technology established.

1.2 Research results for sodium-ion batteries

In this section the research results for anode materials (subsection 1.2.1) and electrolytes (subsection 1.2.2) in sodium-ion technology are summarized. Since there was only little progress in the research of anode materials and electrolytes for sodium-ion batteries since the 1990s, it is most likely that the development of these will help sodium-ion technology most on the way towards commercialisation.

For sodium cathode materials significant progress was made within the last 15 years; therefore these will not be summarized here in detail and the reader is referred to the reviews on sodium cathode materials in the bibliography.[6–18]

1.2.1 Anode materials

Since the successful implementation of graphite as the anode in lithium-ion batteries that led to the rapid domination of lithium-ion technology in the field of electrochemical energy storage, there were attempts to find suitable anode materials for sodium-ion batteries as well, to create a comparably well-working and reliable battery based on sodium. The strongest driving force was, and still is, the promise that sodium-based batteries could work in a similar reliable manner as LIBs, but with a much lower price, due to widespread and worldwide evenly distributed sodium resources. From the start on, this *copy & paste* process of electrodes and electrolytes from lithium to sodium cells was difficult, due to the larger ionic radius of sodium ions and the resulting differences of thermodynamic and kinetic properties, such as the change of products upon charging[36] or solvation properties.[37]

Experiences made during the development of lithium-ion batteries had and still have significant influence on what kind of electrodes are considered as potential anode materials for sodium-ion batteries.[5,19–22] Metallic sodium anodes would exhibit high

theoretical specific capacities (1165 $^{mAh}/_{g}$) and low negative redox potentials (-2.71 V vs. SHE). Despite all that they have not been intensively studied due to safety concerns arising from critical events such as dendrite formation, the subsequently possible thermal runaway and fire risks, of cells containing metallic lithium electrodes in the 1980s (see the next paragraph "Sodium metal").[38–43]

The most prominent example for the failure in transferring the basic working principles of lithium-ion onto sodium-ion technology is graphite as anode material and will be described in detail in the second paragraph ("Graphite") of this section.

Other viable, but still next-generation anode materials, such as non-graphitic carbons, conversion type materials, titanates and alloy forming anodes were investigated intensively in the last years but still suffer from major problems such as high irreversible losses in the initial cycles and large volume expansion during sodium ion insertion (see paragraphs "Non-graphitic carbons" and "Conversion type materials, alloys and titanates").

Sodium metal

Apart from high temperature cell designs, such as sodium/sulphur and ZEBRA cells, which work with a solid electrolyte (β''-alumina, Al_2O_3) and liquid sodium metal at around 300 °C, there are no commercial sodium battery systems containing sodium metal today.[6,12,35] Sodium/sulphur cells at ambient temperatures were studied intensively, due to their beneficial key data such as cheap and abundant reactants, but their strong dependency on the electrolyte composition still causes a lot of problems that have to be solved before they can fully be commercialised.[44]

Recently, sodium/oxygen cells (Na/O_2 cells) have been studied containing metallic sodium as anode material.[9,12,36,45] These cell types are working with sodium superoxide as reaction product and linear glycol ethers ("glymes") as electrolyte solvents. Very recently, these glymes were found to be beneficial when combined with metallic sodium anodes forming a very thin and flexible surface layer (SEI) and enable good reversibility and cycling behaviour.[46]

Graphite

The fact that graphite is not suitable to store sodium ions to a significant amount between its layers was a huge setback to the development of sodium-ion batteries.[31–33] Apart from sodium, all alkali ions are known to form so-called binary graphite intercalation compounds (***b***-GIC) of the composition $A^+C_n^-$, with C_n being n carbon atoms of the graphite lattice and A^+ an alkali metal ion.[34,47–53] For more details of the insertion mechanism see section 2.2.1. The unfavourable size mismatch between the sodium ions and the graphite structure, however, leads to an electrochemically inactivity of graphite towards the insertion of sodium ions.[34,50,54]

Recently, Wen *et al.* successfully circumvented this mismatch. They oxidized a synthetic graphite by the HUMMER's oxidation method[55] and afterwards heated it at 600 °C under reductive Argon atmosphere.[56] The interlayer distance of graphite was expanded by this treatment by around 28 % and then allows the reversible storage of sodium ions in between the galleries of this expanded graphite material (around 280 $^{mAh}/_{g}$ at a discharge current of 20 $^{mAh}/_{g}$ for several thousand cycles). Strictly speaking, the resulting carbon materials can no longer be considered as graphite since the qualitative intercalation behaviour does resembles the one of non-graphitic carbon.

Carbons

Apart from graphite many different kinds of carbon materials were proposed as anode materials for lithium-ion[51–53] and sodium-ion batteries.[19–22,57–62] These non-graphitic carbons exhibit a disordered structure which deviates more or less from the well-ordered structure of graphite. These carbons contain crystalline, graphitic domains consisting of single-layer graphene or/and small stacks of few graphene layers within a disordered, non-crystalline matrix. This means that these carbons do not exhibit a long-range order. The graphene stacks are slightly tilted towards each other and may have an expanded gallery height or exhibit a non-ideal parallel orientation towards each other. Due to the tilted stacks, nanopores/nanocavities

form additionally. This structural motive is denoted as "house-of-cards" or "falling cards" model.[53,57] Because of their special structure the insertion of alkali ions is different when compared to graphite. The ions can be stored in between two layers of graphitic domains, at the edges of the single stacks or by the accumulation inside nanopores or nanocavities, allowing a higher charge storage capacity than graphite. The reversible intercalation starts for both, Li^+ and Na^+, at potentials of around 1.0 V *vs.* the corresponding redox couple and the voltage characteristics show no staging behaviour as in graphite. At 1.0 V the population of the graphitic domains occurs, at lower potentials the nanopores and nanocavities are filled by adsorption or accumulation of Li^+ or Na^+ clusters or agglomerates.[53] Unfortunately, the charge storage is not fully reversible in the initial cycles. Most non-graphitic carbons exhibit irreversible charge losses up to 60 % of the reversible capacity and are therefore just not ready to be implemented into commercial cells.[19–22] Only few commercial producers entered the market till today.[63]

In other approaches it was tried to tailor the nanostructure of carbon synthetically to develop structures with just the right dimensions to accommodate sodium ions, such as porous carbons,[64] carbon nanosheets,[65] hollow carbon nanospheres[66] or hollow carbon nanowires.[67] Since these synthetic approaches mostly are complex and costly, there are still many problems and challenges to solve before a possible commercialisation of these tailored nanocarbons.

Conversion type materials, alloys and titanates

One way to improve energy densities of electrodes for sodium-ion batteries is to selectively increase the ion storage capacities of the electrode material. One possible approach is to use conversion reactions as electrode reaction. Thereby, a transition metal compound M−X (M = transition metal ion, X = fluorides, oxides, phosphides, sulphides,...) undergoes a reaction with an alkali metal forming the alkali compound (A−X) and metallic nanoparticles, layers or dendrites from the transition metal (M), yielding much higher capacities than intercalation materials.[6–8,10,11,20,68]

Another approach is to use alloy-forming metals such as Sn, Pb, Si, Ge, Sb or many others to form binary alloys with sodium, such as Na_x-M. These compounds are attractive materials for charge storage since a single atom may be combined with multiple Na ions and so yield much higher capacities than hard carbon or graphite.[6–8,10,13,19,20,69] Especially, the bulk materials and nanostructured material of tin[70–73] and antimony[74] have been studied recently.

One main problem of conversion type and alloy-forming materials so far lies in the significant volume expansion of the electrode material during insertion of the sodium ions, leading to structural disintegration of the electrode. Another issue are significant charge losses within the first few cycles,[13,19,20,68] but the fact that there are manifold combinations for electrode reactions in conversion and alloy type cells and consequently very variable equilibrium voltages combined with high capacities ($> 400\ \frac{mAh}{g}$) still triggers activity in this research field.

Apart from these, layered host materials are studied as well. Titanates, such as $Na_2Ti_3O_7$ or $NaTi_3O_6(OH) \cdot 2H_2O$ being the most promising materials for NIBs, offering flat potentials at reasonably low intercalation potentials ($> 1.0\,V$) delivering capacities between $80\ \frac{mAh}{g}$ and $150\ \frac{mAh}{g}$.[75]

1.2.2 Electrolytes

The research on suitable electrolytes for sodium-ion batteries is still in its infancy. For a long time, it was exclusively tried to establish carbonate based electrolytes, comparable to those implemented into lithium-ion batteries. But since the solvation properties and the formation of electrode surface layers are distinctively different from those in lithium based systems no lasting progress was made in this research field so far.[76–81]

The *state-of-the-art* electrolyte for sodium-ion batteries at the moment is sodium hexafluorophosphate ($NaPF_6$) as conductive salt in PC (propylene carbonate) or a mixture of PC and EC (ethylene carbonate) as electrolyte solvent. In case of electrode materials with a high volume expansion, such as alloy based electrodes, the addition

of fluoroethylene carbonate (FEC) is common.[79,82] Propylene carbonate (PC) is not used in commercial LIBs since it is not compatible with graphite electrodes. Already in the 1970s it was found that, when PC was used, as electrolyte solvent it is co-intercalated into the graphite structure which triggers gas evolution and the structural decomposition of the electrode.[83–85]

Other electrolyte solvents that are more beneficial for sodium-ion than for lithium-ion batteries are "glymes" (a group of linear ethers with different chain length, ethylene glycol (dimethyl ethers)). These were proposed as solvents due to their beneficial thermodynamic properties and viscosities[86] and were tested as electrolyte solvents in metal-air cells (Li/O_2 and Na/O_2 cells) which contain metallic alkali metals as anode material.[87,88] While glymes seem not to form a stable SEI on metallic lithium, leading to dendrite formation and capacity fading,[89,90] they seem to be working very well for sodium-oxygen cells,[36,91] were a thin and flexible surface film is formed atop of the sodium metal surface.[46]

2 Graphite as intercalation host

Aim of this research project was to activate graphite for the electrochemical insertion of sodium ions. Graphite electrodes were prepared by the standard procedure currently used in lithium-ion technology, however, due to the inability of graphite and sodium ions to form binary graphite intercalation compounds (***b***-GIC), it was necessary to find another electrode reaction by modifying the electrolyte composition.[31–33]

In this chapter the definition of the term "graphite intercalation compound" (GIC) will be recalled and the applicable characterization methods for these compounds are summarized (section 2.1). Furthermore, the basic insertion mechanisms into graphite are described (section 2.2). Finally a model is proposed to use the electrolyte solvent as active cell component (section 2.3), changing the electrode reaction from intercalation (section 2.2.1) to co-intercalation reaction (section 2.2.2).

2.1 Structure and characterisation

Graphite intercalation compounds are a material class with a great variety of structure and compositions based on the ability of storing different species in between the relatively weakly interacting graphene layers. Thereby graphite shows an redox-amphoteric behaviour forming donor (*e.g.* with alkali metal ions) as well as acceptor compounds (with $FeCl_3$ for example). GICs were first described in a scientific paper in 1840 by Schafhäutl.[92] He observed the formation of *yellow* and *blue* graphite alongside with a dilation of the graphite flakes when treating them with sulphuric acid or other oxidizing agents. They were first described as electrode material in

1938 by Rüdorff and Hofmann.[47]

Per definition, intercalation compounds are formed by the insertion of atomic or molecular layers of guest species (atoms, ions, molecules or complexes) between the layers of a host material. No major structural modification of the host structure takes place.[93] A charge transfer between the guest species (intercalant) and the host structure occurs. An intercalation-ready material exhibits strong *intra*-planar binding and weak *inter*-planar forces.[93–100] The most prominent examples for intercalation-ready materials are graphite and transition metal dichalcogenides.[96,101,102] The resulting fundamental structural unit of the forming intercalation compound is depending on the host material. In the case of graphite, for example, usually atomic monolayers of the intercalants are formed in between two adjacent layers of the graphite host, while for transition metal dichalcogenide such as TiS_2 a three-layered sandwich of S-Ti-S of the host structure is formed and separates the intercalant layers.[102] An overview of the most important vocabulary of intercalation reactions is listed in table 2.1; a graphical representation is shown in figure 2.1.

The formation mechanisms of graphite intercalation compounds haven been extensively studied in the 1970s and 1980s and are described in a number of seminal review articles and books.[93–102] In contrast to the ***b***-GICs, the ***t***-GICs are scarcely investigated up until today. The ternary compounds were studied from the 1960s till 1990s mainly in Germany and Japan with the focus on their synthesis and structural analysis.[97,103–108] Overall, the underlying principles of the GIC formation can be summarized as follows:

- During the intercalation of intercalants into an intercalation host, an ordering mechanism occurs, the so-called *staging*.
- The intercalants are not randomly intercalated but instead in a periodic arrangement of n layers of the host material in between the intercalant layers, with n denoted as stage index. Due to its highly ordered structure, graphite exhibits the most distinct *staging* behaviour and the highest accuracy of the formatted stages of all known intercalation hosts.

Table 2.1: Vocabulary and definitions of intercalation reactions.[93–98]

term	description
intercalation host	a layered, lamellar material with strong *intra*-planar binding forces and weak *inter*-planar binding forces
intercalant	chemical species intercalated into an intercalation host (atoms, ions, molecules or complexes)
intercalation	insertion of intercalants into an intercalation host, without major structural modification of the host
staging	ordering phenomena during intercalation; intercalants are only situated in a fraction of the interlayer spaces, which exhibit a defined distance towards each other
stage 1	single layers of intercalant and graphite layers alternate; highest, possible amount of intercalant species that can be stored inside a given host material
stage 2	two layers of graphite layers separate each intercalant layer from each other
stage n	n layers of graphite layers separate each intercalant layer from each other

- This staging mechanism is, firstly, caused by a stronger interaction between intercalant–intercalant than the interaction between the intercalant and the intercalation host. The introduction of each intercalant layer secondly adds a substantial strain within the crystal lattice of the intercalation host due to the necessary expansion in c-direction. The avoidance of strain favours the intercalation of a minimum of intercalant layers at a given intercalant concentration. Therefore, the minimal energy necessary corresponds to a close-packed, in-plane intercalant arrangement with the largest possible separation between the minimum amount of intercalant layers.

Due to the amphoteric behaviour and weak van-der-Waals *inter*-planar interaction, graphite is suitable to form a wide variety of intercalation compounds. The most important structural motives are listed in table 2.2. The most prominent graphite intercalation compounds are:

a) binary Li-GICs for lithium-ion batteries[53,94,109] based on the reversible intercalation /deintercalation of lithium ions

b) binary alkali-GICs into transition metal dichalcogenide for physical studies on selective Fermi level filling and electronic conductivity[102]

c) the chemical formation of ternary GICs as an intermediate stage that decomposes and releases solvent molecules with the graphite lattice and therefore triggers exfoliation to obtain graphene as reaction product.[110]

Graphite intercalation compounds can be prepared by chemical route or electrochemically; details will be discussed in section 2.2.

Characterisation methods

The easiest way to track the formation of graphite intercalation compounds and their stages is measuring the dilation of the graphite particles during intercalation and deintercalation *in-situ* or *ex-situ* via microscopic methods or diffraction.[96,100,111–115] The stage formation and therefore the formation of GICs can be tracked via electrochemical measurements such as galvanostatic cycling and cyclic voltammetry.[100] Since the electrochemical characterisation and X-ray diffraction deliver the most accurate overview over the stages formed during intercalation reaction this study will focus on these methods and they are described in detail in the following paragraphs. When handling graphite intercalation compounds, especially those containing alkali ions, it always has to be kept in mind that these might be highly reactive towards water and oxygen, for example, and therefore should best be handled under protective atmosphere.

Table 2.2: Vocabulary and definitions of graphite intercalation compounds.[93,95–98]

term	description
GIC	graphite intercalation compound, formed by intercalation of an intercalant into a graphite host structure
acceptor-GIC	intercalation of an intercalant with acceptor properties, this means the graphite intercalation host is donating electrons (for example $C_8^+Br^-$)
donor-GIC	intercalation of an intercalant with donor properties, the graphite intercalation host is accepting electrons (for example $K^+C_8{}^-$)
***b*-GIC**	*binary GIC:* intercalation host of a single intercalant
***t*-GIC**	*ternary GIC:* intercalation of two different intercalants
homogeneous GIC	two intercalants are located in the same gallery of the host structure, ordered or disordered structure of the guest layers depending on the intercalant-intercalant and intercalant-host interactions
heterogeneous GIC	two intercalants are located in different gallerys of the host or form separated layers within the same gallery

Electrochemical methods: The staging phenomena occurring during the intercalation of intercalants into the graphite structure allows the observation of the kind and degree of intercalation (*i.e.* the determination of the corresponding stages) via electrochemical measurements. For each stage an free Gibbs reaction enthalpy can be calculated according to:

$$\Delta_r G = -z \cdot F \cdot E \tag{2.1}$$

With z being the number of the transferred electrons, F the Faraday constant and E the cell voltage.

When reducing graphite electrochemically in an electrolyte containing the intercalating species, specific potential plateaus do occur, indicating the two-phase regions in between two stages (*i.e.* coexistence of two phases). The highest packing density of the intercalant inside the graphite host is denoted as stage 1 and is dependent on the species that is intercalated (*i.e.* spatial requirements, intercalant-intercalant and intercalant-host interactions). Since the intercalation potentials depend on the kind of GIC that is formed, galvanostatic cycling measurements can additionally be used to distinguish which kind of compound is formed. Under potentiodynamic control (cyclic voltammetry) the region where two stages coexist can be determined as current peaks.[53]

X-ray diffraction: The intercalation of a guest species is always accompanied by an increase of the interlayer distance of two adjacent graphite planes (*i.e.* c-direction of the crystal lattice). Therefore, X-ray diffraction (XRD) is a versatile option to track the formation of GICs either by *in-situ* or *ex-situ* measurements.[48,58,96,115–119]

Calculation of the reflex positions: The change of the average interlayer distance leads to a series of new reflexes which can be easily distinguished from the reflexes of pristine graphite (figure 2.2). One method to determine the stage number and interlayer distance between graphite layers including the intercalants is to calculate structural factors and has been described in detail by Abe *et al.*.[108] A more convenient method is the following:

- Each of the new occurring reflexes is indexed by $(00l)$, since the well-oriented graphite only exhibits these and the $(hk0)$ reflexes therefore can be ignored.
- From the series of appearing diffraction lines, with help of the Bragg equation (2.2), the d-spacing can be calculated.

- Multiplying the d-value with the index l of the reflex leads to the most probable repeat distance, called I_c.

This value describes the repeat distance along the c-direction of the graphite intercalation compound (equation 2.3).[96,119–121] It is an indicator which stage of a graphite intercalation compound is formed. All calculations are simply based on geometrical assumptions and the formation of the pure intercalation stages (equation 2.3 and figure 2.1). The quantities used in equations 2.2 and 2.3 are listed and described in table 2.3.

$$n_{xrd} \cdot \lambda = 2 \cdot d \cdot sin(\theta) \tag{2.2}$$

$$I_c = \Delta d + n \cdot c_0 = d_i + (n-1) \cdot c_0 = l \cdot d_{(00l)_n} = (l+1) \cdot d_{(00l)_{n+1}} \tag{2.3}$$

Table 2.3: Description of the quantities used in the Bragg equation (equation 2.2) and for the repeat distance (equation 2.3).

quantity	description
n_{xrd}	scattering order, positive integer; here $n_{xrd} = 1$
λ	wavelength of the incident beam; here Cu-$K_{\alpha 1} = 1.54\,\mathring{A}$
θ	scattering angle between the incident beam and the planes of graphite
I_c	repeat distance of the graphite intercalation compound
n	stage number
c_0	pristine graphite gallery height; c_0= 3.355 nm[53]
Δd	thickness of one intercalant layer
d_i	gallery height of an intercalated layer
$d_{(00l)_n}$	distance of plane spacings of the $(00l)$ plane of stage n
l	index of the $(00l)$ plane

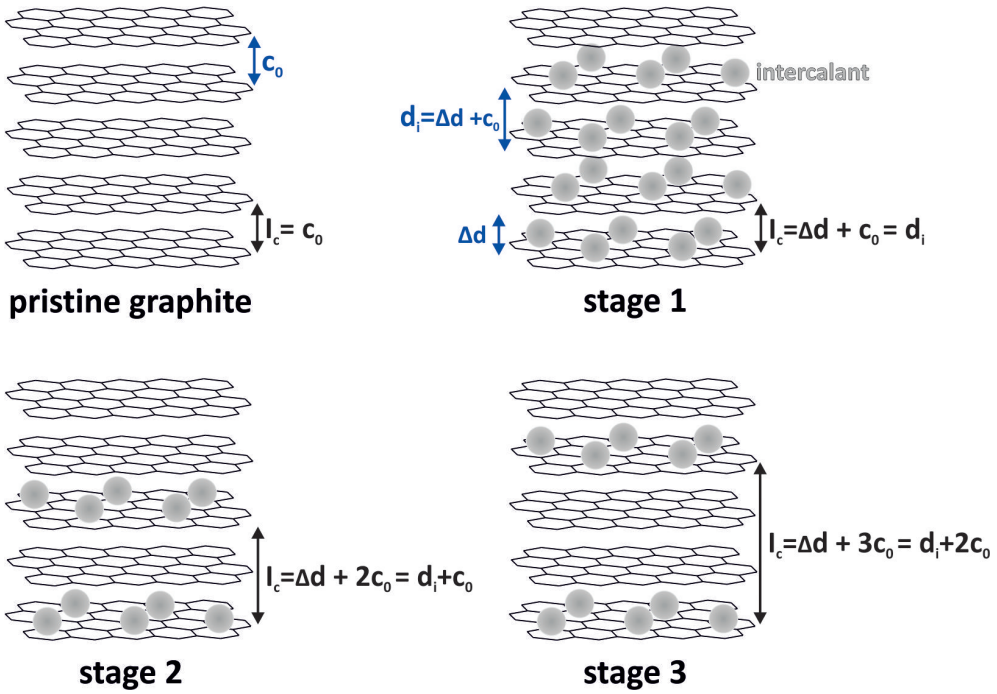

Figure 2.1: Schematic drawing of the staging mechanism occurring during intercalation of an intercalant into the graphite host structure (model by Rüdorff[49]). The equations for calculating the repeat distance, the thickness of one intercalant layer and the gallery height of an intercalated layer are shown for the highest three stages (stage 1 - stage 3). This model represents an idealized case for the intercalation in a graphite material with perfect long-range order. A practically more relevant staging model was proposed by Daumas and Herold[122] and confirmed by electron microscopy and *in-situ* Raman spectroscopy.[123,124] This model is more applicable for stages higher than 1, since it proposes the necessary bending of single graphene layers at certain points. In contrast to the above shown model where an intercalant layer is extended from one end of a graphite crystal to the other, in this model multiple intercalant islands are formed. However, for a stage 1 compound, which is examined solely in this study, no difference between the Daumas-Herold model and the above shown Rüdorff model can be observed and therefore is neglected.

The reflexes of pure intercalation stages without any deviation from the ideal structure can be calculated according to:[120,125–127]

$$d_{(00l)_n} = \frac{1}{l} \cdot [d_i + (n-1) \cdot c_0] \tag{2.4}$$

In figure 2.2 the reflex positions for the pure intercalation stages of LiC_6 and KC_8, LiC_{12} and LiC_{18} are calculated and shown in comparison with the most intense diffraction line of pristine graphite. The introduction of a guest species leads to a downwards shift of the main diffraction line along with the appearance of a series of new and equidistant reflexes. How strong the main reflex shifts depends on the species that is intercalated (the bigger the intercalant the more pronounced the shift) and on the stage that is formed (the stages with higher numbers, i.e. stages with lower intercalant density, exhibit more reflexes with a lower spacing between them).

Without the calculation of structural factors it can only be estimated what the intensity ratios of the different reflexes will be. Roughly, it can be said that the reflex with the highest intensity in stage n is *(00n)* for binary Li^+-GICs and K^+-GICs. For bigger intercalants and ternary GICs it is know to be *(00 n+1)* or *(00 n+2)* depending on the intercalant layer thickness Δd.[125–127] As a rule-of-thumb, the most intense line is always the one closest to the main diffraction line of pristine graphite ($d_{(002)}$=3.355 $\AA$). This is especially true for higher stage numbers, since due to the higher dilution of the intercalant within the graphite lattice, only small deviations from the pristine graphite structure are caused.

With the equations described above ***t***-GICs can be identified easily, if it is ensured that they are handled under protective atmosphere to prevent their decomposition. The easiest way is to prepare the samples inside an argon-filled glovebox and cover them with a polyethylene foil[128] or a Kapton tape[129] before the measurement. Since these covers may weaken the intensities of the reflexes at low scattering angles, these should be neglected and only the main diffraction line or reflexes at higher scattering angles be used to determine the intercalant thickness.[130]

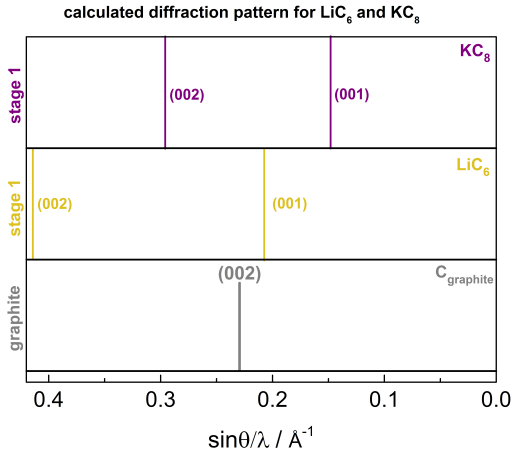

(a)

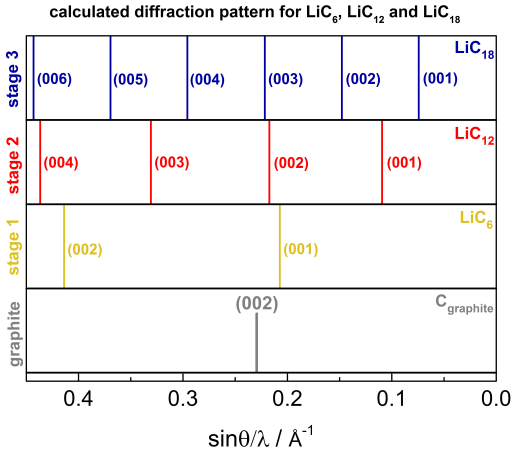

(b)

Figure 2.2: Calculated reflex positions (using eq. 2.4) for (a) graphite, LiC_6 and KC_8, (b) graphite, LiC_6, LiC_{12} and LiC_{18}. The introduction of an intercalant into graphite leads to a downwards shift of the diffraction line with the highest intensity along with the appearance of a series of equidistant reflexes. How strong the shift is depends on the intercalant and stage.

2.2 Insertion mechanisms into graphite

There are two kinds of reversible insertion mechanisms for graphite materials. Firstly, the intercalation of a guest species forming GICs. Secondly, the adsorption of the species on the edges of individual graphene layers or in nanopores developed by the tilt of single graphene stacks towards each other in graphite materials with small particle sizes or graphitic carbons with a less distinct long-range order.[53] Since this study was focused on synthetic graphite with large particles and a high long-range order, the adsorption mechanisms are not described in detail here. For more information see section 1.2.1 in the subsection "Carbons" alongside with the references of relevant publications on this research topic.

The next subsections will focus on the details of intercalation and co-intercalation reactions and sum up the most important research results (sections 2.2.1 and 2.2.2) describing chemical and electrochemical routes to prepare them. The most relevant reviews on graphite intercalation compounds are listed in table 2.4.

Table 2.4: Survey of reviews on graphite intercalation compounds.

Reviews on GICs	**year/author**	**Ref.**
Chemistry of GICs	*1976/Ebert*	[95]
Physics of GICs	*1981/Dresselhaus*	[96]
Review on GICs as electrode material	*1982/Flandrois*	[99]
Review of theory of GICs	*1985/DiVincenzo*	[50]
Book chapter: Review of physics of GICs	*1986/Dresselhaus*	[101]
Physical review on layered materials	*1987/Dresselhaus*	[102]
Physics of ***t***-GICs	*1988/Solin*	[97]
IUPAC nomenclature of GICs	*1994/Boehm*	[98]
Electrochemistry of GICs	*1998/Noel*	[100]
IUPAC *Goldbook* on intercalation reactions	*2007/Aleman*	[93]
Theoretical paper on ***b***-alkali-GICs	*2013/Nobuhara*	[34]

2.2.1 Intercalation into graphite

The term intercalation is typically used to describe the introduction of a single species into the graphite lattice without disturbing the planarity of the graphite planes significantly. The products of this cell reaction are denoted as *binary graphite intercalation compounds* (***b***-GICs). Graphite is showing amphoteric behaviour, allowing the reversible intercalation of cationic and anionic species.[131]

Donor-type ***b***-GICs:
(graphite reduction & cation uptake)

$$C_n + xe^- + xI^+ \rightleftharpoons \mathbf{I_x^+ C_n^-} \tag{2.5}$$

Acceptor-type ***b***-GICs:
(graphite oxidation & anion uptake)

$$C_n + xI^- \rightleftharpoons xe^- + \mathbf{I_x^- C_n^+} \tag{2.6}$$

With C_n being n carbon atoms of the graphite lattice, I^+/I^- being cationic and anionic intercalant species, e^- being electrons and x a positive integer.

Well-studied examples for cation intercalation are the alkali ions Li^+ and K^+ forming LiC_6 and KC_8, respectively.[30,48] While the LiC_6 formation is used commercially as charge storing electrode reaction in lithium-ion batteries, so far there are no practical applications for the binary potassium-GICs.[132,133] Prominent examples for the intercalation of anions into the graphite structure are the hexafluorophosphate anion (PF_6^-) and the trifluoromethanesulfonylimide anion ($TFSI^-$).[134,135] These anion intercalation mechanisms are intensively studied for their application in so-called *Dual-Ion cells*. These cells are based on a hybrid mechanism in between batteries and supercapacitors, where the energy is stored by intercalating cations into a graphite anode while intercalating anions into a graphite cathode. This kind of cell reaction is mainly hindered by the electrochemical stability window of the electrolyte,

which leads to decomposition of the electrolyte before anion intercalation.[119,131]

In the following paragraphs relevant publications on the chemical and electrochemical formation of binary graphite intercalation compounds are described and listed (table 2.5 and table 2.6).

Chemical formation of *b*-GICs

The chemical intercalation of anions and cations into graphite proceeds mainly *via* two different approaches. Firstly, *via* melt-infiltration where the intercalant and graphite are placed in evacuated vessels and are heated until the intercalant is liquid or gaseous.[31,48,49,92,115,136] Secondly, *via* solution methods where a salt containing the intercalant species is dissolved in an appropriate solvent and mixed with the graphite host material and a reducing or oxidizing agent in an appropriate, usually organic, solvent at ambient or slightly increased temperature (30 °C-100 °C).[47,109,116] In contrast to the other alkali metals only a minor fraction of sodium ions can be chemically intercalated into graphite (NaC_{64} vs. LiC_6, KC_8, RbC_8 and CsC_8).[31,49]

Table 2.5: Literature survey on ***b***-GICs prepared by chemical preparation routes.

Chemical preparation *b*-GICs	**year/author**	**Ref.**
First description of GICs: Colour & dilatation	*1840/Schafhaeutl*	[92]
b-HSO_4^--GIC: Preparation and characterisation	*1938/Ruedorff*	[47]
b-K-GIC: Preparation and characterisation	*1954/Ruedorff*	[48]
b-Na-GIC: Preparation of NaC_{64}	*1959/Asher*	[31]
b-K,Rb,Cs-GICs: Preparation & characterisation	*1959/Ruedorff*	[49]
b-HSO_4^--GICs: Preparation and characterisation	*1978/Besenhard*	[109]
b-K,Rb,Cs-GICs: X-ray diffraction	*1978/Chung*	[115]
b-K-GIC: Stability of different stages	*1996/Oh*	[136]
b-$TFSI^-$-GIC: Anion intercalation & XRD study	*1998/Zhang*	[116]

Electrochemical formation of *b*-GICs

The electrochemical formation of ***b***-GICs is more advantageous than the chemical formation, since the amount of stored charge and therefore the formed stage can be easily controlled by measuring the cell voltage. Furthermore it allows the synthesis at room temperature. It proceeds mainly through the galvanostatic reduction/oxidation of graphite *vs.* a metallic counter electrode in organic solvents or a mixture of organic solvents,[78,117,132,134,137] polymer electrolytes[32,33,112] or ionic liquids,[119,131,135] depending on the voltage range where the intercalation of the guest species occurs. Just as the ***b***-GICs formed *via* chemical preparation routes, all alkali metals except sodium can electrochemically be intercalated to a sufficient and comparable amount (NaC_{64} vs. LiC_6, KC_8).[32,117,132]

Table 2.6: Literature survey on ***b***-GICs prepared electrochemically.

Electrochemical preparation *b*-GICs	**year/author**	**Ref.**
b-Na-GIC: Formation of NaC_{64}, polymer electrolyte	*1988/Ge*	[32]
b-Na-GIC: Formation of NaC_{70}, polymer electrolyte	*1993/Doeff*	[33]
b-Li-GIC: Structural characterisation	*2000/Hightower*	[117]
b-PF_6^--GIC: Anion intercalation & structure	*2009/Maerkle*	[134]
b-K-GIC: Electrochemistry & structure	*2010/Liu*	[112]
b-$TFSI^-$-GIC: Electrochemistry anion intercalation	*2012/Placke*	[135]
b-$TFSI^-$-GIC: XRD study anion intercalation	*2013/Schmuelling*	[119]
b-Anion-GICs: Different anions & XRD study	*2014/Placke*	[131]
b-K-GIC: Electrochemistry and XRD study	*2015/Komaba*	[132]

2.2.2 Co-intercalation into graphite

The term co-intercalation describes the introduction of a single species alongside another intercalant species into the graphite lattice. The second intercalating species is either another intercalant species or the solvation shell of the first species. The simple term “co-intercalation” is more commonly used for the co-intercalation of

a cationic or anionic species alongside with their solvation shell. The products of both of these cell reactions are denoted as *ternary graphite intercalation compounds* (***t***-GICs).

Generally, co-intercalation phenomena are regarded as harmful for the cycle stability of an electrode material, since the intercalation of the solvation shell is often linked to exfoliation of the graphite material. In LIBs, the co-intercalation of solvents often leads to the exfoliation and subsequently to the disintegration of the graphite electrode. To increase the cycle life of LIBs it is regarded as absolutely necessary to suppress co-intercalation reactions[51–53,106,138,139] (by formation of protective solvent-impermeable surface films, SEI[29]) or to prevent them (by decreasing the solvation number of the alkali ions[140,141]).

This study will focus on ***t***-GICs formed by the co-intercalation of solvent molecules. As for the binary compounds, in theory graphite shows amphoteric behaviour, allowing the reversible intercalation of cationic and anionic species or complexes.[97]

Donor-type ***t***-GICs:
(graphite reduction & cation + solvent uptake)

$$C_n + xe^- + xI^+ + y \cdot \text{solv} \rightleftharpoons \mathbf{I_x^+(solv)_yC_n^-} \tag{2.7}$$

Acceptor-type ***t***-GICs:
(graphite oxidation & anion + solvent uptake)

$$C_n + xI^- + y \cdot \text{solv} \rightleftharpoons xe^- + \mathbf{I_x^-(solv)_yC_n^+} \tag{2.8}$$

With C_n being n carbon atoms of the graphite lattice, I^+/I^- being cationic and anionic intercalant species, $x{\cdot}e^-$ being x electrons, $y{\cdot}solv$ being y solvent molecules.

A well-studied example for a cation and solvent co-intercalation is Li^+ and DMSO (Dimethylsulfoxide) or Li^+ and DME (Dimethylether) forming $Li(DMSO)C_{24}$ and $Li(DME)C_{18}$, respectively.[104,105,107,142,143] To the best of the author's knowledge

there is no practical example for the anion and solvent co-intercalation to be found in scientific literature, but in theory it should work like the cation and solvent co-intercalation. The missing of reliable, experimental data maybe due weak solvation of the "large" anions due to their lower charge density compared to cations.

The intercalation of solvents into graphite sometimes leads to the exfoliation of the graphite into single graphene layers or small graphene stacks, depending on the solvent-graphite interaction. It was therefore proposed as large-scale preparation technique for graphene.[110]

In the following paragraphs relevant papers on the chemical and electrochemical formation of ternary graphite intercalation compounds are described and listed (table 2.7 and table 2.8).

Chemical formation of *t*-GICs

The chemical co-intercalation of cations and their solvation shells into graphite proceeds *via* solution methods where a salt containing the intercalant species is dissolved in an appropriate solvent and mixed with the graphite host material and a reducing or oxidizing agent. As solvent usually an organic solvent at ambient or slightly increased temperature (30 °C - 100 °C) is used, comparable to the chemical formation of the ***b***-GICs. As co-intercalating solvents, mostly linear or cyclic ethers with different amounts of coordinating oxygen atoms are chosen, such as THF (tetrahydrofuran),[108,118] or glymes.[128,144,145] Amides and sulphonamides as co-intercalating solvents are studied less intensely.[103,146]

In contrast to the formation of the ***b***-GICs, the ***t***-GICs of sodium and solvents can be synthesized easily to the same degree as for all other alkali metals.[128,144,145]

Table 2.7: Literature survey on ***t***-GICs prepared by chemical preparation routes.

Chemical preparation *t*-GICs	**year/author**	**Ref.**
t-Li,Na-GICs: Co-intercalation of amides	*1968/Ginderow*	[103]
t-Li,K,Rb,Cs-GICs: Co-intercalation of THF	*1997/Mizutani*	[108]
t-Na-GIC: Co-intercalation of ethers	*1998/Tanaike*	[144]
t-Li,K-GICs: Co-intercalation of ethers	*2001/Inagaki*	[145]
t-Li,K,Rb,Cs-GICs: Co-intercalation diff. solvents	*2002/Mizutani*	[128]
t-Li-GIC: XRD study, co-intercalation of THF	*2011/Henderson*	[118]
t,q-Li,Na-GICs: Structural characterisation	*2012/Maluangnont*	[146]

Electrochemical formation of *t*-GICs

The electrochemical formation of ***t***-GICs proceeds mainly through the galvanostatic reduction/oxidation of graphite *vs.* a metallic counter electrode in organic solvents. It is more advantageous than the chemical route, since the amount of stored charge and therefore the formed stage can be easily controlled by measuring the cell voltage and it allows the synthesis at room temperature. Additionally, it gives evidence about thermodynamic and kinetic properties of the proceeding electrode reaction and allows conclusions about the reversibility of the co-intercalation mechanism.

Thereby linear and cyclic ethers as well as DMSO were found to co-intercalate in reasonable amounts.[104–107,142,143,147]

Just like the ***t***-GICs formed via chemical preparation routes, the ternary compounds of sodium and solvents can be co-intercalated easily to the same degree as for all other alkali metals.

Table 2.8: Literature survey on ***t***-GICs prepared electrochemically.

Electrochemical preparation *t*-GICs	**year/author**	**Ref.**
t-NMe_4^+,Li/DMSO,DME-GIC: Cyclic voltammetry	*1974/Besenhard*	[104]
t-Alkali,NMe_4^+/DMSO,DME-GIC: Staging	*1976/Besenhard*	[105]
t-Alkali,NMe_4^+/DMSO,DME-GIC: Staging	*1980/Besenhard*	[142]
t-GIC: Review on ***t***-GIC	*1983/Besenhard*	[106]
t-Li/DMSO-GIC: Staging phenomena	*1991/Schoderboeck*	[107]
t-Li/solvent-GIC: Co-intercalation vs. intercalation	*2003/Abe*	[147]
t-Li/DMSO,DME-GIC: *De*-solvation energies	*2004/Abe*	[143]

2.3 Model for co-intercalation of glymes

While lithium and the larger alkalis such as potassium, rubidium, caesium do form binary graphite intercalation compounds voluntarily, leading to LiC_6 and KC_8, RbC_8, CsC_8, respectively, no such compound can be chemically or electrochemically prepared with sodium ions.[31–33] The fact that sodium ions do not form binary graphite intercalation compounds as the other alkali metals is usually explained by a size mismatch between the sodium ion and the graphite lattice. Evidently, sodium ions cannot energetically favourably be positioned inside the geometry of a graphite crystal. According to density functional theory calculations, the non-existence of sodium-rich ***b***-GICs in based on thermodynamic reasons. The insertion of sodium ions into the graphitic host structure would be accompanied by a strong stretching of the carbon-carbon bond and is therefore unfavourable.[34]

Since there is no viable option to shrink the sodium ions down to the size of a lithium ion, the enlargement of the sodium ion may be a way to circumvent the mismatch between graphite and sodium ions. One way may be the co-intercalation of the sodium ions alongside with their solvation shell into graphite (equation 2.7). For sodium ions the co-intercalation of solvent molecules into graphite was described in detail before but without any links to electrochemical measurements focusing mainly on their structural characterisation.[108,118,128,144–146]

To ensure a reversible co-intercalation / *de*–co-intercalation, an appropriate solvent should offer atoms that strongly coordinate sodium as central ion and form ideally a flexible solvent shell around the sodium ion. Both conditions are necessary to provide a sufficient stability and flexibility of the complex within the graphite lattice.[148] Generally, crown ethers are known to form stable and highly ordered complexes with alkali ions. Their stability is determined by the donor-acceptor interaction between the oxygen and the alkali ion and the size match between the alkali ion used and the void in the middle of the crown ether.[149] In case of sodium ions, [15]-crown-5 exhibits a high complex stability (figure 2.3, left), but since crown ethers are relatively expensive and dissolve only small amounts of the conductive salts that are needed for their application in batteries, it seems their use will not be feasible. A more appropriate solvent based on the same structural element is diglyme (Bis(2-methoxyethyl) ether, figure 2.3, right). With the same coordinating oxygen atoms it offers similar complex stability combined with a higher flexibility due to its linear ether chain and beneficial properties as electrolyte solvent, is already studied alkali/oxygen cells,[36,87,88,91] especially relating to their beneficial filming properties of the alkali metals[46,89,90] and their basic physcial properties such as conductivity and solubility of conductive salts.[86]

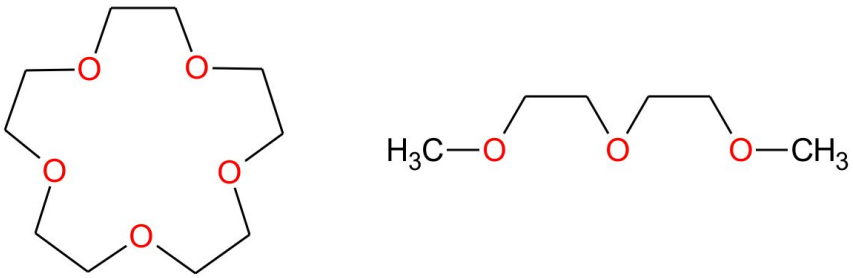

Figure 2.3: Skeletal formulas of [15]-crown-5 (1,4,7,10,13-Pentaoxacyclopentadecane, left) and diglyme (Bis(2-methoxyethyl) ether, right).

A possible co-intercalation mechanism for diglyme and the alkali ions (Li^+, Na^+) is schematically drawn in figure 2.4. The proposed mechanism is based on the as-

sumption that each ion is coordinated by six ether oxygen atoms, based on the most common coordination number (CN) 6 for complexes in liquids.[150] The intercalation mechanism for diglyme and the alkali ions is still under discussion and object of intense research. All assumptions and conclusions in this work are based on the essential assumptions made in figure 2.4.

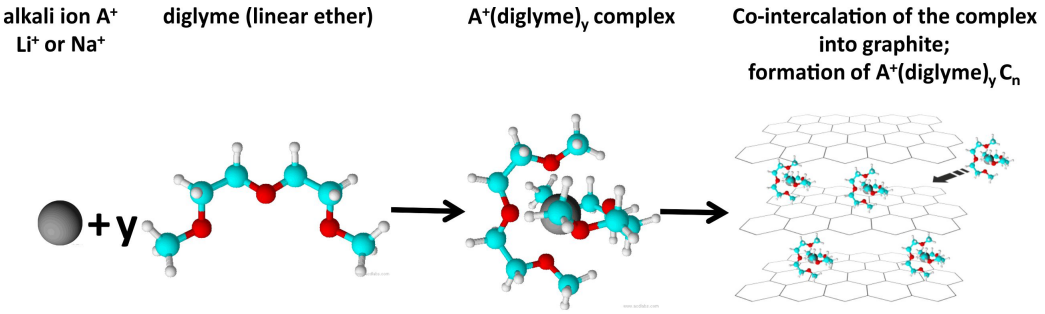

Figure 2.4: Model of the electrochemical insertion reaction into graphite based on solvent co-intercalation: An alkali-ion is coordinated by y diglyme molecules via an alkali ion-oxygen interaction. The resulting complex can reversibly be inserted / *de*-inserted into a graphite electrode. When the solvent shell is inserted alongside with the alkali ion this process is referred to as co-intercalation.[51] Concept from Jache *et al.*.[129]

3 Experimental results and discussion

In this chapter a first test of the proposed co-intercalation electrode reaction from section 2.3 is carried out (experimental details in section 3.1). At first, the inability to intercalate "bare" sodium ions into a graphite electrode from a carbonate based electrolyte is reproduced and compared to analogously constructed lithium cells (section 3.2). Afterwards, measurements in a diglyme based electrolyte are conducted and characterized by electrochemical measurements and X-ray diffraction (section 3.3), proving that the solvent molecules participate in the electrode reaction. An preliminary conclusion is given in section 3.4.

In section 3.5 the effect of different chain lengths of the linear ethers (glymes) is tested to make a statement about coordination effects that may affect the co-intercalation process. Furthermore, the steric hindrance for the co-intercalation electrode reaction is increased by using linear ethers with side groups. Concluding this study, first electrochemical measurements on sodium-ion full cells based on graphite/diglyme/P2-$Na_{2/3}Ni_{1/3}Mn_{2/3}O_2$ are shown in section 3.6.

3.1 Experimental details

Electrode slurries were made from graphite powder as-received (SFG-44, synthetic graphite, particle size 44 μm, *Imerys S.A.*), polyvinylidene fluoride (PVDF *Solef 1310, Solvay*), and N-methyl-2-pyrrolidone (NMP, *Sigma Aldrich*). The content of graphite and binder was 90 wt% and 10 wt%, respectively. Electrodes were prepared by doctor blading a slurry onto copper foil (d=10 μm, *Schlenk*). The thickness of the electrodes was approximately 40 μm - 50 μm in the dried state. Circular elec-

trodes (d=1.2 cm) were punched out and contained 4 mg–5 mg graphite as active mass each. These were further dried at 120 °C for 2 h under vacuum (*Büchi* tube furnace) to evaporate residual NMP and then transferred into an argon-filled glovebox (*GS Glovebox System Technik*), where three-electrode Swagelok type cells for cyclic voltammetry and two electrode coin cells (CR2032, MTI *Corporation*) for galvanostatic cycling measurements were assembled. Lithium foil (*Rockwood Lithium*) or sodium (*BASF SE*) were used as the counter and reference electrodes. *Whatman* glass microfibre filters (*GF/A*) were used as separators. A commercially available 0.5 M solution of lithium hexafluorophosphate ($LiPF_6$) in 1:1 w/w% ethylene carbonate and dimethyl carbonate (EC/DMC, LP30, Selecti-Lyte, *Merck*) and a self-made electrolyte containing 0.5 M of sodium hexafluorophosphate ($NaPF_6$, purity >99.0 %, *Alfa Aesar*) in 1:1 w/w% EC/DMC (purity >99.0 %, *Sigma Aldrich*) were used as the electrolytes. Furthermore single solvent electrolytes based on different glymes were prepared (monoglyme (1G) purity >99.5 %, diglyme (2G) purity >99.5 %, triglyme (3G) purity >99.0 %, tetraglyme (4G) purity >99.0 %; Di(propylene glycol) methyl ether (DPGDME) purity >99.1 %, Diethylene glycol dibutyl ether (Butyl-2G) purity >99.0 %, 1,5-Dimethoxy pentane (1,5-DMP) purity >98.0 % and tetrahydrofuran (THF) without inhibitor purity >99.9 %, all used as received from *Sigma Aldrich*) with 1 M lithium triflate (LiOTf; purity >99.995 %, *Sigma Aldrich*) or 1 M sodium triflate (NaOTf; purity >98.0 %, *Acros*). The solvents were dried over molecular sieves and the purity was verified by ^{1}H-NMR measurements (200 MHz), (see supplementary information figure 7.1). No significant amounts of impurities - especially no water - could be determined.

Electrochemical measurements were conducted at 25 °C in a climate chamber using a *Maccor* battery cycler (Model 4300). Cells were cycled galvanostatically at a constant current of 37.2 $^{mAh}/_{g}$ (per gram active material) unless otherwise noted between 0.01 V and 3.0 V. All potentials reported herein were measured against a lithium or sodium metallic reference electrode, respectively. Capacities are given in mAh per gram of active material. Furthermore, cyclic voltammetry was conducted (*Biologic* VMP3) with a voltage sweep rate of 0.05 $^{mV}/_{s}$ for at least ten cycles. Wide-

angle X-ray diffraction patterns were recorded with a *PANanalytical EMPYREAN* ($Cu - K_\alpha$ source, 40 kV, 40 mA) in a 2θ angular range between 10 ° and 80 ° under a protective self-adhesive Kapton foil (*VWR*) to avoid exposure of the sample to air. The diffraction patterns were taken in Bragg-Brentano geometry with an automatic slit on the side of the X-ray source. This ensures that always the same area of the sample is irradiated and enables good resolution even at higher scattering angles, though it may lead to a decrease in reflex intensity at small scattering angles. In this research project the GICs are identified by reflex position solely, so the intensity ratios of the reflexes could be neglected. For the correct prediction of intensity ratios the structural factors can be calculated, which can be referred to in the previous papers.[108] In this work the notation of the reflexes follows the concepts described in section 2.1.

The analysis of diffraction patterns of binary and ternary GICs was carried out within a cooperation project with Prof. Takeshi Abe from the University of Kyoto.

3.2 About the absence of sodium-rich *b*-GICs

To prove the suitability of the prepared graphite electrodes and reproduce the *state-of-the-art* of ***b***-alkali-GICs, half cells with lithium and sodium were build using a carbonate based electrolyte.[1] As half cells those cells are denoted where an active material, in this case graphite, is measured against a metallic alkali electrode.

While for the lithium half cells the formation of LiC_6 is expected, it should not be possible to form and to characterise the corresponding sodium-rich compounds ("NaC_x"), meaning that graphite is an electrochemically almost inactive material towards sodium ion intercalation.[32,53]

[1] Part of the experimental data and figures shown were published in *Angewandte Chemie International Edition* and were adapted from Ref. [1] for this work with permission from the *John Wiley and Sons*.

3.2.1 Electrochemical characterisation in carbonates

Carbonates offer beneficial properties for their application as electrolyte solvents. Especially mixtures of ethylene carbonate and other carbonates (such as dimethyl carbonate (DMC), ethyl methyl carbonate (EMC), diethyl carbonate (DEC), and others) offer a good compromise exhibiting a high relative permittivity, low viscosities, inertness against inactive cell components, a wide liquid region over a wide temperature range and are non-toxic and economically viable.[78,137] Additionally, carbonates do form stable surface films (SEI layers) on graphites and carbon electrodes that act as a sieve for lithium ions and prevent the exfoliation of the electrode and thereby enhance the cycle stability.[29,52,53,151] So far, the transfer of those beneficial properties to sodium cells and the intercalation of sodium ions into graphite has been proven to be difficult to impossible. Due to the different solubilities of sodium compounds in contrast to lithium compounds in the electrolyte solvents and an insufficient surface film formation, several adjustments for sodium cells are necessary. The development of carbonate based sodium electrolytes is therefore still in progress.[76–79,81,152]

The theoretically obtainable capacity for the formation of LiC_6 is 372 $^{mAh}/_{g}$, calculated by equation 3.1. For the, so far unobserved and therefore undefined, sodium-rich binary GICs ("NaC_x") it might be something between 372 $^{mAh}/_{g}$ ("NaC_6") and 279 $^{mAh}/_{g}$ ("NaC_8"), if sodium ions would behave exactly the way lithium or potassium ions do. Sodium-lean ***b***-GICs have been described in literature before (such as NaC_{64}).[31,32]

$$q_{th} = \frac{\nu_{e^-} \cdot F}{M_x} \tag{3.1}$$

With ν_{e^-} the number of transferred electrons during the discharge reaction, F the Faraday constant (96,485.33 $^{C}/_{mol}$ = 26,801.48 $^{mAh}/_{mol}$) and M_x the molar mass of the reaction product upon full reduction of the electrode.

The first discharge/charge cycle of the graphite electrodes in analogous lithium and sodium half cells measured by galvanostatic cycling and cyclic voltammetry (CV) are shown in figure 3.1. As expected, for lithium the stage-wise formation of the ***b***-GIC can be traced, which manifested itself as potential steps in the capacity-voltage plot and as current peaks in the CV plot. The differential capacity plot, *i.e.* relative change of the capacity (increase or decrease) during intercalation/*de*-intercalation as a function of the voltage, allows additionally the deconvolution of the current peaks of the CV measurement and allows, to a certain extent, the identification of overlapping multi-electron processes (shown in the appendix 7.2b). For sodium almost no intercalation of sodium ions into graphite can be determined, neither by galvanostatic cycling nor cyclic voltammetry.

Additionally the cycle stability of the cell reaction was tested by executing galvanostatic cycling for at least fifty cycles. The specific capacities of the first fifty cycles for both alkali half cells are shown in the appendix in figure 7.2a. The lithium cells do show capacity fading during prolonged cycling, however this may be due to the fact that the graphite material used is not optimized for the application in lithium cells and the formation of LiC_6. It is most likely that the relatively large particles of the graphite material of around 44 μm suffer from exfoliation, leading to declined kinetics of the electrode compared to commercially applied graphites.[53,134,151,153] However, this fading should not be a problem in proving the proposed co-intercalation mechanism from section 2.3. From these results it can be concluded that the prepared graphite electrodes behave just as expected from literature study and that they are suitable for testing their behaviour towards the co-intercalation mechanism.

3.2.2 XRD-analysis of *b*-alkali-GICs

The structural analysis of the electrochemically formed ***b***-alkali-GICs was done by X-ray diffraction. For lithium the formation of LiC_6 can be traced clearly (see table 3.1 and figure 3.2). The values for the reflex positions and the intercalant layer thickness are in good agreement with the literature.[117,154] For sodium no changes

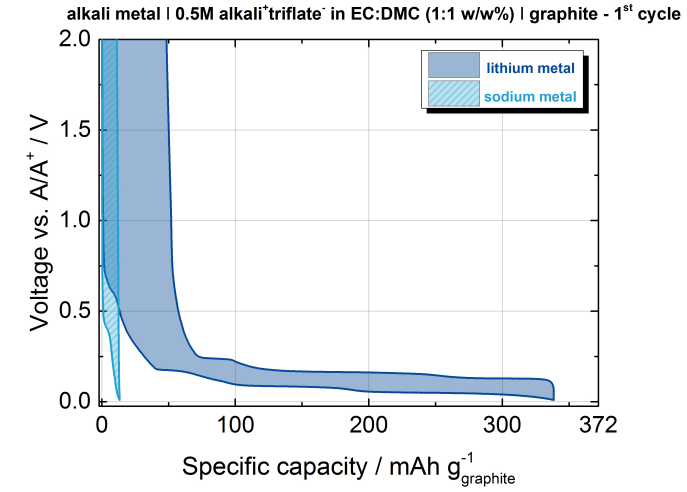

(a) voltage characteristics

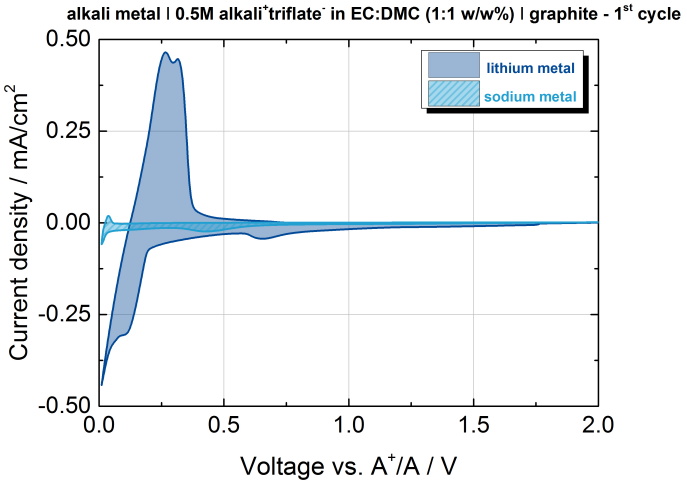

(b) cyclic voltammetry

Figure 3.1: (a) Voltage characteristics at a constant current of 37.2 $^{\mathrm{mA}}/_{\mathrm{g}}$ and (b) cyclic voltammograms at a scan rate of 0.05 $^{\mathrm{mV}}/_{\mathrm{s}}$ of graphite electrodes in lithium and sodium half cells in a carbonate based electrolyte.

in the diffraction pattern can be determined, which can be taken as clear evidence that no Na-GIC is formed during electrochemical discharge of graphite in a carbonate based electrolyte which is in good agreement with literature, as well.[32–34]

Table 3.1: Reflex positions and interlayer distance calculated from equations 2.2 and 2.3 of electrochemically prepared ***b***-alkali-GICs at stage 1 (i.e. full lithiation) determined with wide-angle X-ray diffraction.

sample	scattering angle 2θ / °	repeat distance I_c / Å	intercalant layer thickness Δd / Å
graphite	26.5	3.36	-
	54.5	3.36	-
LiC_6	23.9	3.72 (10.7 %)	0.36
	48.9	3.72 (10.7 %)	0.36

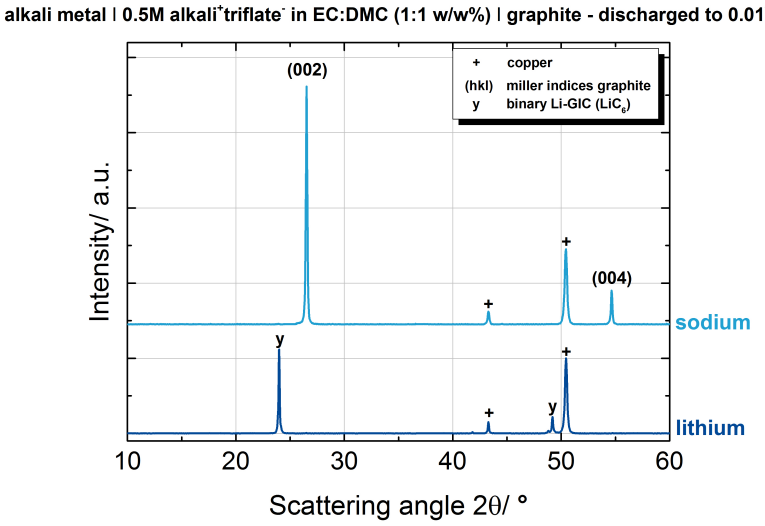

Figure 3.2: X-ray diffraction patterns of graphite electrodes in lithium and sodium half cells in a carbonate based electrolyte. Insertion products recorded at 0.01 V versus the corresponding redox couple after three cycles.

3.3 Formation of *t*-alkali-2G-GICs

To make a *proof-of-principle* of the model for the co-intercalation of glymes into graphite electrodes proposed in section 2.3, half cells of lithium and sodium were built using a diglyme based electrolyte.[2]

Due to the flexibility of the linear ether chain of diglyme similar stability of the complexes formed are expected for both alkali metals, forming $A^+(\text{diglyme})_y C_n^-$, respectively.[149] The electrolyte properties of different glymes were tested elsewhere, exhibiting sufficiently high dielectric constants and low viscosities.[86] However, there are reports results as well that glymes do react with lithium metal surfaces and do not form a protective layer comparable to carbonate solvents, and are therefore not suitable to be used in lithium-ion batteries.[89]

3.3.1 Electrochemical characterisation in diglyme

The first discharge/charge cycle of the graphite electrode in analogous lithium and sodium half cells measured by galvanostatic cycling and cyclic voltammetry are shown in figure 3.3. For both alkali metal ions, the formation of an intercalation phase is detected, which manifests itself as potential steps in the capacity-voltage plot and as current peaks in the CV plot. The differential capacity plot is shown in the appendix 7.3b for comparison.

For both alkali ions the intercalation is starting at potentials higher than the "classical" intercalation of "bare" lithium ions in carbonate-based electrolytes. From the CV plot it can be determined that the intercalation reaction occurs reversible between 1.30 V – 0.60 V vs. Li^+/Li for the lithium ions (with an irreversible fraction below 0.1 V) and between 1.05 V – 0.13 V vs. Na^+/Na for the sodium ions (figure 3.3b). These values are a first hint on the successful co-intercalation of ions and their solvent shells since co-intercalation reactions are typically known to occur at higher

[2] Part of the experimental data and figures shown were published in *Angewandte Chemie International Edition* and were adapted from Ref. [1] for this work with permission from the *John Wiley and Sons*.

equilibrium potentials compared to the formation of the binary GICs.[155]

The specific capacities of the first fifty cycles for both alkali half cells are shown in the appendix in figure 7.3a. The lithium cells do not show capacity fading during prolonged cycling as they had done under similar conditions when using the carbonate based electrolyte. This was unexpected, since the co-intercalation of a ion-solvent complex into the graphite electrode was expected to lead to a more distinct exfoliation than the intercalation of the smaller, "bare" lithium ions.[53,134,151,153]

For both alkali ions similar specific capacities of approximately 100 $^{mAh}/_{g}$ are determined, and the sodium half cells show a more stable cycling behaviour during prolonged cycling. We have been able to cycle these unoptimized sodium cells for 600 cycles without capacity fading (figure 7.4). Recalculating the intercalation species from the capacity values using equation 3.1 $A^{+}(diglyme)_{y}C_{20}^{-}$ - $A^{+}(diglyme)_{y}C_{21}^{-}$ are obtained, which is in good accordance to values reported in literature for similar compounds formed by solvent co-intercalation.[104,105,109,142,156]

To verify that no side reactions with the battery inactive materials do occur and somehow contribute to the electrode reaction during cycling, reference experiments were conducted. The cycle stability of different current collectors and different conductive salts (i.e. different anions) were tested (figures 7.5 and 7.6).

When different current collectors at the backside of graphite are used, a strong link of the choice of collector material on the cycle stability and achievable specific capacity can be found. The more flexible, stretchable and ductile the collector material is, the better the cycle stability and the higher the specific capacity. This effect is mostly likely caused by the large volume expansion of the graphite active material upon sodiation, which is around 250 % (subsection 3.3.2). When the active mass is applied onto a Whatman separator, without using any metallic current collector and graphite is directly electrically contacted, the electrochemical performance is better than for the surface-treated copper foil from *Schlenk* and much better than for untreated aluminium foil with a smooth surface (figure 7.5a). These findings are mostly likely linked to the fact that the formation of ***t***-alkali-2G-GICs is accompanied by a large volume expansion of the graphite particles which can be coped best by a

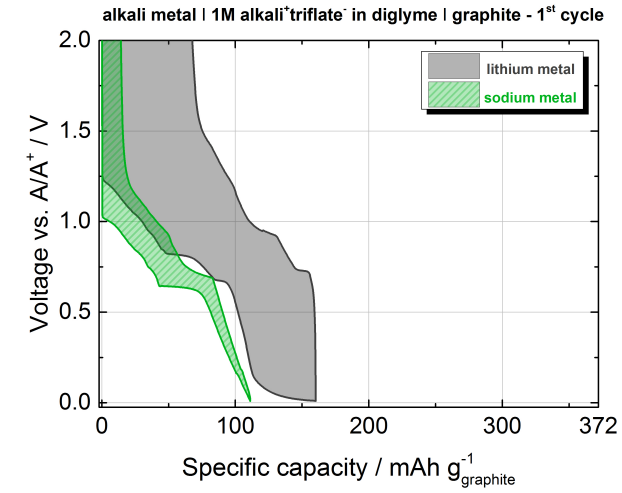

(a) voltage characteristics

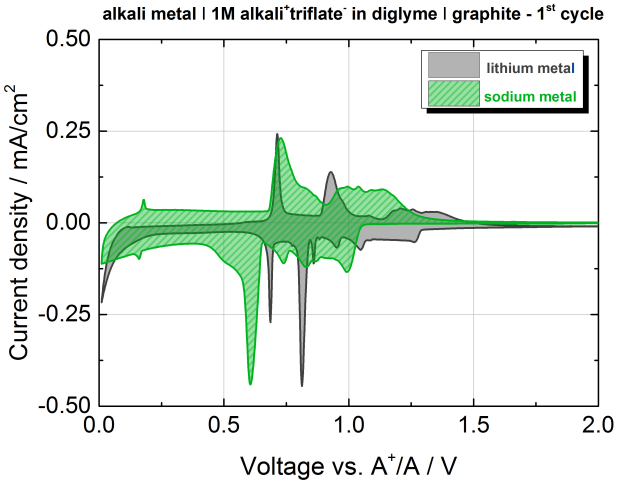

(b) cyclic voltammetry

Figure 3.3: (a) Voltage characteristics at a constant current of 37.2 $^{\mathrm{mA}}/_{\mathrm{g}}$ and (b) cyclic voltammograms at a scan rate of 0.05 $^{\mathrm{mV}}/_{\mathrm{s}}$ of graphite electrodes in lithium and sodium half cells in a diglyme based electrolyte.

flexible supporting material with a rough surface, *i.e.* a flexible current collector is beneficial for the cycle stability and the achievable capacities of the co-intercalation electrode reaction. For the basic co-intercalation potentials no difference due to the choice of current collector can be determined (figure 7.5b).

Figure 7.6 shows the results for different conductive salts and their impact on the charge/discharge characteristics and cycle stability. In conclusion, the formation of ***t***-alkali-2G-GICs is almost the same for all tested salts (NaI, NaOTf and $NaPF_6$) and the choice of conductive salt does not make a significant difference for the cycle stability or the achievable capacities of the electrode reaction.

Scan rate-dependent cyclic voltammetry measurements

To examine the insertion mechanism of the alkali-diglyme complex into graphite electrodes scan rate-dependent cyclic voltammetry measurements were conducted and analysed. The dependence of cyclic voltammograms on the scan rates can be used to distinguish between Faradaic and pseudo-capacitive charge storage.[157–159] For electrochemical reactions the Faradaic peak currents scale with the square route of the scan rate and capacitive currents scale linearly with the scan rate. The following two mathematical expressions were used for analysis with j being the peak current of a selected redox step and ν the scan rate:

1. The power law dependence of the current density on the scan rate; with b=0.5 for the Faradaic case, b=1 for the pseudo-capacitive case. Plotting *log (j)* vs. *log (ν)* at a constant electrode potential, the slope b is used to conclude on the Faradaic or pseudo-capacitive nature of the electrochemical process.

$$j = a \cdot \nu^b \quad \Longrightarrow \quad log(j) = b \cdot log(\nu) + log(a) \tag{3.2}$$

2. The superposition of Faradaic and pseudo-capacitive currents, plotting $j/\sqrt{\nu}$ vs. $\sqrt{\nu}$ at a constant electrode potential. The slope k_C and the y-axis intercept

k_F are taken as measures for the pseudo-capacitive ($k_C \cdot \nu$) and the Faradaic ($k_F \cdot \sqrt{\nu}$) currents.

$$j = k_C \cdot \nu + k_F \cdot \sqrt{\nu} \quad \Longrightarrow \quad \mathrm{j}/\sqrt{\nu} = k_C \cdot \sqrt{\nu} + k_F \tag{3.3}$$

Figure 3.4 shows the CV current responses at scan rates between 0.05 $^{\mathrm{mV}}/_{\mathrm{s}}$ - 1.25 $^{\mathrm{mV}}/_{\mathrm{s}}$ for both alkali metals. Several cathodic and anodic current peaks are evident, but the peak currents are significantly lower for the lithium based cells than for the sodium based cells. For the main co-intercalation step at around 0.60 V - 0.75 V the peak currents (marked with A_{red}/B_{ox}) are analysed in detail (appendix figure 7.7).

Figure 3.5 shows the separation of the redox peaks A_{red}/B_{ox} at the different scan rates. From these values it becomes clear that the redox peak separation (i.e. the overpotential of the electrode reaction) is smaller for the insertion of Na/2G into graphite than for Li/2G; which is in accordance with the results from galvanostatic cycling measurements of these systems. The separation between the peak potentials E_{anodic} and $E_{cathodic}$ is increasing with increasing scan rates for both alkali metals, indicating kinetic limitations for both systems. Additionally, and especially for the lithium-based system, a broadening of the redox peaks can be determined when scan rates are increased.

When *log (j) vs. log (ν)* is plotted at a constant electrode potential, according to equation 3.2, a linear fit of the data offers information on the b-value. A b-value close to 1 generally indicates that the electrode reaction is surface-limited, i.e. that capacitive charge storage is proceeding; b-values close to 0.5 points to a diffusion controlled charge storage reaction. The resulting values are listed in table 3.2 and from these it can be assumed that the co-intercalation electrode reaction is based on both, Faradaic and pseudo-capacitive charge storage.

When $\mathrm{j}/\sqrt{\nu}$ is plotted *vs.* the $\sqrt{\nu}$, according to equation 3.3, it is possible to

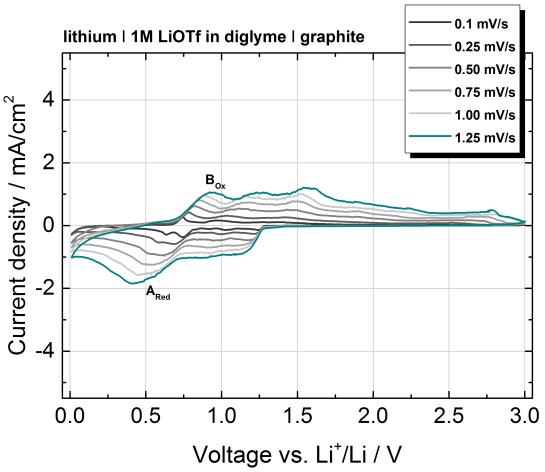

(a) lithium half cells

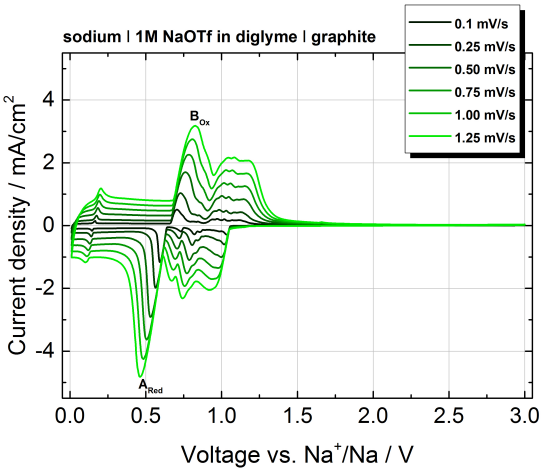

(b) sodium half cells

Figure 3.4: Scan rate-dependent cyclic voltammetry measurements of graphite electrodes in (a) lithium and (b) sodium half cells in a diglyme based electrolyte. To examine the insertion mechanism of the alkali-diglyme complex the peak currents (A_{red}/B_{ox}) are analysed to distinguish between Faradaic and pseudo-capacitive charge storage.

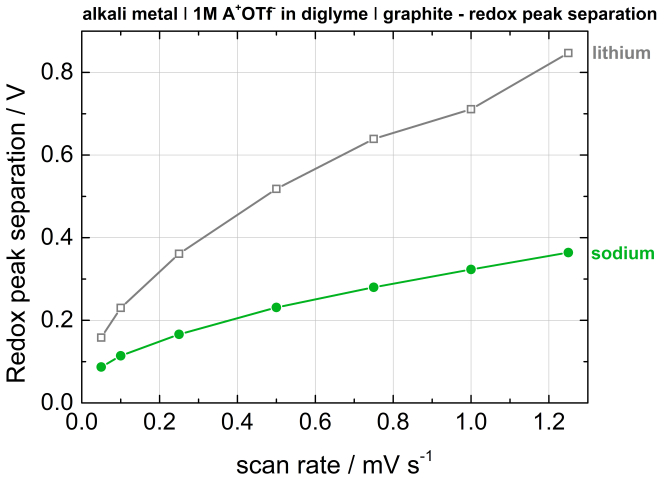

Figure 3.5: Redox peak separation determined from scan rate-dependent cyclic voltammetry measurements of graphite electrodes in lithium and sodium half cells in a diglyme based electrolyte.

quantitatively separate the contributions of the surface-limited (pseudo-capacitive) and diffusion-controlled (Faradaic) elements of the reactions. From this graph, with the slope corresponding to k_C and the y-axis intercept k_F, the contributions the co-intercalation reaction were determined and are listed in table 3.2.

For both mathematical expressions it becomes apparent that the co-intercalation/ *de*-co-intercalation reaction is almost equally based on surface-controlled and diffusion-controlled processes. These results are in good accordance with values reported by other groups working on co-intercalation electrodes. Kang *et al.* found for their graphite-diglyme co-intercalation system a b-value close to 0.8 and a Faradaic contribution close to 70 %.[156] The different values compared to this study might originate from a different electrode composition (i.e. different current response due to changed electronic conductivities). The group of Kang *et al.* added 20 wt% of a conductive agent to their graphite active material, while the electrode in this study contained

Table 3.2: Results of the analysis of the charge storage mechanism of Li^+/Na^+ in diglyme based electrolytes into graphite electrodes by scan rate-dependent cyclic voltammetry measurements (see figure 3.4).[157–159] b-values according to equation 3.2 and contributions of the pseudo-capacitive and faradaic processes on the anodic/cathodic peak current as function of the scan rate according to equation 3.3.

System	b-value (A_{red}) / s/mV	b-value (B_{ox}) / s/mV	$k_F\sqrt{\nu}$ (A_{red}) / %	$k_F\sqrt{\nu}$ (B_{ox}) / %
Li/2G	0.74	0.74	67%	68%
Na/2G	0.76	0.72	65%	73%

no conductive agent at all.

It needs to be mentioned that the above described theory and the presented mathematical connections of the peak current densities and the scan rate do imply that peak currents scale exactly with $\sqrt{\nu}$ or ν and that there is no broadening or rate-dependent shifting of the current peaks with increasing scan rates.[158] This behaviour was not observed for the here studied alkali-diglyme systems. Therefore, such *isopotential plots* of peak current densities *vs.* scan rates do not properly take into account scan rate-dependent changes of the peak potentials and peak widths and may therefore not deliver physical meaningful results for this type of electrochemical system.

3.3.2 XRD-analysis of *t*-alkali-2G-GICs

The structural analysis of the electrochemically formed ***t***-alkali-GICs was preformed by X-ray diffraction. Just like the reflexes for the ***b***-GICs a series of reflexes can be determined for the ***t***-GICs. Since expansion of the interlayer distance is larger when forming the ternary compounds the diffraction lines are more closely situated than for the binary compounds (for further explanations see section 2.1).[127] Since the solvation shell is presumably similar for the lithium and sodium ions the interlayer

expansion should be solely dependent on the co-intercalated alkali ion.

Figure 3.6 does not show the (001) reflexes of the respective ***t***-GIC. These can normally be detected below 2θ=10 °,[128] but with a low intensity due to the used measurement setup, *i.e.* using a Bragg-Brentano geometry and an automatic slit. In this study, only the reflexes in the angular range of 10 ° to 60 ° are used for analysis, which is possible since graphite is a highly ordered structure. The (001) reflexes of the ternary compounds could be detected in transmission mode under adjusted conditions.[130,152] For both alkali metals the formation of $A^+(diglyme)_yC_n^-$ can be traced (see table 3.3). The values for the reflex positions and the thickness of one intercalant layer are in good agreement with the data from other research groups which prepared the compounds via a chemical route.[126–128] The reflex with the highest intensity is found to be the *(00 n+2)* reflex for both alkali metals, which is in accordance with the theoretical background described in section 2.1.

Noticeable is the expansion of the interlayer distance of graphite (i.e. the repeat distance at stage 1), which is around 230 % for the lithium-diglyme solvent complex, and around 250 % for the sodium-diglyme solvent complex. The differences in the thickness of one intercalant layer are around 6.4 % when the central ion of the alkali-glyme complex is exchanged (from 7.8 Å for the lithium ion to 8.3 Å for the sodium ion) and around 95.4 % when the ternary GICs is formed instead of the binary one (from 0.36 Å for LiC_6 to 7.8 Å). These high values are not intuitive, since it is usually assumed that such high expansion of the interlayer distance may lead to exfoliation of graphite and therefore to the structural decomposition of the electrode material.[53,110,151] Hence, the good cycle stability, especially of the Na^+/2G and graphite electrodes is unexpected. One possible explanation may be a stabilizing effect of the positively charged complex towards the negatively charge graphite planes.

Table 3.3: Reflex positions and interlayer distances of electrochemically prepared ***t***-alkali-2G-GICs at stage 1 determined with X-ray diffraction.

sample	scattering angle / 2θ	repeat distance I_c / Å	intercalant layer thickness Δd / Å
graphite	26.5	3.36 (-)	-
	54.5	3.36 (-)	-
$Li^+(2G)_yC_n^-$	15.8	11.2 (233.3 %)	7.8
	23.8	11.2 (233.3 %)	7.8
	31.9	11.2 (233.3 %)	7.8
	40.2	11.2 (233.3 %)	7.8
	48.7	11.2 (233.3 %)	7.8
	57.6	11.2 (233.3 %)	7.8
$Na^+(2G)_yC_n^-$	15.1	11.7 (248.2 %)	8.3
	22.9	11.7 (248.2 %)	8.3
	30.7	11.7 (248.2 %)	8.3
	38.6	11.7 (248.2 %)	8.3
	46.7	11.7 (248.2 %)	8.3
	55.0	11.7 (248.2 %)	8.3

Stability of *t*-alkali-GICs

Since GICs can be reactive side reactions with the electrolyte may occur. To study the stability of the ***t***-alkali-2G-GICs open circuit voltage (OCV) and X-ray diffraction measurements were conducted (figures 3.7 and 7.8) to test the stability of these compounds toward self-discharge and their shelf life.[3]

Figure 3.7a shows the evolution of the OCV after cells were galvanostatically discharged to 0.01 V *vs.* A^+/A. To avoid analysing irreversible processes, occurring in the first cycles, the third discharge/charge cycle was analysed. For the lithium-based system the OCV increases up to >0.5 V within the first two hours. Afterwards the voltage subsequently increases up to 0.67 V within 48 hours. For the sodium cells the

[3] The experimental data and figures were published in *Physical Chemistry Chemical Physics*. Reproduced from Ref. [2] with permission from the PCCP Owner Societies.

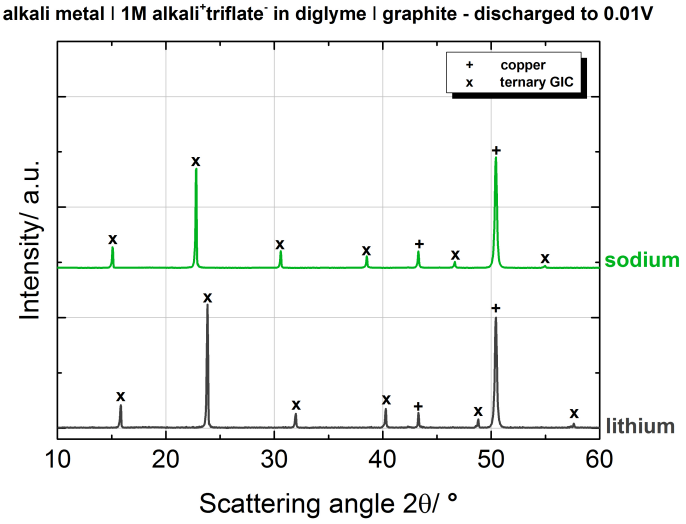

Figure 3.6: X-ray diffraction patterns of graphite electrodes in lithium and sodium half cells in a diglyme based electrolyte.

increase in voltage is less pronounced, reaching 0.04 V within two hours and 0.08 V after 48 hours. In both cases, equilibrium is not reached, as the OCV still continuously rises after 48 hours. After measuring for 48 hours the cells were charged (*i.e.* delithiated/desodiated) up to 1.6 V (lithium cell)/ 1.2 V (sodium cell) and the OCV was measured for another 48 hours in the following. For both alkali metals within half of an hour the OCVs decrease to defined voltages and afterwards remain stable (U_{Li}=1.30 V, U_{Na}=1.07 V). To interpret this behaviour the differential capacities of the galvanostatic cycling of the half cells were analysed (figure 3.7b). From these it can be seen that the electrochemical activity during *de*-intercalation reaction is starting around 1.25 V vs. Li^+/Li and around 1.06 V vs. Na^+/Na (marked as red rectangles). These values fit well to the OCVs reached after 48 hours. Therefore it can be concluded that the electrodes are in equilibrium and are not degrading. The redox activity for the co-intercalation starts around 0.70 V vs. Li^+/Li and around

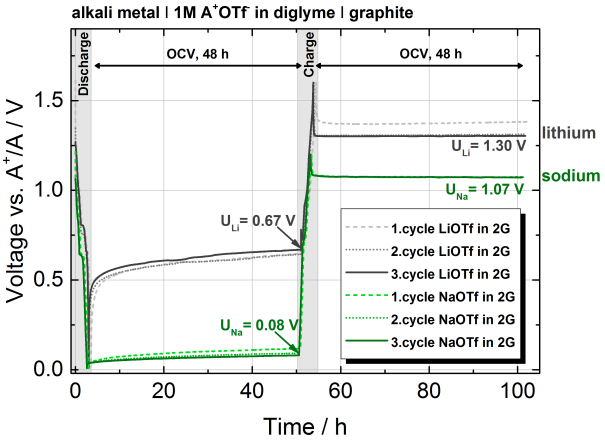

(a) OCV evolution

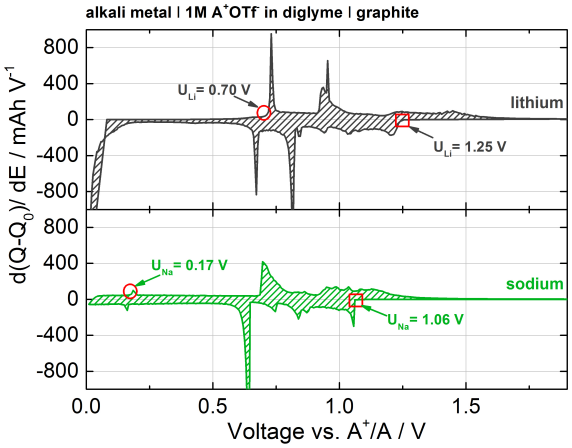

(b) Differential capacities

Figure 3.7: Experimental data about the self-discharge of *t*-2G-GICs prepared by electrochemically driven co-intercalation of diglyme and lithium or sodium ions into graphite electrodes. (a) Open circuit voltage after discharge after three cycles, (b) differential capacity plot in the 3^{rd} cycle of the cells shown in (a).

0.17 V vs. Na^+/Na (marked as red circles). These values are in good accordance with the OCV values measured after the 48 hours. A clear indication for side reactions would also become apparent when comparing coulombic efficiencies for cells cycled with and without the OCV measurements. Without OCV measurements, coulombic efficiencies in the third cycle are typically around 97 % (Na) and 96 % (Li). With OCV measurements we found 97.9 % (Na) and 92.7 % (Li). Overall, the measurements indicate a sufficient stability in the case of sodium whereas slight indications for side reactions are found for lithium.

The structural stability (or shelf life) of the ***t***-2G-GICs was tested by X-ray diffraction. Thereto, lithiated/sodiated graphite electrodes were removed from the coin cells and diffraction patterns were taken immediately and after storing them for four weeks in empty coin cells without electronic contacts under argon atmosphere. The comparison between the diffraction patterns shows no sign of structural degradation for both alkali metals (figure 7.8).

3.4 Preliminary summary

In summary, in the last three sections a *proof-of-principle* of the co-intercalation model was demonstrated that was proposed in section 2.3. We demonstrated that graphite, in contrast to the general view, can be activated as intercalation host for sodium-ion batteries by forming ternary graphite intercalation compounds instead of binary ones. The electrolyte solvent participates in the electrode reaction and can be reversibly co-intercalated into the graphite structure. The important features of this co-intercalation reaction for sodium are small irreversible charge losses, low overpotentials and a superior cycle life. The exceptional stability might simply be related to the fact that ***b***-GICs between sodium and graphite do not form. Additionally it was shown that the ternary compounds of diglyme, sodium and graphite exhibit sufficient stabilities against self-discharge and structural decomposition (shelf life). In summary, these results suggest an alternative route to search for new electrode reactions for sodium-ion batteries.

3.5 Other co-intercalating ethers

After successfully proving the principles of the co-intercalation model proposed in section 2.3, in this section the transfer of this concept is tested and described for other, coordinating ethers.[4] The effect of different chain lengths of the linear ether (glyme) is tested to make a statement about coordination effects that may affect the co-intercalation process (*e.g.* chelate effect, macrocyclic effect, denticity; subsection 3.5.1). Furthermore, the steric hindrance for co-intercalation is increased by using linear ethers containing side groups (subsection 3.5.2). Overall, the focus will be on the electrochemical properties of the above mention systems, concentrating on galvanostatic cycling, cyclic voltammetry and X-ray diffraction of the co-intercalated graphite electrodes.

3.5.1 Linear ethers with different ether chain lengths

After showing that the co-intercalation of sodium ions into graphite alongside with their diglyme-based solvation shell is highly reversible it worth to study the electrochemical properties of other glymes as electrolyte solvents as well. As glymes solvents of the chemical group of the *ethylene glycol dimethyl ethers* are denoted (appendix table 7.1, figure 3.8). To study the effect of the length of the ether chain (i.e. the effect of more or fewer ether oxygen atoms acting as alkali ion coordinating species) monoglyme (1G), diglyme (2G), triglyme (3G) and tetraglyme (4G) were chosen as electrolyte solvents. The basic structural composition of the glymes is:

$$\mathbf{CH_3\text{-}(O\text{-}CH_2)_n\text{-}O\text{-}CH_3} \text{ with n=1,2,3,4}$$

The donor numbers according to Gutmann[5] of glymes are in the range of 14.0 - 24.0 (1G: 24.0, 2G: 19.2, 3G: 14.0, 4G: 16.6) and are within the range of conventionally

[4] The experimental data and figures were published in *Physical Chemistry Chemical Physics*. Reproduced from Ref. [2] with permission from the PCCP Owner Societies.

[5] The Gutmann donor number is a quantitative measure of the strength of solvents as Lewis bases, *i.e.* as electron pair donors. It is defined as the negative enthalpy value ($^{kcal}/_{mol}$) for the 1:1 adduct formation between the solvent and the standard Lewis acid $SbCl_5$.[160]

(a) monoglyme (b) diglyme (c) triglyme (d) tetraglyme

Figure 3.8: Ball-stick models of the different glymes (*ethylene glycol dimethyl ethers*) tested in this subsection. *Blue balls:* carbon atoms, *red balls:* oxygen atoms and *white balls:* hydrogen atoms.

used carbonate solvents (EC: 16.4 and DMC: 15.1).[86,160,161] For the better evaluation of coordination effects, analogous measurements of all corresponding lithium systems were conducted.

Cycle stability, reversibility and voltage characteristics of *t*-alkali-glyme-GICs

The specific capacities of the co-intercalation or lithiation/sodiation step of graphite electrodes in lithium and sodium half cells using glyme based electrolytes are shown in figure 3.9. The reversible formation of ***t***-GICs takes place in all cases.

The reversible capacities for all alkali/glyme systems are in the range between 55 $^{mAh}/_{g}$ - 100 $^{mAh}/_{g}$. Thereby, the sodium based systems outperform the lithium based systems significantly, with respect to capacity retention. For both alkali ions the electrode reactions based on diglyme co-intercalation do show the highest capacities and the best capacity retention. Noticeably different is the performance of triglyme in the sodium based cells. For this combination lower capacities of around 50 $^{mAh}/_{g}$ - 60 $^{mAh}/_{g}$ were obtained, compared to 84 $^{mAh}/_{g}$ - 100 $^{mAh}/_{g}$ for monoglyme, diglyme and tetraglyme. For the lithium half cells tetraglyme exhibits the lowest reversible capacities of around 60 $^{mAh}/_{g}$, while triglyme shows a degrading perfor-

mance. The specific capacities and the coulombic efficiencies in the 50^{th} cycle and the irreversible capacity in the first cycle of all combinations of glymes and alkali ions are listed in table 3.4.

The voltage characteristics of all alkali/glyme cells in the 50th cycle are shown in figure 3.10. All sodium-based systems show overall lower internal resistances compared to the lithium-based systems. Apart from the combinations of Li/1G and Li/3G no side reactions, which might be related to electrolyte composition, are seen within the first 50 cycles. For the sodium based cells, 3G again is exhibiting a distinctively different behaviour compared to the other glyme/sodium combinations.

Taking a closer look at the data listed in table 3.4, it can be seen that the sodium-based cells show a throughout better electrochemical cycling performance compared to the lithium cells. The highest coulombic efficiencies were measured for the combinations of Na/1G and Na/2G (>99.6 %), while Na/3G and Na/4G do show minor side reactions (coulombic efficiencies of about 100.1 % - 100.5 %). The efficiencies for Li/1G, Li/2G and Li/4G are somewhat lower with values of >98.0 %. Due to side reactions, the efficiency for Li/3G is much lower (86.0 %). The irreversible losses are mainly limited to the first cycle (appendix figures 7.9, 7.10, 7.11 and 7.12) and are on the average lower for the sodium systems (10 $^{mAh}/_{g}$ - 30 $^{mAh}/_{g}$) than for the lithium systems (20 $^{mAh}/_{g}$ - 60 $^{mAh}/_{g}$).

The specific capacities upon lithiation/sodiation in the different glymes, when different constant currents were applied, are shown in figure 3.11. Apart from 4G, the sodium-based systems show only slightly lower capacities when higher discharge currents are applied and good kinetic properties of the electrode reaction in Na-glyme systems can be concluded. For 4G slowly increasing capacities can be found, which are mostly likely linked to the higher viscosity of this solvent when compared to the shorter glymes (appendix table 7.1). All lithium based cells deliver very low or almost no reversible capacities at higher currents. After the application of higher currents the return to lower currents does not lead to a recovery of the reversible capacities, indicating an irreversible damage of the electrode material at higher current (appendix figures 7.9 and 7.10). For the sodium systems no such degradation can be

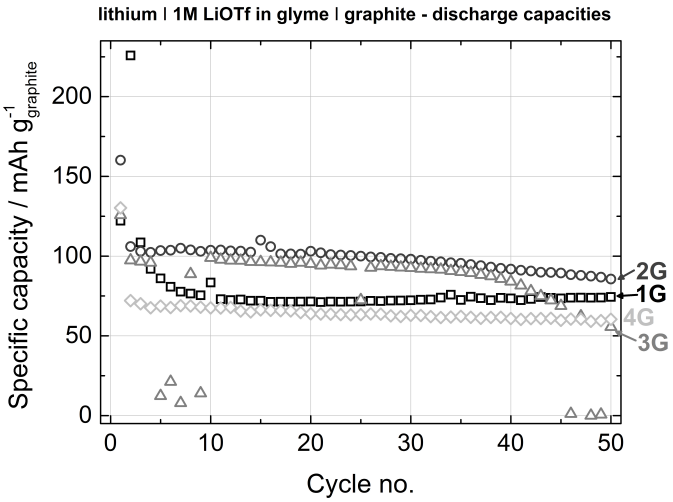

(a) lithium half cells

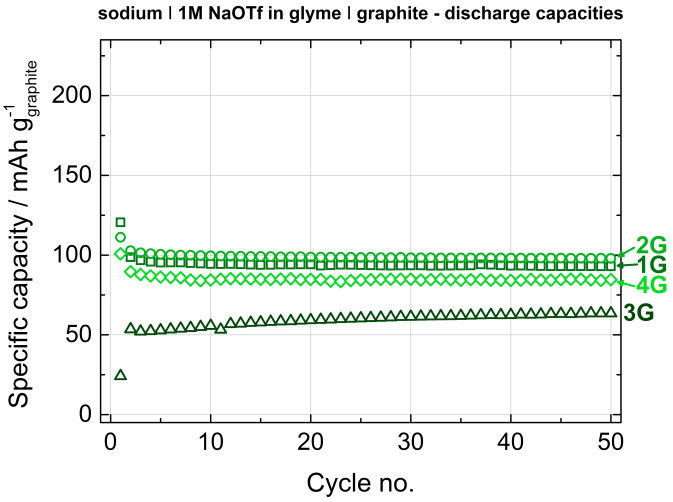

(b) sodium half cells

Figure 3.9: Specific capacities per cycle of graphite electrodes in (a) lithium and (b) sodium half cells in glyme based electrolytes.

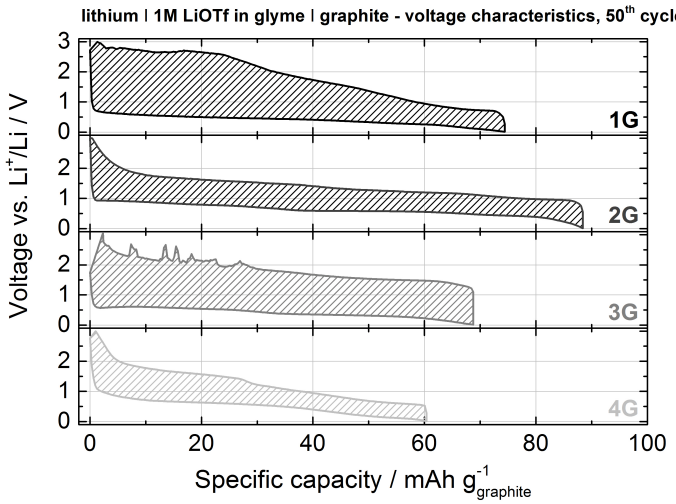

(a) lithium half cells

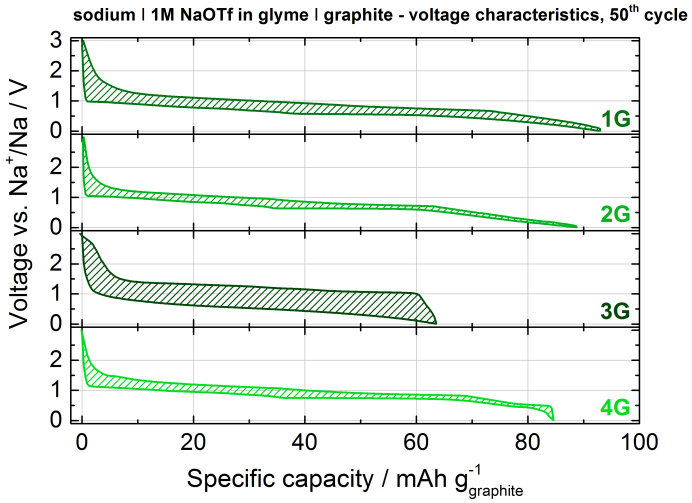

(b) sodium half cells

Figure 3.10: Voltage characteristics of graphite electrodes in lithium and sodium half cells in a diglyme based electrolytes in the 50^{th} cycle.

Table 3.4: List of the specific capacities of the co-intercalation and *de*-co-intercalation steps, coulombic efficiencies in different glyme-based cells for sodium and lithium systems in the 50^{th} cycle and irreversible capacities in the first cycle.

System	Co-intercalation capacity 50^{th} cycle/$\frac{mAh}{g}$	*De*-co-intercalation capacity 50^{th} cycle/$\frac{mAh}{g}$	Coulombic efficiency 50^{th}cycle/%	Irrev. capacity 1^{st} cycle/$\frac{mAh}{g}$
Li/1G	74.4	73.1	98.2	23.2
Li/2G	85.6	85.5	99.8	62.7
Li/3G	55.6	47.8	86.0	30.8
Li/4G	60.4	59.4	98.3	64.0
Na/1G	93.0	92.7	99.8	28.0
Na/2G	98.0	97.6	99.6	13.4
Na/3G	63.5	63.9	100.5	-26.7
Na/4G	84.6	84.7	100.1	14.2

determined; after cycling at a current of 372 $^{mA}/_{g}$ the original reversible capacities can be obtained (appendix figures 7.11 and 7.12).

In summary, when graphite electrodes are cycled galvanostatically against an alkali metal electrode in different glyme based electrolytes, the overall electrochemical performance is best when 2G is used, closely followed by 1G and 4G. For both, lithium and sodium, 3G shows the weakest performance and lowest efficiency. The performance of the sodium cells is significantly more stable in all glymes than for analogue lithium cells.

Cyclic voltammetry of *t*-alkali-glyme-GICs

Cyclic voltammetry was used to study the electrode reactions in more detail. The results are summarized in figure 3.12 for the lithium cells, in figure 3.13 for the sodium cells. For each alkali-glyme system the current response in the first and 20^{th} cycle are shown. From these results some general conclusions can be drawn:

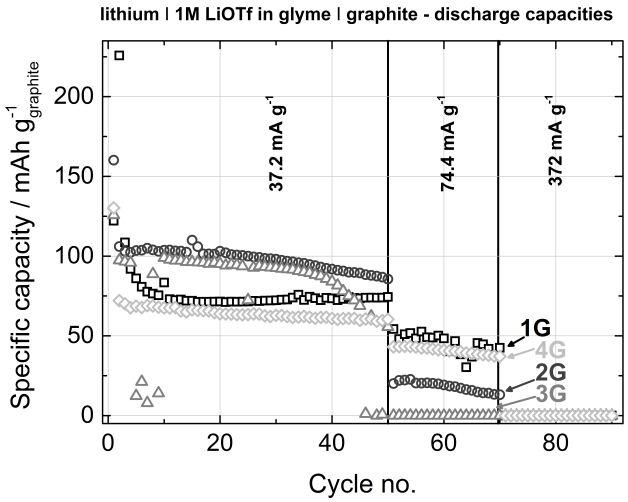

(a) lithium half cells

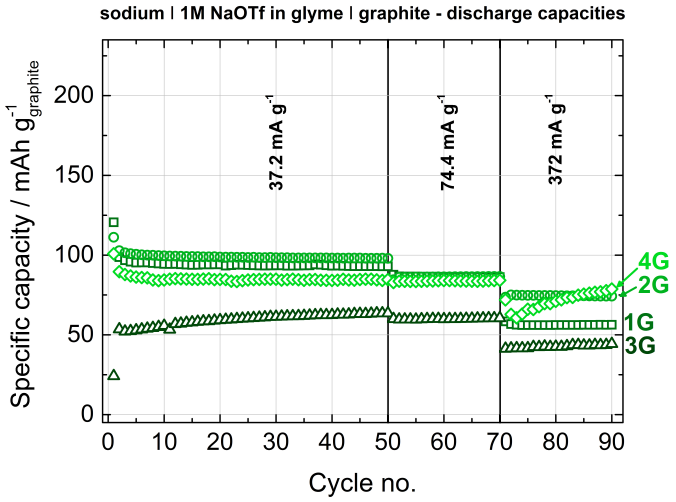

(b) sodium half cells

Figure 3.11: Specific capacities at different constant currents of graphite electrodes in (a) lithium and (b) sodium half cells in glyme based electrolytes.

- The general pattern of the voltammograms in the first cycle is similar for all systems, except for Na/3G. Several maxima can be determined and indicate a complex, staged charge storage mechanism. The voltammogram of Na/3G in contrast is less well-defined (which is in line with the findings made by galvanostatic cycling measurements, figure 3.10b). The different pattern for Na/3G might be related to a geometrically unfavourable coordination of the sodium ions by the 3G solvent molecules, resulting in a steric hindrance which leads to higher internal resistances and poorly defined redox potentials. Taking the preferred coordination numbers of Li^+ and Na^+ in solution (CN = 4 - 7) the cation-glyme complexes listed in table 3.5 are plausible.[90,149,162–164] From this, due to their similarity to crown ether complexes, the combinations of Li/3G and Na/4G should be favourable. Furthermore, the combinations of Li/1G, Li/2G, Na/1G and Na/2G might enable complexation in a similar way, offering 2 or 3 oxygen atoms per glyme molecule. Triglyme offers four oxygen atoms for coordination, therefore it is likely that it forms less "ideal" complexes with sodium ions, which prefers due to its size, a coordination number >4. To reach higher coordination numbers a second triglyme molecule would be necessary. The second molecule, however, is too long, *i.e.* offers more ether oxygen atoms than necessary, and the non-coordinating parts of this second molecule are likely causing steric hindrance during co-intercalation. Hence, for Na/3G a peculiar current response in the CVs can be observed. Despite this effect, the Na/3G system is also highly reversible. For the combination of Li/4G the same argument of steric hindrance might be applied.

- The peak current densities of all lithium system are higher and do show poorer cycle stability compared the analogue sodium systems. This is supported by the results from galvanostatic measurements where lithium-glyme combinations do show high irreversible capacities decay at higher discharge/charge currents. Since there is no indication for impurities, the most likely reason for the poorer cycle life is that the solvation shell is stripped off at the electrode surface or

inside the electrode, leading to degradation of the graphite. The smaller ionic radius of lithium compared to sodium might lead to less stable complexes with glyme molecules. Additionally, there is a thermodynamic driving force to form ***b***-GICs, which do not exist for sodium ions. So at potentials close to 0 V *vs.* Li^+/Li the formation of ***t***-GICs competes with the formation of ***b***-GICs.

Table 3.5: Possible cation-glyme-complexes based on the preferred coordination numbers of the alkali ions in solution and the complexation of these ions by crown ethers.[90,149,162–164]

Solvent	**Oxygen atoms per molecule**	Glyme molecules per Li^+	Coordination no.
1G	**2**	2	4
2G	**3**	2	6
3G	**4**	1 ([12]crown-4-like)	4
4G	**5**	1	5
Solvent	**Oxygen atoms per molecule**	Glyme molecules per Na^+	Coordination no.
1G	**2**	3	6
2G	**3**	2	6
3G	**4**	1-2	4-6
4G	**5**	1 ([15]crown-5-like)	5

Comparing the co-intercalation potentials of the different alkali-glyme systems it is obvious that the redox potential is a function of the glyme length. For better comparison the first cycles from figures 3.12 and 3.13 are replotted in figures 3.14a/b and 3.15a/b. Figures 3.14c and 3.15c show the main redox potentials of the co-intercalation and *de*-co-intercalation plotted against the electrolyte solvent. From this representation it can be clearly seen that the redox potentials are functions of the glyme length for both alkali ions.

The lithium based cells show a steady increase of the co-intercalation potential

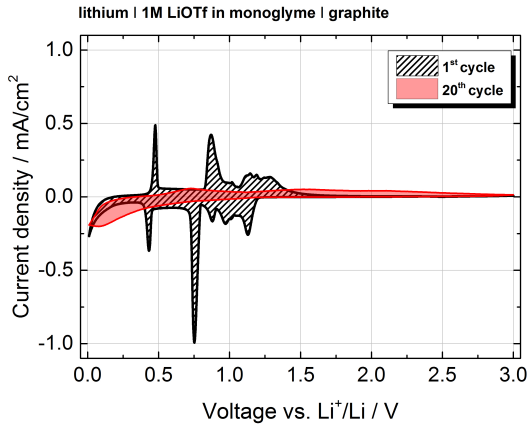

(a) Li/1G

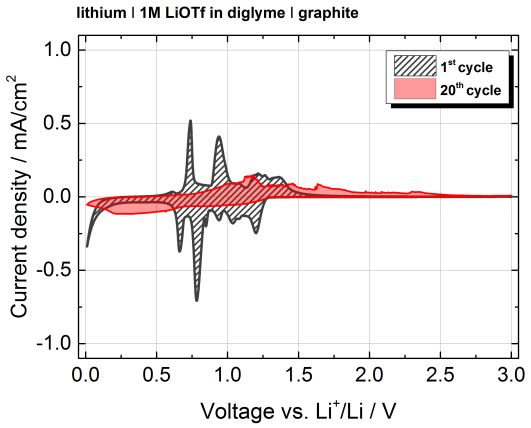

(b) Li/2G

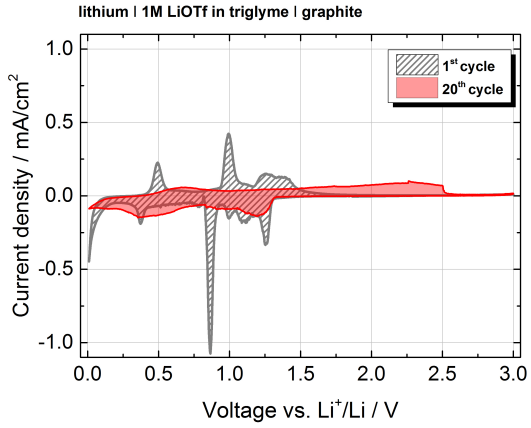

(c) Li/3G

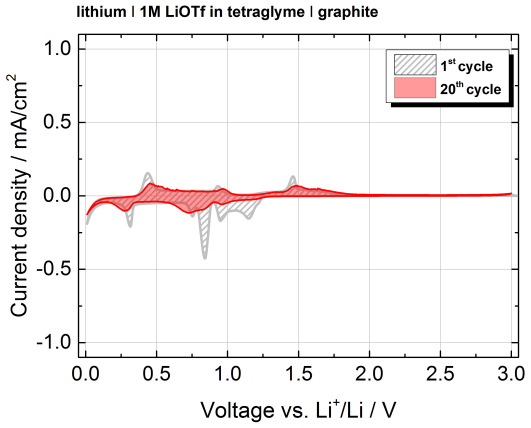

(d) Li/4G

Figure 3.12: Cyclic voltammograms of graphite electrodes in lithium half cells in different glyme based electrolytes in the first and in the 20th cycle.

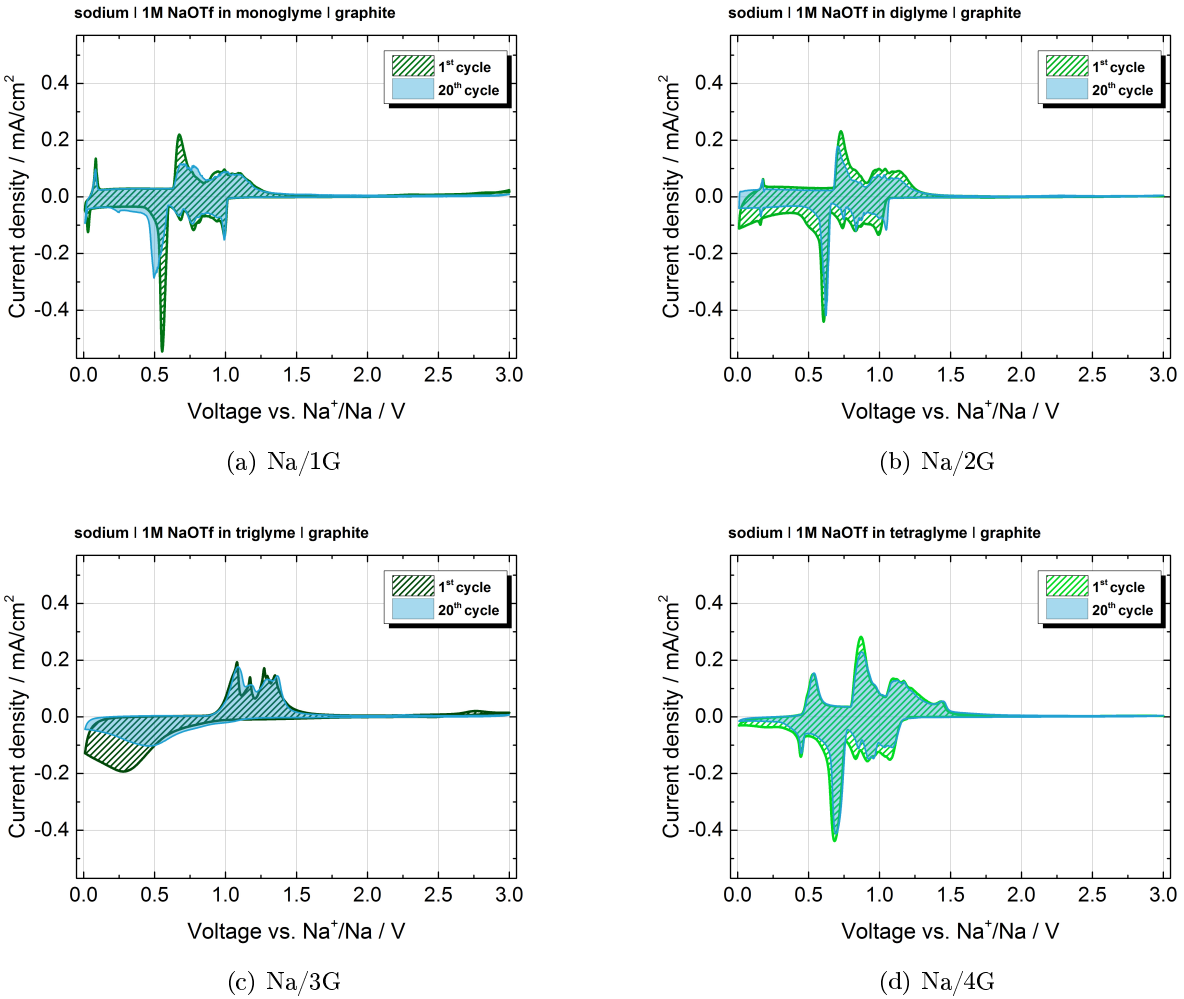

(a) Na/1G

(b) Na/2G

(c) Na/3G

(d) Na/4G

Figure 3.13: Cyclic voltammograms of graphite electrodes in sodium half cells in different glyme based electrolytes in the first and in the 20th cycle.

from $E_{1G} < E_{2G} < E_{3G}$ without any significant change in the intercalation pattern (3.14a/b). For Li/4G the current response is changing slightly, alongside with a much lower insertion potential and a much higher *de*-insertion potential. For the sodium cells a steady increase from $E_{1G} < E_{2G} < E_{4G}$ can be identified, excluding 3G and its peculiar behaviour (3.15a/b). The combination of Na/3G shows, analogue to Li/4G, lower insertion and higher *de*-insertion potentials. In both cases, these changes might be linked to less favourable coordination numbers compared to the other alkali-glyme combinations and will be further analysed. Overall, the co-intercalation potential seems to be dependent of the ether chain length of the co-intercalated glyme solvent ($E_{1G} < E_{2G} < E_{4G}$) and the alkali ion ($E_{Na} < E_{Li}$).

The effect of the ether chain length on the redox potential is even stronger at lower potentials. At low potentials, when large amounts of solvent are co-intercalated to form the higher stages, this indicates strong differences in Gibbs energies of the formation at high degrees of sodiation.

Summary: For both electrochemical methods applied to these alkali-glyme systems, 2G is found to exhibit the best electrochemical performance for both alkali ions. The reversibility of the co-intercalation reaction is more stable for the sodium than for the lithium cells. Due to the dependency of the co-intercalation potentials on the ether chain length of the glyme used it may be plausible to tailor the redox potential of the co-intercalation reaction by mixing two or more glymes in a specified ratio.

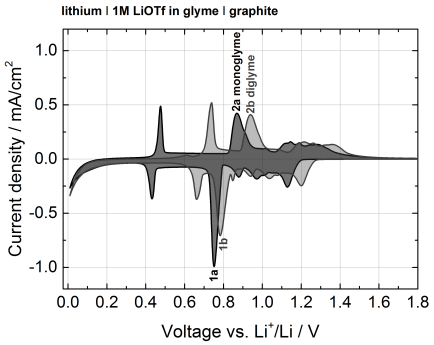

(a) CV data of Li/1G, Li/2G

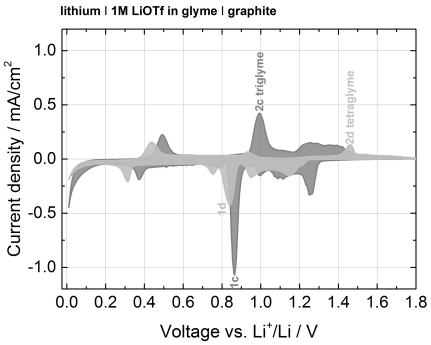

(b) CV data of Li/3G, Li/4G

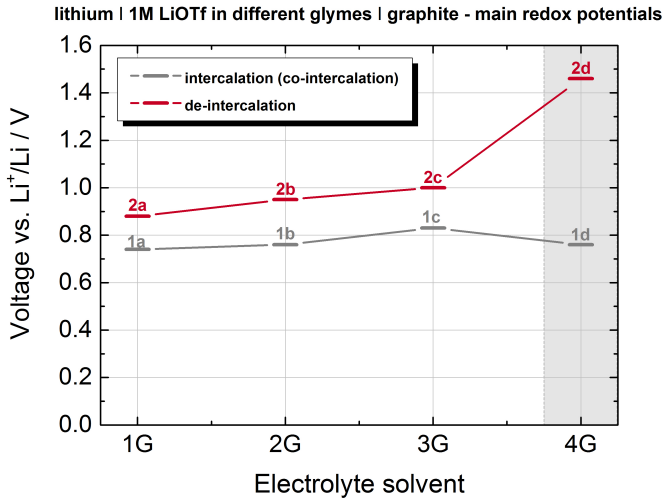

(c) Dependence of the redox potential on the ether chain length in lithium half cells

Figure 3.14: Dependence of the redox potential of the co-intercalation electrode reaction on the glyme length in lithium half cells. Cyclic voltammetry data of the first cycle of (a) 1 G, 2 G and (b) 3 G, 4 G; data replotted from figure 3.12. (c) Dependence of the main co-intercalation potential on the glyme length of the electrolyte solvent. The respective potentials are marked in (a)/(b).

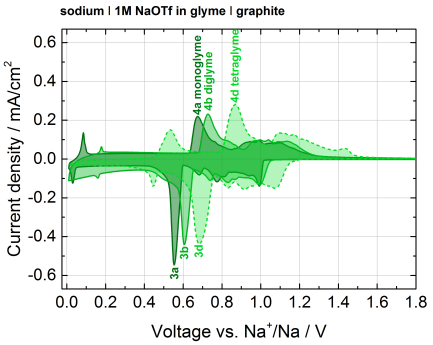

(a) CV data of Na/1G, Na/2G, Na/2G

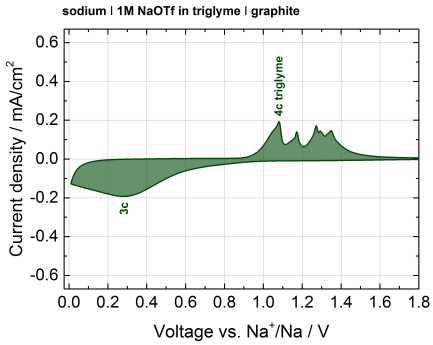

(b) CV data of Na/3G

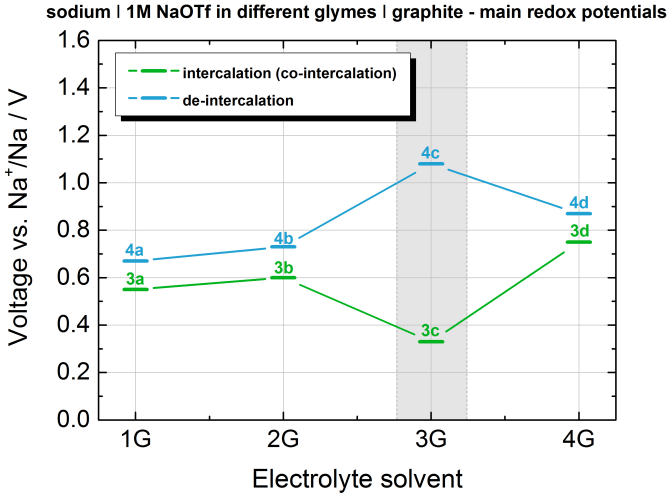

(c) Dependence of the redox potential on the ether chain length in sodium half cells

Figure 3.15: Dependence of the redox potential of the co-intercalation electrode reaction on the glyme length in sodium half cells. Cyclic voltammetry data of the first cycle of (a) 1 G, 2 G, 4 G and (b) 3 G; data replotted from figure 3.13. (c) Dependence of the main co-intercalation potential on the glyme length of the electrolyte solvent. The respective potentials are marked in (a)/(b).

X-ray analysis of *t*-alkali-glyme-GICs

To prove that co-intercalation of the alkali-glyme complexes into the graphite electrode did occur, X-ray diffraction in an angular range between 10 ° to 60 ° was conducted (appendix figure 7.13 survey and figure 3.16 detail diffraction pattern). For all combinations of alkali ions and glymes a significant shift of the (002)-diffraction line to lower scattering angles was measured. For the lithium systems an average shift of $2\theta = 2.7\,°$, for the sodium systems of $2\theta = 3.7\,°$ was determined. Additionally, a series of reflexes occurs for all systems. Their origin is described in detail in section 2.1 and was described for the LiC_6 formation before.[51,53,96,116,119]

From the diffraction patterns it becomes apparent that the solvation shell (*i.e.* in this case the glyme length) only has a minor influence on the expansion in interlayer distance. The expansion of the interlayer distance of graphite, *i.e.* the repeat distances at stage 1, is around 230 % - 236 % for the different lithium-glyme solvent complexes, and around 248 % - 254 % for the different sodium-glyme solvent complexes. The thickness of one intercalant layer Δd differs between 7.7 Å–7.9 Å for the lithium based cells leading to overall repeat distances I_c of 11.1 Å–11.3 Å. For the sodium based cells it differs around 8.3 Å–8.5 Å leading to repeat distances of 11.7 Å–11.9 Å. The average repeat distances of the fully lithiated/sodiated *t*-alkali-glyme-GIC are summarized in table 3.6; a more detailed analysis can be found in the appendix in tables 7.2 and 7.3.

Studying the shift of the main diffraction line in more detail, minor differences between the different glyme chain lengths can be determined (figure 3.16). For the Li/glyme co-intercalation, the shift of the diffraction lines is in 0.07 ° steps from 2G > 3G > 4G; from 1G to 2G it is around 0.25 °. The higher offset between 1G and 2G might be explained by different coordination numbers (which are mostly likely CN = 4 for 1G and CN = 6 for 2G) or the higher volatility of 1G (appendix 7.1). For the sodium-based systems a gradual increase in interlayer spacing can be determined, in around 0.05 ° steps from 1G > 2G > 4G (figure 3.16b). Just like for the electrochemical characterization methods Na/3G takes a special position within

the glyme series. The change in interlayer distance for the co-intercalation of Na/3G is smaller than for the rest of the glymes (compare Na/1G: 3.65 ° > Na/3G: 3.55 °). The difference might be explained again by a different coordination number for 3G. If two 3G molecules do coordinate a sodium ion not all available ether oxygen atoms within the 3G chain are able to coordinate with the ion. This may result, in contrast to 1G, 2G and 4G, in a less "ideal" geometrical alignment. While for 1G, 2G and 4G an almost spherical solvation sphere can be assumed, it is not possible in the same way for Na/3G; leading to a nearly spherical shell with non-coordinating side groups sticking out. In summary, the increase in repeat distance (interlayer distance) is >200 % during the formation of ***t***-alkali-glyme-GICs, which is remarkable considering the excellent reversibility of the electrode reactions, especially for the sodium cells.

Table 3.6: Reflex positions and interlayer distances of electrochemically prepared ***t***-alkali-glyme-GICs at stage 1 determined with X-ray diffraction.

sample	repeat distance I_c /Å(increase in %)	intercalant thickness Δd /Å
graphite	3.36 (-)	-
$Li^+(1G)_yC_n^-$	11.1 (230 %)	7.7
$Li^+(2G)_yC_n^-$	11.2 (233 %)	7.8
$Li^+(3G)_yC_n^-$	11.3 (236 %)	7.9
$Li^+(4G)_yC_n^-$	11.3 (236 %)	7.9
$Na^+(1G)_yC_n^-$	11.7 (248 %)	8.3
$Na^+(2G)_yC_n^-$	11.7 (248 %)	8.3
$Na^+(3G)_yC_n^-$	11.6 (245 %)	8.2
$Na^+(4G)_yC_n^-$	11.9 (254 %)	8.5

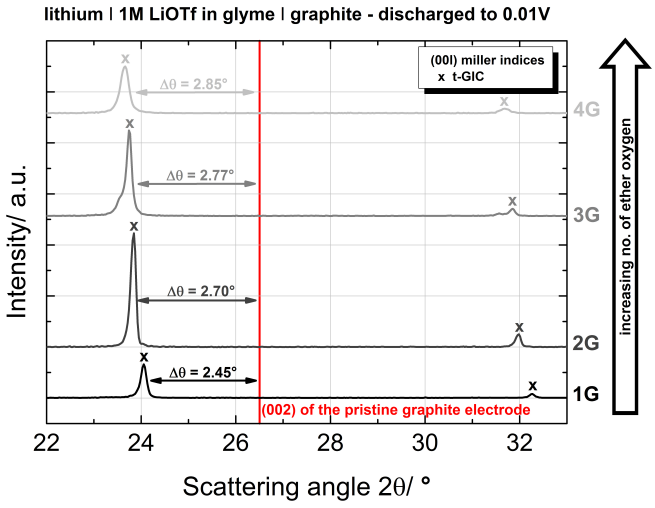

(a) lithium half cells

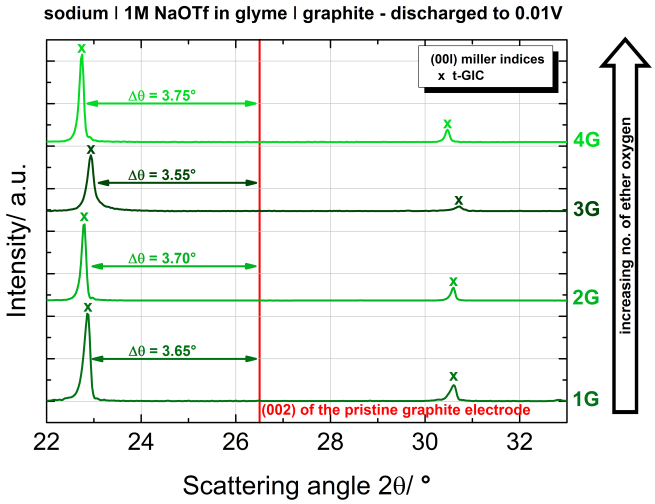

(b) sodium half cells

Figure 3.16: X-ray diffraction patterns of graphite electrodes in (a) lithium and (b) sodium half cells after full lithiation/ sodiation using different glymes.

Effect of the glyme mixtures on the co-intercalation reaction

As already discussed in the former subsections, cells based on Na/3G behave very differently from sodium half cells which contain 1G, 2G or 4G as electrolyte solvent. Mostly likely, an unfavourable complexation of the sodium ions by the 3G molecules is the reason for that specific behaviour. The mixing of glymes with different chain length should lead to a competition between the different glymes for forming ion-solvent complexes. This competition should affect therefore the redox behaviour of the electrode materials. To test this hypothesis, an electrolyte consisting of a 1:1 mixture of 1G and 3G was prepared; *i.e.* containing equal numbers of 1G and 3G molecules. Thereby, both glymes will act as chelate ligands, where 3G will act as an tetradentate ligand and 1G as a bidentate ligand. From this it might be assumed that if one sodium ion is complexed by one of each glyme molecules a six-fold coordination sphere would be achieved.

The specific capacities obtained at different discharge/charge currents of electrolytes based on 1G, 3G or the mixture of 1G/3G are shown in figure 3.18a alongside with the corresponding voltage profiles in the 50^{th} cycle (figure 3.18b). The differential capacities calculated out of the galvanostatic cyclic data are shown in the appendix in figure 7.14. The electrochemical performance of the mixture is similar to that of 3G. The most probable explanation for this similarity would be that the sodium ions are preferentially coordinated by 3G molecules which leads to a preferred co-intercalation of those complexes. This preference would be in accordance with the thermodynamically driven *chelate effect* or the kinetically driven *macrocyclic effect*. These are described in literature for a variety of ligands, but so far not for sodium-glyme complexes:[148]

- According to Holleman *et al.* the *chelate effect* describes the enhanced affinity of chelating molecules for a metal ion compared to the affinity of a collection of similar monodentate (non-chelating) molecules for the same metal ion.[148] It can be thermodynamically described by the standard Gibbs free energy $\Delta G^{\ominus}$ and the equilibrium constant K:

$$\Delta G^{\ominus} = -RT \cdot ln(K) = \Delta H^{\ominus} - T\Delta S^{\ominus} \tag{3.4}$$

With the gas constant R, the temperature T, the standard enthalpy change of the reaction $\Delta H^{\ominus}$ and the standard entropy change $\Delta S^{\ominus}$.

The larger the equilibrium constant is, the higher the concentration of the complex would be. Since the enthalpy is assumed to be approximatively the same for both complex forming reactions (equation 3.5 and 3.6), the difference in stability constants K is only due to the effects of entropy. In equation 3.5 three particles on the left side of the reaction are combined to one complex on the right side. While in equation 3.6 four particles on the left side are combined to one the right side. This means the decrease in entropy is smaller for equation 3.5 than for equation 3.6, resulting in a higher stability constant for the 3G based sodium complexes.

$$Na^+ + 2 \cdot (3G) \rightleftharpoons [Na(3G)_2]^+ \tag{3.5}$$

$$Na^+ + 3 \cdot (1G) \rightleftharpoons [Na(1G)_3]^+ \tag{3.6}$$

- Kinetically the chelate effect can be explained according to Schwarzenbach.[148] At similar concentrations of chelating molecules of different denticities the probability to form the complex with the molecules with the higher denticity is higher, since the velocity of the occupation of the second and all higher coordination sites for the multidentate solvent molecule is higher than for the monodentate solvent (so-called macrocyclic effect).

However, taking a look at the redox potentials and the results from cyclic voltammetry, especially during charging, differences between the 3G based electrolyte and the mixture of 3G and 1G can be determined (3.17 and figure 3.18b). From the

CV measurements again the current response looks similar to that of the 3G based electrolyte, but with a slightly higher insertion and a slightly lower *de*-insertion voltage. From the described results, it is not easily possible to conclude whether these differences in electrochemical performance are dominated by thermodynamic or kinetic properties. However, it is reasonable to assume that in mixtures of glymes with different chain lengths, different co-intercalation mechanisms compete, leading to new and/or mixed redox potentials. Despite the fact that the effect is small so far, mixing of glymes might be an attractive route to tailor redox behaviour of the co-intercalation based electrode reactions and their kinetics. As a side remark it should be noted that the addition of carbonates into a diglyme based electrolyte does suppress the co-intercalation reaction fully and is therefore no viable option for tailoring the redox behaviour of the graphite electrode.[165]

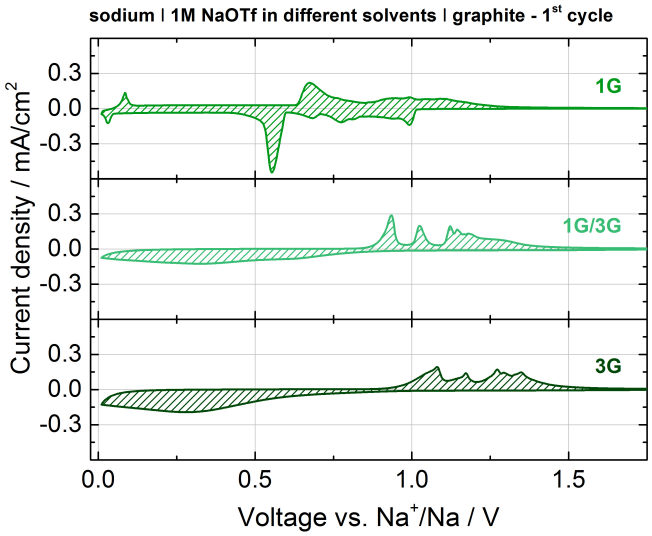

Figure 3.17: Cyclic voltammograms at a scan rate of 0.05 $^{mV}/_{s}$ of graphite electrodes in sodium half cells in monoglyme, triglyme or a a 1:1 mixture of 1G/3G based electrolyte.

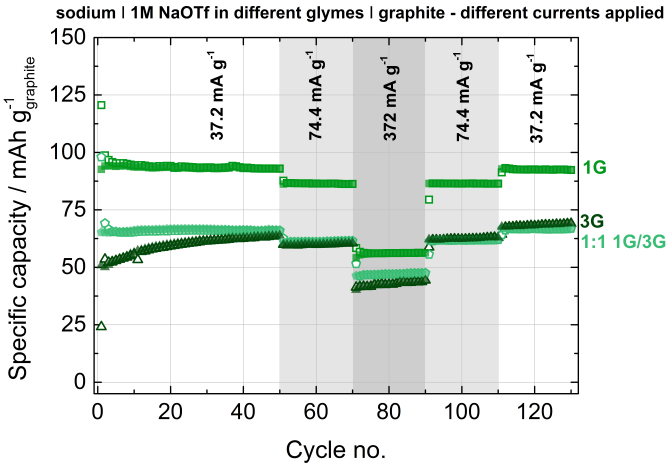

(a) specific capacities

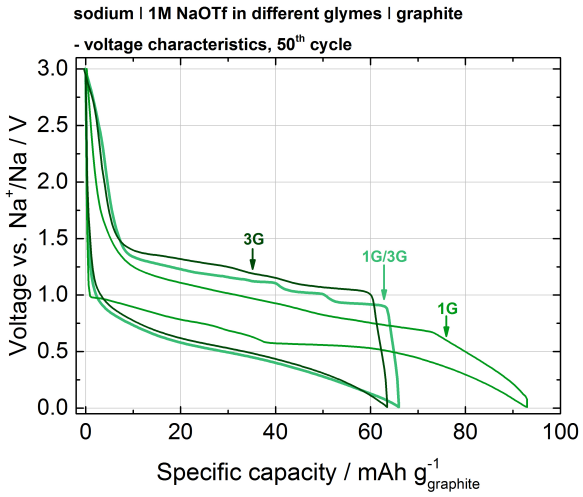

(b) voltage characteristics

Figure 3.18: (a) Specific capacities per cycle and (b) voltage characteristics in the 50^{th} at different applied currents of graphite electrodes in sodium half cells in monoglyme, triglyme or a a 1:1 mixture of 1G/3G based electrolyte.

Effect of a *pre*-formed SEI on the co-intercalation reaction

A well-studied phenomena in LIBs is that the compatibility between graphite electrodes and carbonate based electrolytes is only possible because a solid electrolyte interphase (SEI) is formed during the first lithiation process.[29] The formation of the film is inevitable since the lithiation of graphite is proceeding outside the electrochemical stability window of the carbonate solvents. But, a rather lucky coincidence, this SEI formed by carbonates on a graphite surface is electronically insulating but permeable for lithium ions, ensuring the lithium ion transport into the graphite structure.[53] Additionally, it is considered an important function of this SEI to prevent the co-intercalation of solvent molecules into the graphite lattice; which may lead to exfoliation and structural decomposition. Though, to form ***t***-GICs the co-intercalation of solvent molecules is required. From this observation the question arises: *Does an SEI form in the case of co-intercalation electrodes?*

Taking into account the low overpotentials of the co-intercalation electrode reaction and the large lattice expansion involved, it may be concluded that virtually no SEI is present for these systems. Or that the formed SEI is highly flexible and dynamic, allowing an easy charge transfer between electrolyte and electrode. From this point of view a very detailed surface and impedance analysis, which is beyond the scope of this work, should be conducted.

To give an example the role of the SEI on co-intercalation electrodes, the effect of a *pre*-formed SEI on a graphite electrode surface on the passing of a glyme based solvation shell was studied. To this end, it was tested whether a glyme based solvation shell is able to pass a SEI layer that had been *pre*-formed on the graphite surface under utilization of a carbonate based electrolyte. For this purpose a graphite electrode was discharged (sodiated) to 0.01 V vs. Na^+/Na in a carbonate based electrolyte (a mixture of EC/DMC, w/w% 1:1) to form an SEI-layer on the graphite surface (figure 7.15).[51,53,166] The graphite electrode with the *pre*-formed SEI was then placed into another sodium cell with a diglyme based electrolyte and cycled in the usual way.

As shown in figure 3.19a virtually no electrochemical activity can be determined

within the first two cycles. This most likely means that the solvent co-intercalation is suppressed by the *pre*-formed SEI-layer. After 25 cycles with fluctuating capacity values, the capacities stabilize and high coulombic efficiencies are achieved. A comparison of the voltage profiles after 50 cycles with and without the *pre*-formed SEI is shown in figure 3.19b. The combined overpotentials for both are very small and similar to almost identical. From this it can be assumed that the *pre*-formed SEI starts to crack at some places when the co-intercalation starts. The pronounced increase in volume expansion during co-intercalation subsequently frees more and more of the graphite surface from the passivating SEI layer leaving behind an interphase with a low resistance and clearly supports the idea of a nearly SEI-free surface. However, the above described experiment does not clarify the nature of the SEI in the case of co-intercalation electrode reactions in detail.

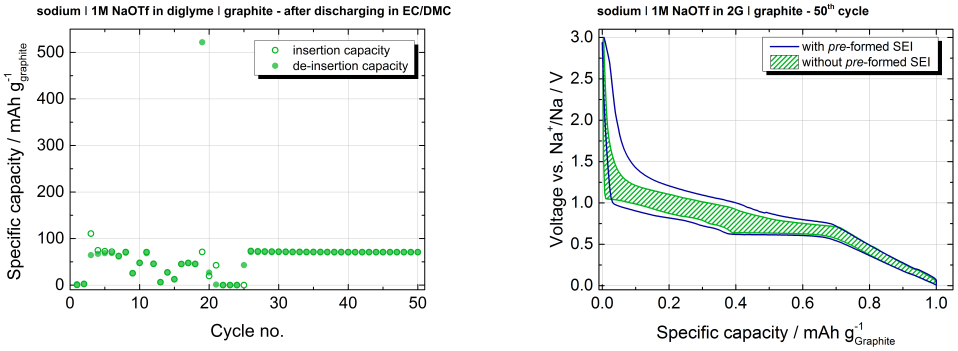

(a) specific capacities (b) voltage characteristics

Figure 3.19: (a) Specific capacities and (b) voltage characteristics of graphite electrodes in sodium half cells with an applied current of 37.2 mA/g. At first the graphite electrode was discharged in a carbonate based electrolyte to form a SEI-layer. (a)/(b) This electrode is then transferred into a sodium cell and cycled with the diglyme based electrolyte.

3.5.2 Ethers with steric hindrance

To further study the influence of the solvation shell on the co-intercalation electrode reaction ethers were purchased and tested which exhibit an increased steric hindrance when alkali-solvent-complexes are formed (figure 3.20, table 3.7). Ethers were chosen which exhibit selected side groups implemented into the linear diglyme base structure (DPGDME and Butyl-2G) or oxygen atoms are replaced by carbon atoms (1,5-DMP); for properties see in the appendix table 7.4. Not from all chosen solvents it was possible to prepare electrolytes (see table 3.8). For example, the dissolution of LiOTf in DPGDME leads to an unintended and unidentified precipitation (appendix figure 7.16). Furthermore, both alkali conductive salts are almost insoluble in 1,5-DMP (table 3.8) or the coordination is to weak; from which it may be concluded that after the absence of the third oxygen atom 1,5-DMP is too non-polar to dissolve the conductive salts to a sufficient amount. From these limitations follows that it was only possible to perform electrochemical characterization measurement on the NaOTF/DPGDME electrolyte and of both combinations of alkali triflate/Butyl-2G.

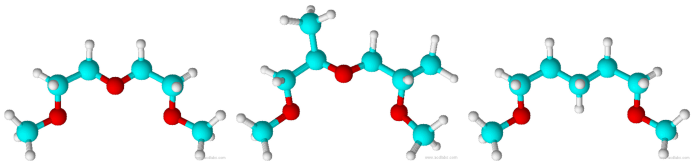

(a) diglyme (b) DPGDME (c) 1,5-DMP

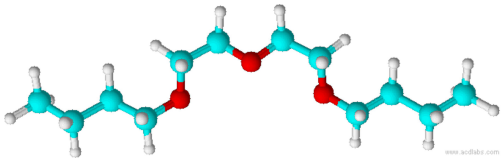

(d) Butyl-2G

Figure 3.20: Ball-stick models of diglyme derivatives studied in this subsection. *Blue balls:* carbon atoms, *red balls:* oxygen atoms and *white balls:* hydrogen atoms.

Table 3.7: Diglyme derivatives: structure names, abbreviations and skeletal formulas. The steric hindrance for solvents co-intercalation was increased by introducing specific side groups into the linear ether chain of diglyme. Physical properties of the solvents are listed in the appendix table 7.4.

Name	Abbr.	Structure
Bis(2-methoxyethyl) ether	2G	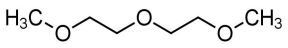
Bis(methoxypropyl) ether	DPGDME	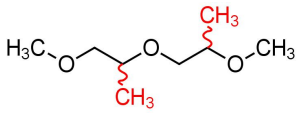
Bis(2-butoxyethyl) ether	Butyl-2G	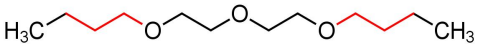
1,5-Dimethoxy pentane	1,5-DMP	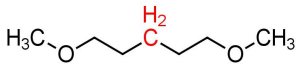

Table 3.8: Prepared electrolytes from the solvents listed in table 3.7. For LiOTf and DPGDME an unexpected precipitation occurred (diffraction pattern in the appendix, figure 7.16). In 1,5-DMP sodium and lithium triflate are almost insoluble, and therefore no electrochemical measurements could be conducted for these systems.

Solvent	LiOTf	NaOTf
DPGDME	Precipitation	1M
Butyl-2G	0.5 M	0.5 M
1,5-DMP	Almost insoluble (<0.2 M)	Almost insoluble (<0.2 M)

In figures 3.21 and 3.22 the results of the electrochemical characterization and the X-ray diffraction for the sodium based electrolytes with DPGDME and Butyl-2G alongside with the results from 2G and 3G are shown.

The specific capacities are summarized in figure 3.21a. The reversible capacities of the diglyme derivatives are around 85 $^{\mathrm{mAh}}/_{\mathrm{g}}$ for Na/DPGDME and around 50 $^{\mathrm{mAh}}/_{\mathrm{g}}$ for Na/Butyl-2G. While the cycling stability is reasonable for both diglyme derivatives, they still lag behind the performance of the glymes. For the DPGDME cells a constant overcharging in every step is determined, which can be linked to undesired side reactions although we do not directly observe electrolyte decomposition. When the discharge/charge currents are increased, especially for Butyl-2G, a distinct decrease in obtainable capacities can be observed; significantly more than for the glymes. This effect might be related to different reasons: (a) the higher viscosity (Butyl-2G[167] 2.3 mm^2/s vs. 2G 1.2 mm^2/s) and/or (b) the increased spatial dimensions of the sodium-Butyl-2G complex. Both may lead to a slower diffusion into the graphite electrode. The irreversible charge losses of Na/DPGDME and Na/Butyl-2G are around 15 $^{\mathrm{mAh}}/_{\mathrm{g}}$, each, and are therefore in the same range as for the glyme-based electrolytes. These losses are most likely linked to side reactions with the surface terminating groups of graphite.

The voltage characteristics in figure 3.21b show an increase of the internal overpotential when non-polar side groups are introduced. The DPGDME solvent shows similar intercalation potentials as 2G, while Butyl-2G resembles more the behaviour of 3G. The same trend can be determined from the results of the cyclic voltammetry shown in figure 3.22a. For DPGDME and 2G similar current responses can be determined, however, the peak currents are a bit lower for DPGDME. This decrease in current might be related to a slower diffusion of the larger ion-solvent complex of DPGDME and Na^+ into the graphite lattice. The voltammogram of Butyl-2G is somewhere in between the pattern for DPGDME and 3G, which might be due to the longer non-polar and therefore not coordinating side groups. The CVs of Butyl-2G and 3G are different upon oxidation, where 3G exhibits sharp current peaks not existent for Butyl-2G. This shift from distinct to broader, less defined voltammograms

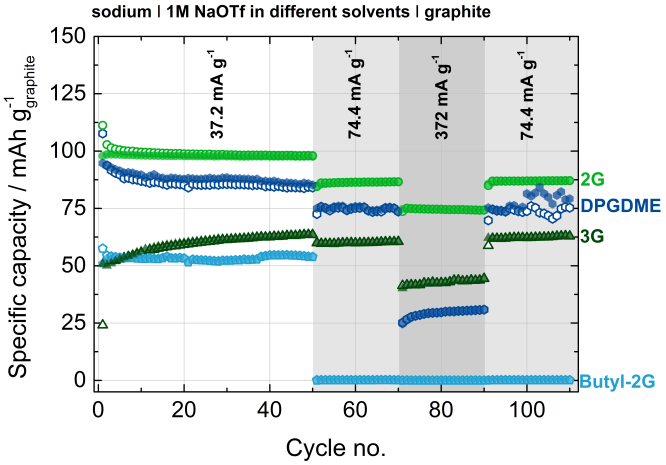

(a) specific capacities

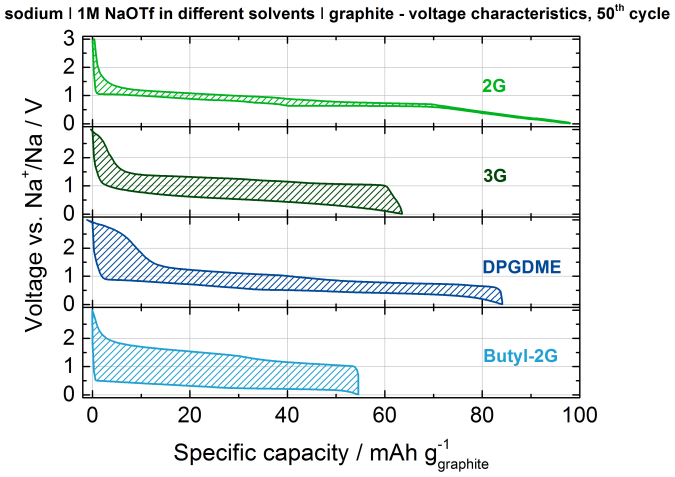

(b) voltage characteristics

Figure 3.21: (a) Specific capacities per cycle at different applied currents and (b) voltage characteristics in the 50^{th} cycle at a constant current of 37.2 $^{mA}/_{g}$ of graphite electrodes in sodium half cells in a diglyme, DPGDME, Butyl-2G or 3G based electrolytes.

from DPGDME to Butyl-2G to 3G is likely related to steric effects. These lead to a "non-ideal" complex formation (*i.e.* less compact complexes) and therefore to slower diffusion of these spatial demanding complexes into graphite. Summing up, the electrochemical characterization of DPGDME and Butyl-2G demonstrates that the introduction of non-polar side groups does not suppress the co-intercalation of solvents with sodium ion into graphite. But, because of the larger size of the ion-solvent complexes, graphite can host fewer sodium ions resulting in lower capacities and poorer C-rate performance.

The X-ray diffraction patterns of the sodiated graphite electrodes prepared by using DPGDME and Butyl-2G based electrolytes are shown in figure 3.22b. While Na/DPGDME exhibits a similar repeat distance of $I_c = 11.7$ Å as Na/2G, Na/Butyl-2G shows a larger distance of $I_c = 11.9$ Å. Overall, the difference between glymes and the diglyme derivatives is quite small.

From the results of the electrochemical characterization and X-ray diffraction it can be concluded that the redox chemistry of the co-intercalation electrode reaction is strongly influenced by the type of solvent that is co-intercalated and hence, by the composition and structure of the solvation shell. This impact can be also be seen for Li/Butyl-2G, where reversible capacities close to zero are measured (appendix figure 7.17). The redox potentials, the kinetics and the degree of insertion of sodium ions is clearly depended on the size of the ion-solvent complex. However, only a minor influence can be determined for the repeat distance of the ***t***-GICs. Most likely, the coulombic interactions between the positively charged ion-solvent complex and the negatively charged graphite layers do dominate the graphite lattice expansion.

Cyclic ethers:

To further test on the boundary conditions of the co-intercalation electrode reaction, tetrahydrofuran (THF) was tested as a cyclic ether as electrolyte solvent and [15]crown-5 as an electrolyte additive (appendix figures 7.18, 7.19 and 7.20). When using THF, the solvation shell is expected to be spatially more demanding than for

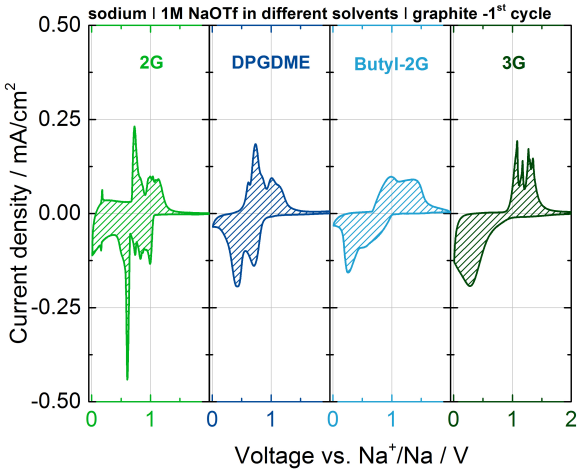

(a) cyclic voltammetry

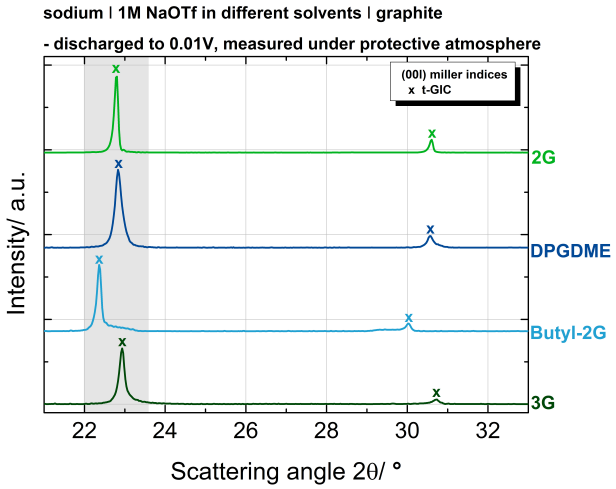

(b) X-ray diffraction patterns

Figure 3.22: (a) Cyclic voltammograms at a scan rate of 0.05 $^{mV}/_{s}$ and (b) X-ray diffraction patterns after full sodiation of graphite electrodes in sodium half cells in a diglyme, DPGDME, Butyl-2G or 3G based electrolytes.

the linear ethers.[119,144,168–170] Nonetheless, co-intercalation does occur for this system, even if it is more difficult and low capacities of around 30 $^{mAh}/_{g}$ after 50 cycles combined with a large voltage hysteresis are achieved.

Due to the chemical similarity to the linear ethers, the circular [15]-crown-5 was used as an additional solvent. This crown ether is known for its strong interaction with sodium ions and is therefore an obvious candidate for co-intercalation electrodes.[90,149] Since it is impossible to dissolve the conductive salt directly within the pure crown ether, 1 mol of the crown ether was added into a solution of 1 M NaOTf in diglyme (1 mol relating to the amount of diglyme, from this follows a salt concentration of the final electrolyte of around 0.8 M). Furthermore, it is assumed that the crown ether complexes are favoured over the diglyme complexes (macrocyclic effect).[148,171] Surprisingly, no electrochemical activity of this electrolyte towards the graphite electrode was measured. Upon cycling only 2 $^{mAh}/_{g}$ of specific capacity were observed. Again, the poorer electrochemical performance in case of the crown ether might be linked to the geometry of the solvation shell, since crown ethers are much more rigid when compared to glymes.

Summary: The introduction of side groups into the linear diglyme structure to selectively increased the steric hindrance of the ion-solvent complex does not prevent any of the systems examined from co-intercalating their solvents into the graphite structure forming ***t***-GICs. While the overall reaction is not suppressed, the steric hindrance leads to increased internal resistances and lower specific capacities. Furthermore, the results for the diglyme derivatives do support the explanation that the peculiar behaviour of 3G is mostly likely due to a non-coordinating side group which leads to an increase of steric hindrance.

3.6 Application in full cells

In a next step the co-intercalation reaction of sodium and diglyme into graphite was used to construct a NIB; *i.e.* a so-called full cell which does not contain any sodium metal but instead a second intercalation material as counter electrode. A crucial boundary condition for the full cell is the compatibility of the intercalation cathode material with the diglyme based electrolyte. To test this compatibility Prof. Shinichi Komaba and his group from *Tokyo University of Science* provided P2-$Na_{2/3}Ni_{1/3}Mn_{2/3}O_2$ (NNMO) as cathode material for the electrochemical characterization in diglyme. The key data of this cathode material is summarized in subsection 3.6.1 alongside with the first results of the electrochemical measurements. The first measurements of sodium-ion full cells based on graphite/diglyme/NNMO are shown in subsection 3.6.2.

3.6.1 Compatibility of Sodium Nickel Manganese Oxide with diglyme

NNMO is a P2-type layered transition metal oxide with a theoretical capacity of 173 $^{mAh}/_{g}$ in which the sodium ions are accommodated at prismatic sites sandwiched between MeO_2 layers, with Me being Ni or Mn.[15,18] The operational voltage is around 3.7 V vs. Na^+/Na based on the redox activity of the Ni^{4+}/Ni^{2+} couple. The practically achievable capacities are fading rapidly during prolonged cycling when charged to voltages $\geq$4.5 V. This is due to a change of the structural motive of the coordination sphere of the sodium ions from prismatic (P2) to octahedral (O3) upon the de-sodiation process. To prevent this fading the voltage needs to be limited to 4.0 V to achieve stable cycling behaviour. However, this limits the reversible capacities to values around 80 $^{mAh}/_{g}$ to 85 $^{mAh}/_{g}$. The synthesis conditions, the structural and electrochemical characterisation of NNMO as electrode material in carbonate based electrolytes has been published elsewhere.[15,18] The circular electrodes (d=1.2 cm) consisting of NNMO, acetylene black and PVDF was 80:10:10 wt% on aluminium foil containing 6 mg - 8 mg active mass, each (experimental in the appendix 7.1). Since aluminium current collectors were used for the cathode material an adjustment of

the diglyme based electrolyte is necessary. Instead of NaOTf, $NaPF_6$ was used to enable a proper passivation of the aluminium surface. As already shown in subsection 3.3.1 and the appendix in figure 7.6 the change of the conductive salt does not affect the co-intercalation electrode reaction. The electrolyte adjustment was requested by Prof. Komaba and was founded on his long-term experiences in this research field.[19]

Electrochemical properties of NNMO in diglyme: When combining NNMO with a diglyme based electrolyte the question arises if the strong complexation of the sodium ions by the diglyme molecules will to lead to problems on the cathode electrode surface. NNMO is a "classical" intercalation material, *i.e.* "bare" sodium ions are intercalated. Therefore it is necessary to strip of the glyme based solvation shell at the electrode surface. This desolvation step might change the kinetic properties of the intercalation reaction or lead to degradation of the electrode material by uncontrolled diglyme co-intercalation. Hence, comparing measurements were conducted.

The group of Prof. Komaba was able to cycle the above described NNMO electrodes in an electrolyte consisting of 1 M $NaPF_6$ in PC for 20 cycles with capacities around 85 mAh/g and coulombic efficiencies >99.9 % with irreversible charge losses limited to the first cycle (see figure 7.21). Figure 3.23 shows the specific capacities and the voltage characteristics determined by galvanostatic cycling. Apart from a slight capacity fading during prolonged cycling the cycle stability and reversible capacities in the diglyme based electrolyte are similar to the cycling performance in the carbonate based electrolyte. However, the leaching of the transition metal ions cannot fully be excluded and may be the main source of the minor capacity fading, since diglyme is mainly used as solvent for organic reactions (such as *Grignard* reactions or metal hydride reductions) due to its ability to chelate small cations, thereby activating the anions for chemical reactions.[167] Apart from this, the cycling performance in diglyme is sufficient to construct first sodium-ion full cells based on graphite, NNMO and the diglyme based electrolyte to gain results on the suitability of the Na/2G co-intercalation as electrode reaction in NIBs.

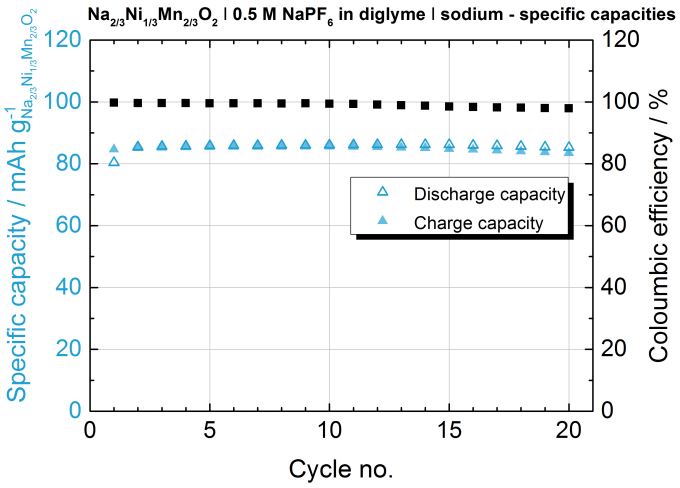

(a) specific capacities and coulombic efficiencies

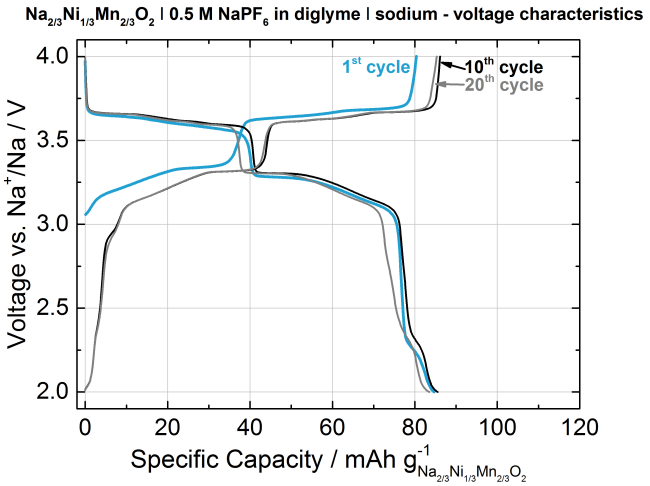

(b) charge/discharge characteristics

Figure 3.23: (a) Specific capacities per cycle and (b) voltage characteristics at an applied currents of 37.2 $^{mA}/_{g}$ of graphite electrodes in sodium full cells in a diglyme based electrolyte.

3.6.2 First results on sodium ion full cells

Theoretical assumptions and boundary conditions: After proving the compatibility of NNMO and the diglyme based electrolyte, sodium-ion full cells were assembled. For this purpose it was necessary to construct cells containing three electrodes instead of the beforehand used two-electrode setup. This additional electrode is necessary to control the half cell potentials and to be able to avoid undesired side reactions that might occur when the electrodes are cycled outside their electrochemical stability window. Since it is not possible to measure absolute potentials of an electrode material, but instead only the potential difference between a working electrode and a counter electrode, it is necessary to introduce a metallic sodium reference electrode. This means all measured potentials will be specified as potentials vs. the sodium redox couple Na^+/Na. Since the average redox potential *vs.* Na^+/Na are 0.65 V for the graphite anode and around 3.7 V for the NNMO cathode the mean obtainable cell voltage of NNMO vs. graphite is expected to be around 3.0 V. Due to the different charge storage capacities of the cathode and the anode material it is necessary to carefully balance the electrode active masses and the charge storage capacities before assembling and to choose them in a way that on both sides of the battery the same amount of charge can be stored (table 3.9).

Table 3.9: Basic electrochemical properties of the half-cell active materials graphite and NNMO tested in a diglyme based electrolyte.

	graphite anode	**NNMO cathode**
Theoretical capacity	105 $\frac{mAh}{g}$	173 $\frac{mAh}{g}$
Reversible capacity	90-100 $\frac{mAh}{g}$	85 $\frac{mAh}{g}$
Electrode reaction	co-intercalation	intercalation
Potential window	0.01 V-3.0 V	2.0 V-4.0 V
Average redox potential *vs.* Na^+/Na	0.65 V	3.7 V
Current collector	copper	aluminium

Theoretical capacities and electrode reactions for the complete sodiation/*de*-sodiation of a NNMO cathode and a graphite anode are calculated by equation 3.1:

Reaction on the positive electrode (q_{th}= 173 mAh/g, intercalation):

$$1.5\ [Na_{2/3}Ni_{1/3}Mn_{2/3}O_2] \rightleftharpoons Na^+ + e^- + 1.5\ [Ni_{1/3}Mn_{2/3}O_2]$$

Reaction on the negative electrode (q_{th}= 105 mAh/g, co-intercalation reaction):

$$Na^+ + y \cdot 2G + n \cdot C + e^- \rightleftharpoons Na^+(2G)_yC_n^-$$

From the operational voltages of the graphite anode and the NNMO cathode a theoretical potential range of the full cells of 0.01 V – 4.0 V *vs.* Na^+/Na can be presumed (figure 3.24). Since side reactions can occur on both active materials when the electrodes are cycled outside their electrochemical stability window an 2-electrode setup is insufficient to evaluate the electrochemical performance. Therefore it seems to be necessary to measure the half cell potentials while cycling the full cell setup.

The following procedure was used for the galvanostatic cycling of the full cell:

- Galvanostatic cycling of the voltage between cathode and anode, *i.e.* "full cell" mode, in a given potential range.
- Meanwhile, recording of the half cell potentials, *i.e.* the voltages between NNMO *vs.* Na^+/Na and graphite *vs.* Na^+/Na.
- Insertion of additional stop criteria for the galvanostatic cycling mode.
  - The charging step is aborted when:
    (a) the cathode reaches its upper limit *vs.* Na^+/Na or
    (b) the anode falls below its lower limit *vs.* Na^+/Na.
  - The discharge step is aborted when:
    (a) the NNMO cathode reaches its lower limit *vs.* Na^+/Na or
    (b) the anode rises above its upper limit *vs.* Na^+/Na.

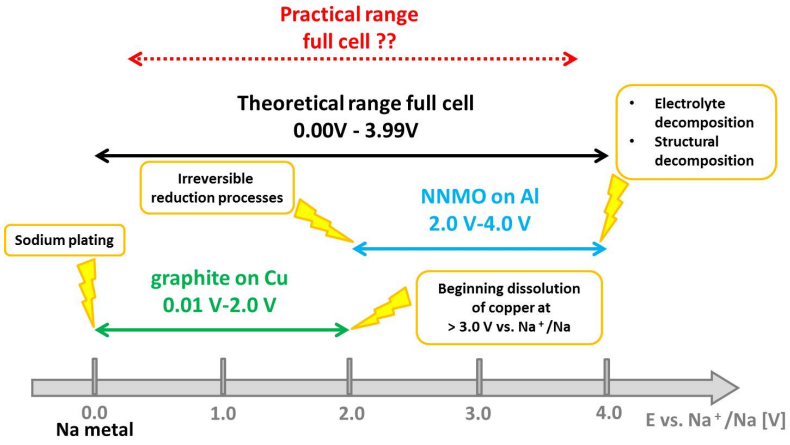

Figure 3.24: Basic assumptions about the electrochemical stability windows of NNMO cathodes on aluminium current collectors and graphite anodes on copper current collectors versus sodium metal reference electrodes.

With this program we are able to cycle the full cells without risking uncontrolled side reactions. Applied to the constructed full cells this means:

The full cell potential $E_{NNMO} - E_{graphite}$ is cycled with an applied current of 12.05 $^{mA}/_{g}$ related to the cathode material ($^{C}/_{20}$ rate) in a potential range of 0.01 V – 4.0 V while the half cell potentials E_{NNMO} and $E_{graphite}$ *vs.* Na^+/Na are recorded. In addition to the potential borders of the full cell there a two more stop criteria added: for charging $E_{NNMO} > 4.0\,V$ and $E_{graphite} < 0.01\,V$ and for discharging $E_{NNMO} < 2.0\,V$ and $E_{graphite} > 2.0\,V$.

Preliminary results: Figure 3.25 shows the specific capacities of NNMO *vs.* graphite in the full cell mode. Sodium metal reference electrodes were inserted to keep track of the cathode and anode potentials *vs.* Na^+/Na for better comparison.

When the two electrodes are combined without balancing the active masses and charge storage capacities it can be seen that the coulombic efficiencies are below

70 % and the capacity retention is not sufficient (detailed data in the appendix figure 7.22).

When the active masses of NNMO and graphite are balanced according to their reversible capacities listed in table 3.9, the coulombic efficiencies, apart from the first cycles, are above 90 %. The fading of the reversible capacities is still apparent (detailed data in the appendix figure 7.23).

Reforming of the graphite anode material stabilizes the reversible capacities significantly (detailed data in the appendix figure 7.24). As reforming of an electrode material typically the preconditioning of an electrode material is denoted. In the industrial fabrication of batteries the preconditioning of an electrode material is usually done by the addition of electrolyte additives. These decompose at higher potentials than the electrolyte compounds and allow the controlled reaction of reactive graphite surface-terminating groups and the formation of a homogeneous SEI layer.[53,151,153] In case of the here shown full cells graphite is reformed by cycling it against a metallic sodium electrode, leading to an controlled reaction of graphite surface-terminating groups with excess electrolyte and sodium ions and/or the controlled and even formation of a SEI on the graphite surface which show limited irreversible charge losses in the full cell setup. This step seems to be reasonable since the amount of sodium ions that can be delivered by the cathode material is limited and should not be "wasted" on irreversible side reactions. Except for the first cycle, where some side reactions do occur, coulombic efficiencies >98.2 % could be found. Although, the capacity retention was better for the reformed graphite electrodes than for the full cells without, the overall retention is still insufficient, exhibiting fading during prolonged cycling. This is unexpected behaviour since both electrode materials have shown sufficient cycle stability in corresponding half cells with this electrolyte under analogue cycling conditions.

The voltage characteristics in the 3^{rd} cycle of the above described full cells and the corresponding half cell potentials (figures 3.26 and 3.27) show the influence of electrode balancing and reforming on the cycling performance. The balancing only causes slight changes in the reversible capacities and voltage characteristics, while the

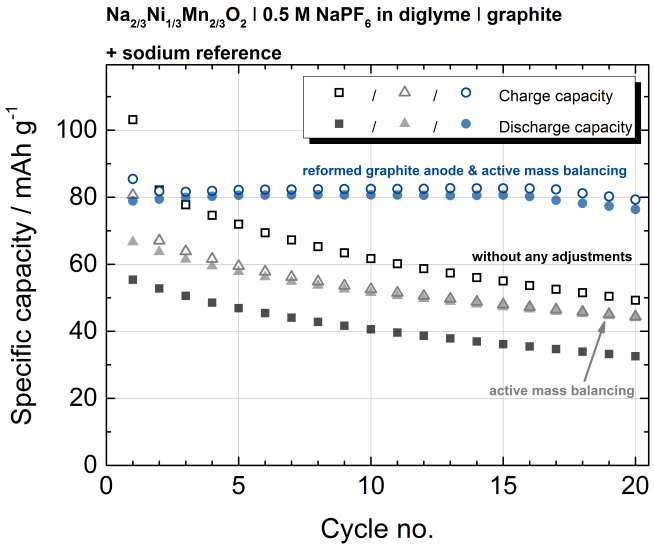

Figure 3.25: Specific capacities of a sodium-ion full cell based on NNMO as cathode and graphite as anode material in diglyme based electrolyte at an applied current of 12.04 mA/g with additional stop criteria (see corresponding text). The influences of active mass balancing and graphite anode reforming are shown.

reforming of the graphite electrode allows the more complete charging/discharging of the cell. Which is linked to the better utilisation of the sodium ion content of the cathode material which can be concluded from figure 3.27.

In summary, the diglyme based electrolyte is compatible with a "classical" intercalation material and first sodium-ion full cells were built and cycled consisting of graphite/diglyme/NNMO exhibiting reasonable cycle stabilities. These batteries therefore may allow further and intensified research in order to develop NIBs.

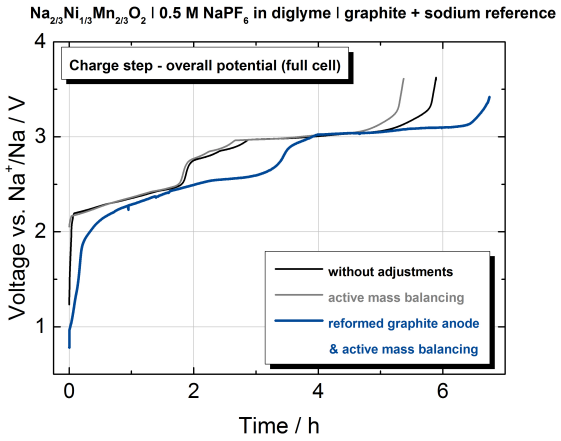

(a) charge characteristics

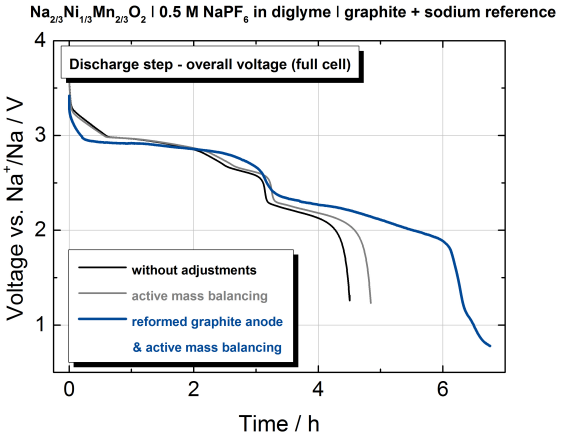

(b) discharge characteristics

Figure 3.26: Voltage characteristics in the 3^{rd} cycle of the full cell potential of a sodium-ion full cell based on NNMO as cathode and graphite as anode material in a diglyme based electrolyte at an applied current of 12.05 $^{mA}/_{g}$ (related to NNMO) with additional stop criteria (see corresponding text). The influence of active mass balancing and graphite anode reforming are shown.

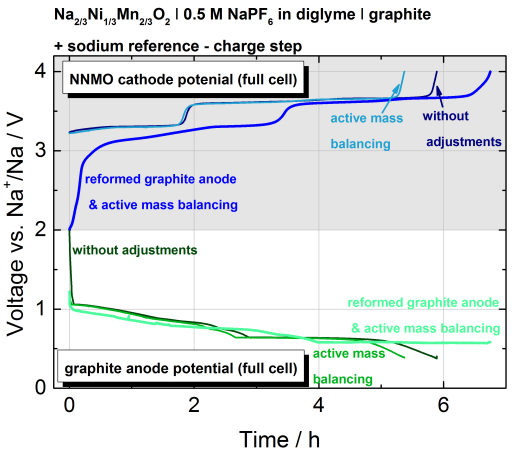

(a) charge characteristics

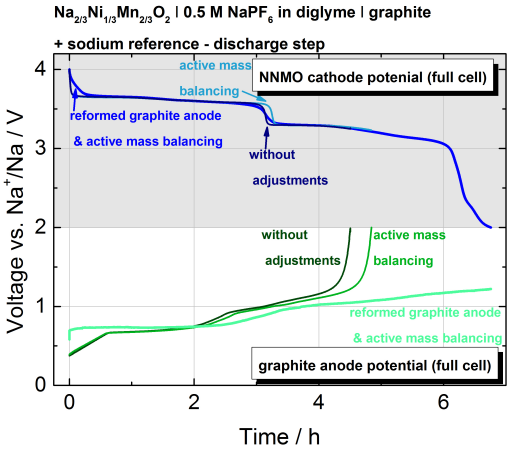

(b) discharge characteristics

Figure 3.27: Voltage characteristics in the 3^{rd} cycle the half cell potentials of a sodium-ion full cell based on NNMO as cathode and graphite as anode material in a diglyme based electrolyte at an applied current of 12.05 $^{mA}/_{g}$ (related to NNMO) with additional stop criteria (see corresponding text). The influence of active mass balancing and graphite anode reforming are shown.

4 Latest research studies

In this chapter the latest research results on the insertion of sodium ions into graphite and non-graphitic carbons are summarized. The described projects were started subsequently after this study or at the same time. The results are organized into four sub-groups:

Table 4.1: Co-intercalation of Na^+ into graphite in glyme-based electrolytes,

Table 4.2: Insertion of Na^+ into graphite related carbons,

Table 4.3: Insertion of Na^+ into non-graphitic carbons

Table 4.4: Other electrode reactions in glyme-based electrolytes

The work of two groups are highlighted since they are close to the topic of this thesis. Kang *et al.* and Chen *et al.* reported about the co-intercalation of sodium ions alongside with their glyme based solvation shell into graphite electrodes shortly after the results of this thesis were published:

Kang *et al.* reported in January 2015 the capability of natural graphite to co-intercalate sodium-glyme complexes.[156] As electrolytes 1 M of $NaPF_6$ in 1G, 2G or 4G with electrodes consisting of 70 wt% natural graphite : 20 wt% conductive agent : 10 wt% PVDF on copper current collectors were used. The characterisation was carried out by galvanostatic cycling, cyclic voltammetry, HR-TEM, FTIR and EIS analysis and delivered comparable results to the ones reported within this work. The slightly higher reversible capacities of 150 $^{mAh}/_{g}$ are most likely due to the high amount of conductive carbon which might deliver additional charge storage capacity. Apart from that no analogue measurements with triglyme or lithium-based cells were conducted. First proof-of-principle measurements on sodium-ion full cells with a

$Na_{1.5}VPO_{4.8}F_{0.7}$ were presented, delivering an energy density of around 120 $^{Wh}/_{kg}$ while maintaining around 70 % of the initial capacity after 250 cycles.

In a second, subsequent paper from July 2015 the same group reported their efforts to investigate the intercalation mechanism of solvated-Na^+ into graphite using *in-operando* X-ray diffraction analysis, electrochemical titration, real-time optical observation, and density functional theory (DFT) calculations.[114] From these results they conclude that the sodium-co-intercalation occurs through multiple staging reactions, which finally form stage 1 GICs within a wide range of Na/C from 1/28 to 1/21. This complex composition is not in accordance with the specific behaviour described for the triglyme electrolyte solvent described in this thesis as an effect of the unfavourable coordination based on the most probable coordination number of sodium (CN=5-7). If only one glyme molecule would be co-intercalated into the graphite electrode it should not be possible to determine a difference between monoglyme, diglyme, tetraglyme and triglyme since the coordination number of the central sodium ion should not have an effect. In both studies no description for the peculiar behaviour of Na^+/3G was given.

In a communication from June 2016 the group compared the co-intercalation phenomena in rechargeable Li-, Na- and K-ion batteries. They found that the specific capacities and insertion mechanisms are similar for all alkali ions despite the different solubility limits of the "bare" ions in graphite. Furthermore, they found that the insertion potentials are dependent on the size of the co-intercalated alkali ion based on an increased interlayer distance upon co-intercalation. Overall, they found and described a similar, reversible co-intercalation mechanism for the potassium ions as already found and described for lithium and sodium ions described in this work.[172]

In a fourth paper from September 2016 the same group conducted theoretical studies based on DFT calculations on the interplay between guest ion, solvents and graphite host upon co-intercalation. They found that the reversible co-intercalation of sodium into graphite is only possible when the co-intercalating solvent strongly coordinates the sodium ions and when the lowest unoccupied molecular orbital level of this so-formed complexes is higher than the Fermi level of graphite.[173]

Chen et *al.* reported in May 2015 about the capability of different graphite materials to co-intercalate sodium-glyme complexes.[174] As electrolytes 1 M solutions of NaOTf or $NaClO_4$ in 1G, 2G or 4G with electrodes consisting of 90 wt% graphite: 10 wt% PVDF or sodium carboxymethyl cellulose (Na-CMC) on copper current collectors were used. The characterisation was carried out by galvanostatic cycling, cyclic voltammetry, SEM, EDX, FTIR, and Raman and delivered comparable results to the ones reported within this work. The minor deviations of the voltage characteristics are most likely due to the low mass loading of the electrodes which was around 1.0 $^{mg}/_{cm2}$–1.5 $^{mg}/_{cm2}$. Apart form that no analogue measurements with triglyme or lithium-based cells were conducted. First proof-of-principle measurements on sodium-ion full cells with a $Na_3V_2(PO_4)_3$-carbon composite cathode were presented delivering around 90 $^{mAh}/_{g}$ at an average voltage of 2.2 V *vs.* Na/Na^+ while maintaining around 80 % of the initial capacity after 400 cycles.

Table 4.1: Latest studies on the co-intercalation of sodium ions into graphite in glyme-based electrolytes.

Active material	Electrolyte /1 M	GICs	Specific capacities (applied current)	Author Date
Natural graphite	$NaPF_6$ /1G, 2G or 4G	***t***	150 $^{mAh}/_{g}$ (100 $^{mA}/_{g}$)	Kang *et. al.* 01.2015 [156]
Natural graphite	$NaPF_6$ /1G, 2G or 4G	***t***	150 $^{mAh}/_{g}$ (100 $^{mA}/_{g}$)	Kang *et. al.* 07.2015 [114]
Natural graphite	NaOTf, $NaClO_4$ /1G, 2G or 4G	***t***	110 $^{mAh}/_{g}$ (100 $^{mA}/_{g}$)	Chen *et. al.* 05.2015 [174]
Natural graphite	$NaClO_4$ 4G	***t***	110 $^{mAh}/_{g}$ (200 $^{mA}/_{g}$)	Scrosati *et. al.* 02.2016 [175]
Natural graphite	NaOTf /2G	***t***	110 $^{mAh}/_{g}$ (100 $^{mA}/_{g}$)	Kang *et. al.* 06.2016 [172]
Graphite	Na^+A^- /diff. solvents	***t***	DFT-calculations	Kang *et. al.* 09.2016 [173]

Table 4.2: Latest studies on the insertion of sodium ions into graphite related carbons (expansion of graphite interlayer distance to facilitate intercalation of "bare" sodium ions).

Active material	Electrolyte /1 M	GICs	Specific capacities (applied current)	Author Date
Flexible graphite film	$NaPF_6$ /2G	***t***	130 $^{mAh}/_{g}$ (100 $^{mA}/_{g}$)	Cui *et. al.* 10.2015 [176]
Graphene	$NaPF_6$ /2G	***t***	100 $^{mAh}/_{g}$ (3 $^{A}/_{g}$)	Pint *et. al.* 11.2015 [177]
Expanded graphite	theoretical	***b***	930 $^{mAh}/_{g}$	Han *et. al.* 07.2015 [178]
Expanded graphite	$NaPF_6$ EC/DEC	***b***	110 $^{mAh}/_{g}$ (37 $^{mA}/_{g}$)	Ramos *et. al.* 11.2015 [179]

Table 4.3: Latest studies on the insertion of sodium ions into non-graphitic carbon materials (expansion of graphite interlayer distance to facilitate insertion of "bare" sodium ions).

Active material	Electrolyte /1 M	GICs	Specific capacities (applied current)	Author Date
Soft carbon (GDL)	0.5 M $NaPF_6$ /2G	***b***/***t***	120 $^{mAh}/_{g}$ (37 $^{mA}/_{g}$)	Janek et *al.* 08.2015[91]
Soft carbon	$NaPF_6$ /EC/DEC(1:1)	***b***	130 $^{mAh}/_{g}$ (100 $^{mA}/_{g}$)	Ji *et. al.* 11.2015 [180]
Soft carbon (mesoporous)	$NaPF_6$ /EC/DEC(1:1)	***b***	330 $^{mAh}/_{g}$ (30 $^{mA}/_{g}$)	Song *et. al.* 03.2016 [181]
Hard carbon	$NaClO_4$ /EC/DEC(1:1)	***b***	200 $^{mAh}/_{g}$ (20 $^{mA}/_{g}$)	Li *et. al.* 04.2016 [182]
Mesocarbon microbeads	$NaPF_6$ /2G	? (capacitor)	93.5 $^{Wh}/_{kg}$ (573 $^{W}/_{kg}$)	Cui *et. al.* 08.2015 [183]
Graphite microbeads	$NaPF_6$ /2G	? (capacitor)	77 $^{Wh}/_{kg}$ (1900 $^{W}/_{kg}$)	Jin *et. al.* 08.2016 [184]

Table 4.4: Latest studies on the enhancement of other electrode reactions by using glyme-based electrolytes.

Active material	Electrolyte /1 M	Specific capacities (applied current)	Author Date
FeS_2	$NaPF_6$ /2G	600 $^{mAh}/_{g}$ (20 $^{mA}/_{g}$)	Wang *et. al.* 02.2015 [185]
TiO_2/graphene	$NaPF_6$ /2G	140 $^{mAh}/_{g}$ (33.5 $^{mA}/_{g}$)	Adelhelm *et. al.* 11.2015 [186]
Pb particles	$NaPF_6$ /2G	55 $^{mAh}/_{g}$ (10 $^{mA}/_{g}$)	Monconduit *et. al.* 11.2015 [187]
CoS /reduced graphene oxide	NaOTF /2G	400 $^{mAh}/_{g}$ (1 $^{A}/_{g}$)	Ramakrishna *et. al.* 03.2016 [188]
Graphite	KPF_6 /2G	100 $^{mAh}/_{g}$ (1 $^{A}/_{g}$)	Pint *et. al.* 09.2016 [189]
Sn	$NaPF_6$ 2G	800 $^{mAh}/_{g}$ (250 $^{mA}/_{g}$)	Tarascon *et. al.* 09.2016 [190]

5 Conclusions

This thesis describes an unexpected reversible sodium ion storage into graphite electrodes by making use of solvent co-intercalation. Starting point of this thesis was that graphite was long been thought to be almost inactive towards the insertion of sodium ions and the formation of sodium-rich binary graphite intercalation compounds. Therefore, to activate graphite as an electrode material for sodium-ion batteries it was necessary to describe and characterize a new kind of electrode reaction for the insertion of sodium ions into the graphite structure.

It was described beforehand in literature that ternary graphite intercalation compounds do form on basis of solvent co-intercalation and on the basis of this knowledge a co-intercalation model was proposed and systematic measurements were successfully conducted and published (sections 3.1 - 3.3) exhibiting a high reversibility of the co-intercalation reaction. This high reversibility was not described, to the best of the author's knowledge, in a scientific publication before.[129]

It was shown that diglyme, a linear ether, acts not just as electrolyte solvent, but that it participates in the electrode reaction. Diglyme forms stable complexes with alkali ions that can be reversibly co-intercalated into the graphite structure. Important features of this co-intercalation electrode reaction for sodium are small irreversible charge losses, low overpotentials and a superior cycle life. The exceptional stability might simply be related to the fact that ***b***-GICs between sodium and graphite do not form. Analogue lithium measurements exhibited a worse reversibility, so that it can be concluded that the competition between the formation of the binary and ternary Li-GICs at low potentials is disadvantageous for the cycle stability of the co-intercalation reaction. Though, the formation of ternary compounds is

linked with increased spatial requirements for the alkali-solvent complex within the graphite lattice and therefore decreased charge storage capabilities. With specific capacities close to 100 $^{mAh}/_{g}$ the sodium-diglyme co-intercalation electrode reaction may not be competitive with lithium-ion technology for portable or mobile applications, but may be complementarily usable for stationary applications where the costs are more relevant than energy densities.

In a next step the co-intercalation concept was transferred to other coordinating ethers (sections 3.5.1 - 3.5.2). When the chain length of the co-intercalated ether is shortened or extended, coordinative effects can be observed, while the reversibility and charge storage capacity for different ethers is not distinctly different. Depending on the preferred coordination number of the central ion, a preference of certain chain lengths can be determined for the different alkali ions. Unfavourable combinations of alkali ions and glymes offering a number of coordinating ether oxygen atoms that is not compatible with the preferred coordination numbers of the alkali ions in solution lead directly to higher internal resistance of the electrode reaction and therefore lower energy efficiencies. For favourable combinations a dependency of the co-intercalation potentials on the ether chain length of the glyme ($E_{1G} < E_{2G} < E_{4G}$) and the alkali ion ($E_{Na} < E_{Li}$) can be observed. Due to this dependency the mixing of two or more glymes in specified ratios is proposed as an approach to tailor the redox potential of the co-intercalation reaction. The expansion of interlayer distances of fully sodiated (co-intercalated) graphite electrodes was determined by X-ray diffraction. From the diffraction patterns it becomes apparent that the solvation shell has only a minor influence on the expansion in interlayer distance. Furthermore, the interlayer distance is found to be >200 % during the formation of ***t***-glyme-GICs, which is remarkable, considering the excellent reversibility of the electrode reactions.

Using diglyme derivatives, *i.e.* ethers which exhibit side groups implemented into the linear diglyme base structure, results in a higher steric hindrance of the cation-solvent complex formed (subsection 3.5.2). From the results of the electrochemical characterization and X-ray diffraction it can be concluded that the redox chemistry of the co-intercalation electrode reaction and the structural evolution is strongly

influenced by the type of solvent co-intercalated and hence, by the composition and structure of the solvation shell. While the redox potentials, the kinetics and the degree of insertion of sodium ions is clearly dependent on the size of the ion-solvent complex, only a minor influence could be determined for the increase in the interlayer distance of the co-intercalated graphite. Furthermore, the results for the diglyme derivatives support the explanation that unfavourable combinations of cations and the number coordination centres influence the co-intercalation behaviour with respect to internal resistances.

Furthermore, the compatibility of the diglyme based electrolyte with a "classical" intercalation material was tested. Prof. Shinichi Komaba and his group from *Tokyo University of Science* provided a layered oxide as sodium cathode material, P2-$Na_{2/3}Ni_{1/3}Mn_{2/3}O_2$ (subsection 3.6). Comparing electrochemical key data for this material in a carbonate based and the ether based electrolyte were measured and analysed and first sodium-ion full cells based on graphite, NNMO and the diglyme based electrolyte were built. Apart from manual problems with the cell construction and irreversible charge losses, due to SEI formation or the reaction of surface-terminating groups of graphite, a reasonable cycle stability could be determined. Since it is possible to cycle these batteries for long-terms and with reasonable charge storage capacities, this cell type may allow further and intensified research in order to understand and develop sodium-ion technology.

Shortly after the publication of the presented results, two other research groups published comparable studies on the co-intercalation of linear ethers and Na^+ into graphite electrodes, agreeing on the here presented results and conclusions.[114,156,174] On the basis of the here described work[1,2] and the results from the two succeeding groups,[114,156,174] a couple of subsequently following paper were published (chapter 4). All of these focus on the application of glyme based electrolytes for sodium ion batteries and examine the effects of glymes solvents in sodium ion full cells[114,156,172–175] or on anode materials[185–190] and agree on the beneficial properties of glyme on the cycle stability in sodium-ion cells.

6 Outlook

The main finding of this thesis is that graphite can act as a highly reversible electrode material for alkali ion based co-intercalation of solvent molecules. Although a number of systematic experiments showed that the electrode reaction is sensitive to a number of parameters, such as the type of solvent or the alkali ion, much is still unknown.

Further and detailed investigations on the formation and insertion of ternary sodium graphite intercalation compounds are still necessary, since it is not clear so far from how many solvent molecules the solvation shell is constructed and how it is intercalated into the graphite host material. Nuclear magnetic resonance (NMR) spectroscopy measurements from the liquid and solid phase and first-principle density functional theory (DFT) calculations and molecular-dynamic (MD) simulations may help clarify the underlying mechanisms. Only one basic work on the insertion of sodium ion into graphite was published by Kang *et al.*[114] They propose the formation of $[\mathrm{Na-glyme}]^{+}$ complexes that are reversibly intercalated and form double layers stacked in parallel to the graphite layers of the graphite host material.

Additionally, the basic question if and from what components an SEI layer is formed on graphite surface in glyme based electrolytes needs to be addressed. Since in a "classical" lithium-ion cell one important function of an SEI is to to prevent the co-intercalation of solvent molecules into the graphite lattice, it becomes apparent that for the formation of solvent based ternary graphite intercalation compounds the SEI layer, if existent at all, needs to be from a different composition and function than in the "classical" intercalation electrode reaction. Taking into account the low overpotentials of the co-intercalation electrode reaction and the large lattice expansion involved, it may be concluded that virtually no SEI can be present for the

sodium-glyme based systems or that the formed SEI is highly flexible and dynamic, allowing an easy charge transfer between electrolyte and electrode. From this point of view a very detailed surface and impedance analysis, which is outside the scope of this study, should be conducted.

Due to the large volume expansion, which might lead to exfoliation during prolonged cycling, further clarifying studies should be conducted. One way would be *in-situ* X-ray nano-tomography which would allow, besides the tracking of the reversible dilation of the graphite material, to make a statement on how the morphology of metallic sodium is developing during prolonged cycling and if dendrite formation occurs.

Since this study focuses on the co-intercalation behaviour of ethereal solvents solely, a further diversification of the solvent range should be considered. Some early work already dealt more or less successfully with the chemically and electrochemically driven co-intercalation of amides or amines.[104,105,142,146] A further interesting class of possible substances might be the group of the silanes, for example dimethyl dimethoxy silane, depending strongly on the basic physical properties such as viscosity, dielectric constants and their ability to dissolve sodium conductive salts to an sufficient amount.

Because the co-intercalation of sodium ions and their glyme based solvation shell into graphite electrodes and the formation of ternary sodium-glyme graphite intercalation compounds are highly reversible and deliver a long term cycle stability this electrode reaction is attractive for application in future sodium-ion batteries. Apart from the beneficial electrochemical properties, the fact that this new kind of electrode reaction requires only low cost materials and uses an already established and well-studied graphite electrode additionally suggest the further implementation into upcoming sodium-ion technology. As the ternary graphite intercalation compounds are also formed with other solvents apart from glymes, the co-intercalation approach provides an alternative route to search for new electrode reactions for sodium-ion batteries.

7 Appendix

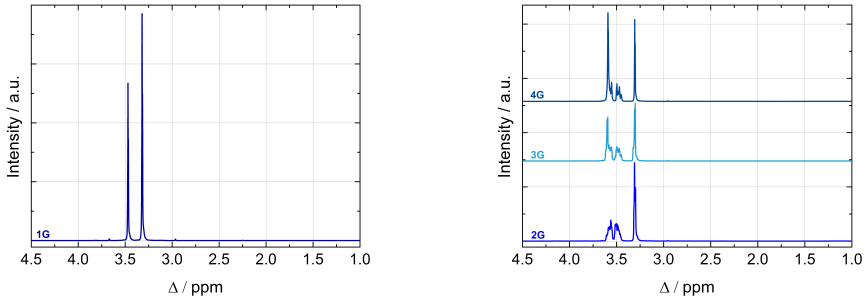

(a) monoglyme (b) diglyme, triglyme, tetraglyme

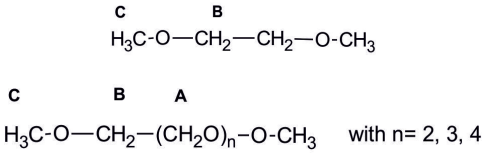

Solvent	(A) CH_2-O	(B) CH_2	(C) O-CH_3
1,2-Dimethoxyethane (monoglyme)	-	3.52 (s)	3.32 (s)
Bis(2-methoxyethyl) ether (diglyme)	3.60 (m)	3.57 (m)	3.31 (s)
Triethylene glycol dimethyl ether (triglyme)	3.60 (m)	3.50 (m)	3.30 (s)
Tetraethylene glycol dimethyl ether (tetraglyme)	3.60 (m)	3.50 (m)	3.30 (s)

Figure 7.1: ^{1}H-NMR 200 MHz of the pure glymes (used as received) in $CDCl_3$ with tetramethylsilane (TMS) as external standard. No significant amounts of impurities could be determined. Chemical shifts in ppm from H. E. Gottlieb *et al.*, *Journal of organic chemistry* **1997**, *62*, 7512-7515.

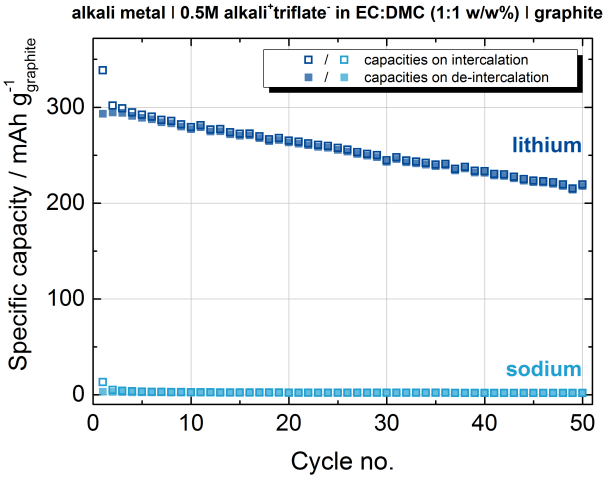

(a) specific capacities

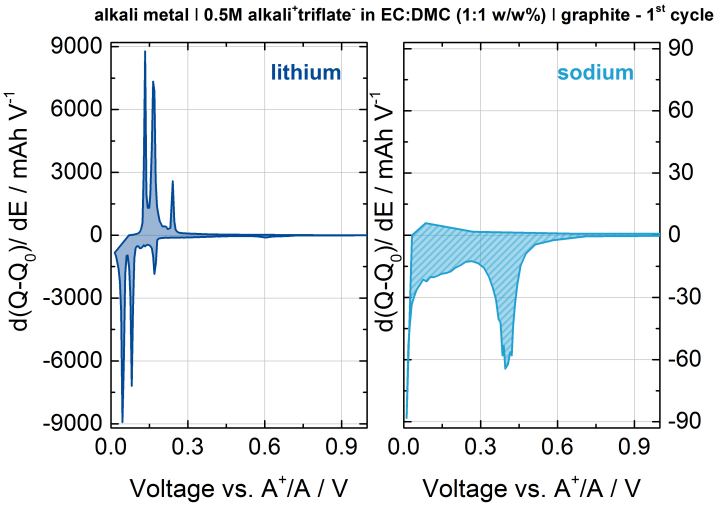

(b) differential capacities

Figure 7.2: (a) Specific capacities per cycle and (b) differential capacities in the first cycle at a constant current of 37.2 $^{mA}/_{g}$ of graphite electrodes in lithium and sodium half cells in a carbonate based electrolyte.

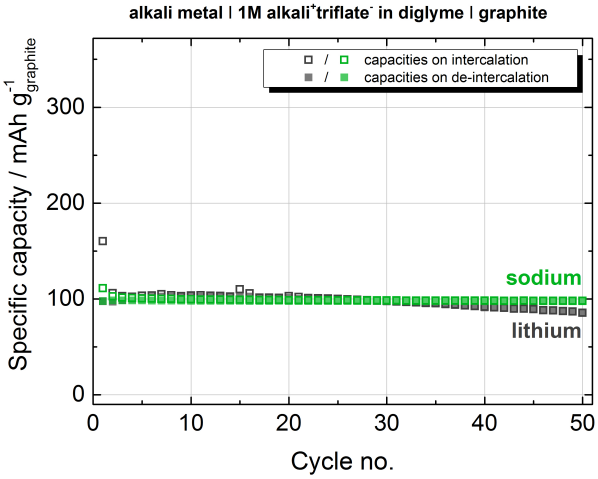

(a) specific capacities

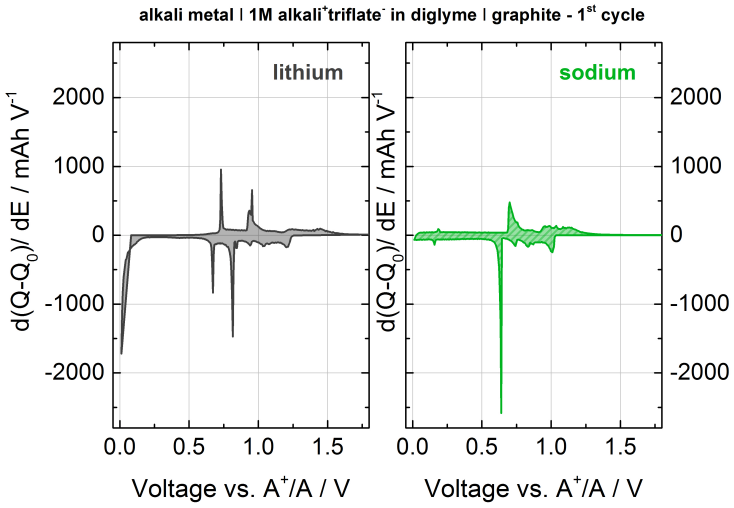

(b) differential capacities

Figure 7.3: (a) Specific capacities per cycle and (b) differential capacities in the first cycle at a constant current of 37.2 $^{\mathrm{mA}}/_{\mathrm{g}}$ of graphite electrodes in lithium and sodium half cells in a diglyme based electrolyte.

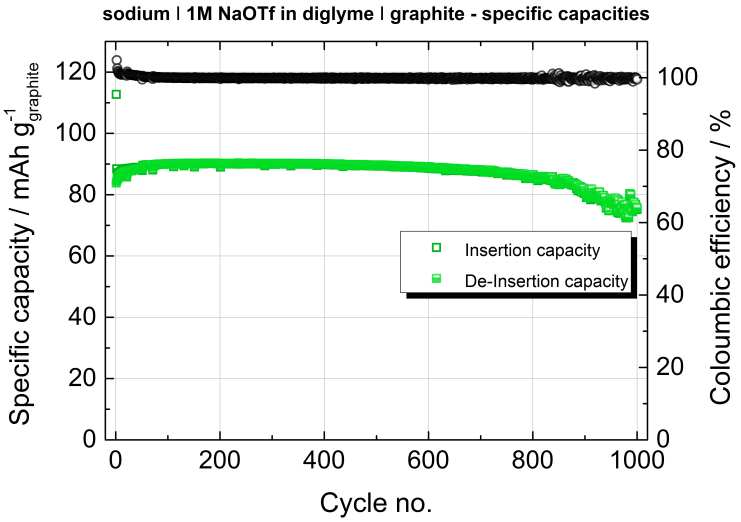

Figure 7.4: Specific capacities of 1000 cycles at a constant current of 37.2 $^{mA}/_{g}$ of a graphite electrode in a sodium half cell in a diglyme based electrolyte.

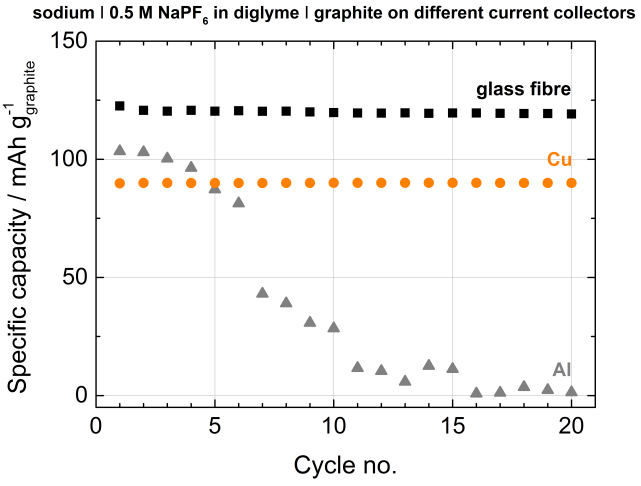

(a) specific capacities

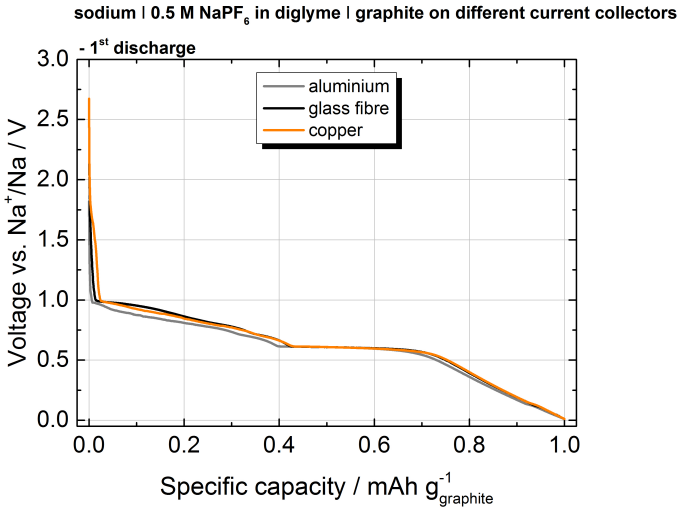

(b) voltage characteristics

Figure 7.5: (a) Specific capacities per cycle and (b) voltage characteristics in the first cycle at a constant current of 37.2 $^{mA}/_{g}$ of graphite electrodes on different current collectors in sodium half cells in a diglyme based electrolyte.

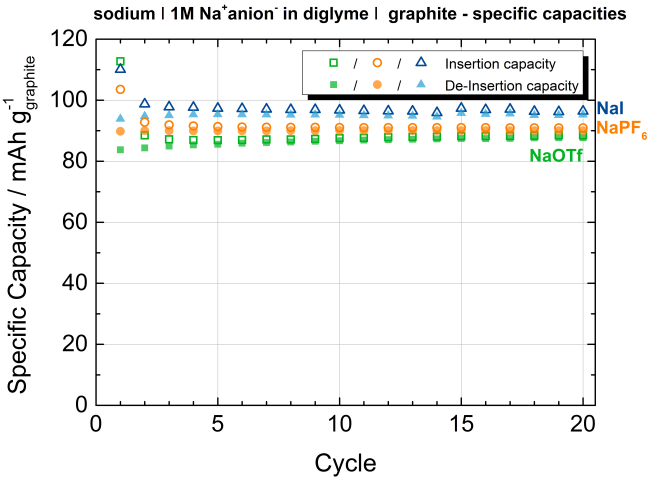

(a) specific capacities

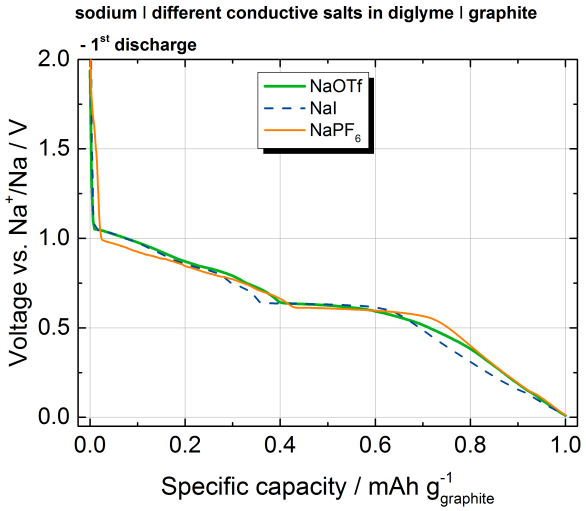

(b) voltage characteristics

Figure 7.6: (a) Specific capacities per cycle and (b) voltage characteristics in the first cycle at a constant current of 37.2 $^{\mathrm{mA}}/_{\mathrm{g}}$ of graphite electrodes in sodium half cells in a diglyme based electrolyte using different conductive salts.

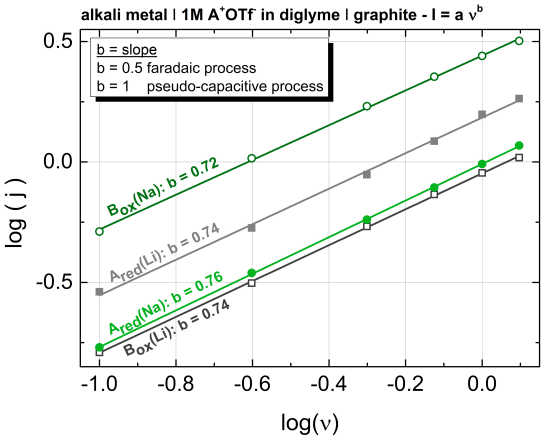

(a) Determination of the b-values according to equation 3.2.

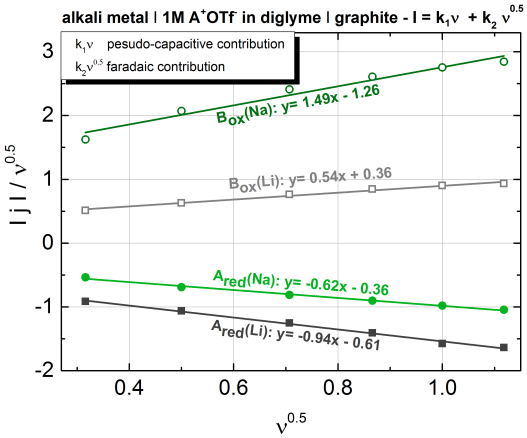

(b) Quantification of the pseudo-capacitive and faradaic contributions of the anodic/cathodic peak current in dependency on the scan rate, according to equation 3.3.

Figure 7.7: Examination of the charge storage mechanism of Li^+/Na^+ in diglyme based electrolytes into graphite electrodes by scan rate-dependent cyclic voltammetry measurements (see figure 3.4).[157–159] For further details see the corresponding text in subsection 3.3.1.

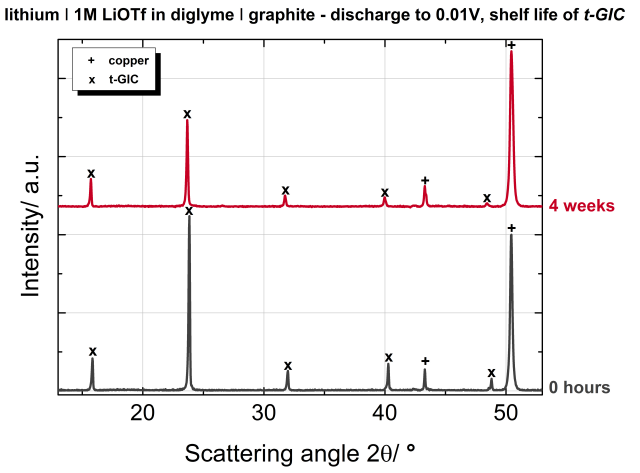

(a) lithium

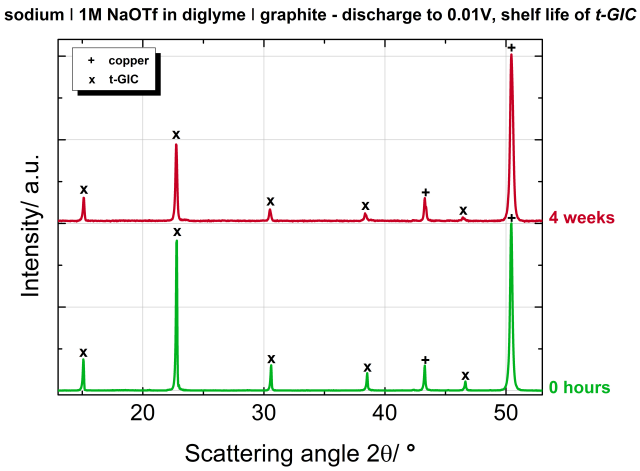

(b) sodium

Figure 7.8: Experimental data about the shelf life of *t*-2G-GICs prepared by electrochemically driven co-intercalation of diglyme and lithium or sodium ions into graphite electrodes. (a) Shelf life of *t*-Li-2G-GICs, (b) shelf life of *t*-Na-2G-GICs.

Table 7.1: Structure names, abbreviations, CAS-numbers, purities, viscosities, flash points and relative densities of monoglyme, diglyme, triglyme and tetraglyme. All data from Sigma Aldrich from where the solvents were purchased and used as received.

Name	CAS-no.	Purity / %	η / $\frac{mm^2}{s}$	b.p. / °	ρ / $\frac{g}{cm^3}$ (25 °)
1,2-Dimethoxyethane (monoglyme, **1G**)	110-71-4	99.5	0.5	85	0.867
Bis(2-methoxyethyl) ether (diglyme, **2G**)	111-96-6	99.5	1.2	162	0.943
Triethyle glycol dimethyl ether (triglyme, **3G**)	112-49-2	99.0	2.5	216	0.986
Tetraethylene glycol dimethyl ether (tetraglyme, **4G**)	143-24-8	99.0	4.1	275	1.009

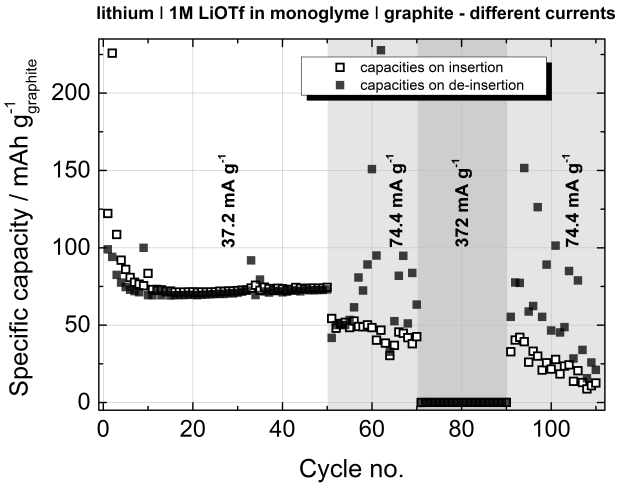

(a) Li/1G

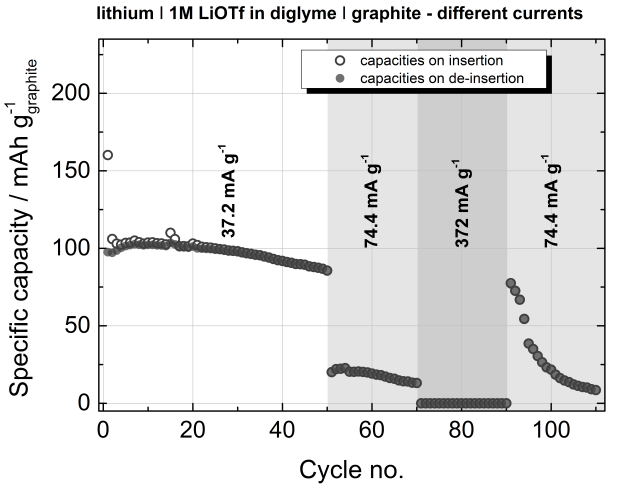

(b) Li/2G

Figure 7.9: Specific capacities per cycle at different constant currents of graphite electrodes in lithium half cells in (a) a monoglyme and (b) a diglyme based electrolyte.

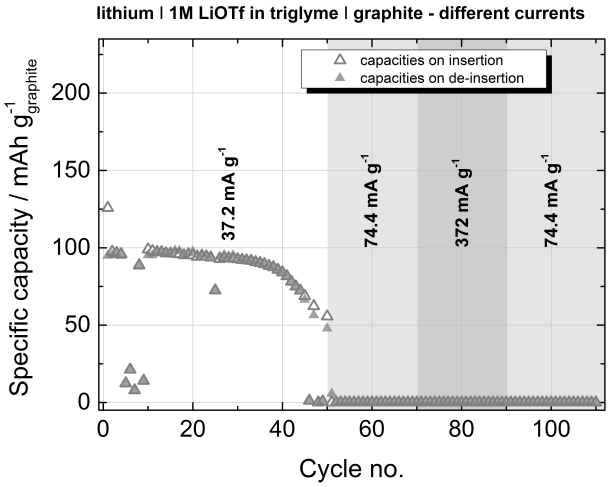

(a) Li/3G

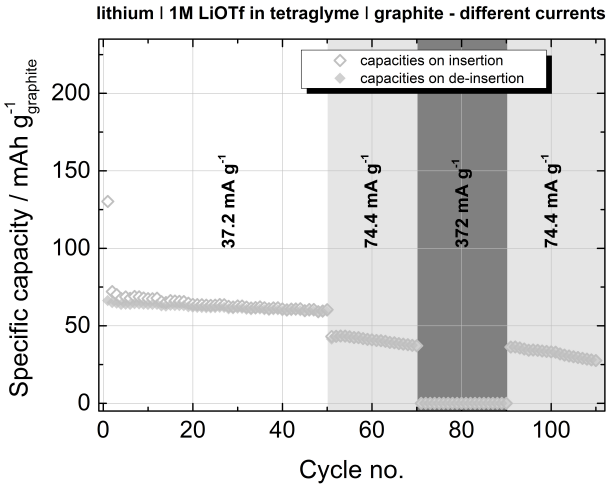

(b) Li/4G

Figure 7.10: Specific capacities per cycle at different constant currents of graphite electrodes in lithium half cells in (a) a triglyme and (b) a tetraglyme based electrolyte.

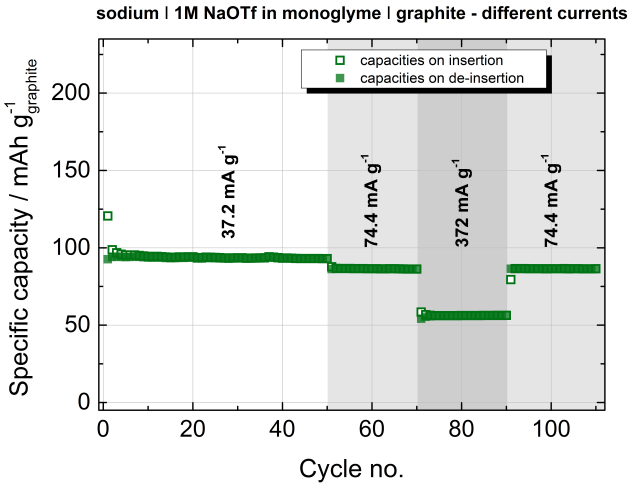

(a) Na/1G

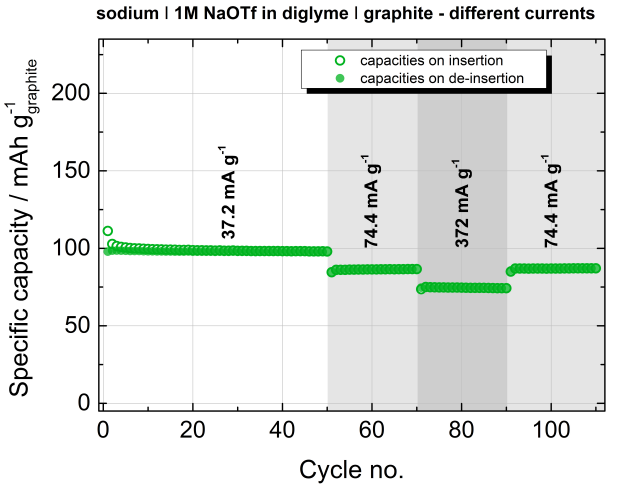

(b) Na/2G

Figure 7.11: Specific capacities per cycle at different constant currents of graphite electrodes in sodium half cells in (a) a monoglyme and (b) a diglyme based electrolyte.

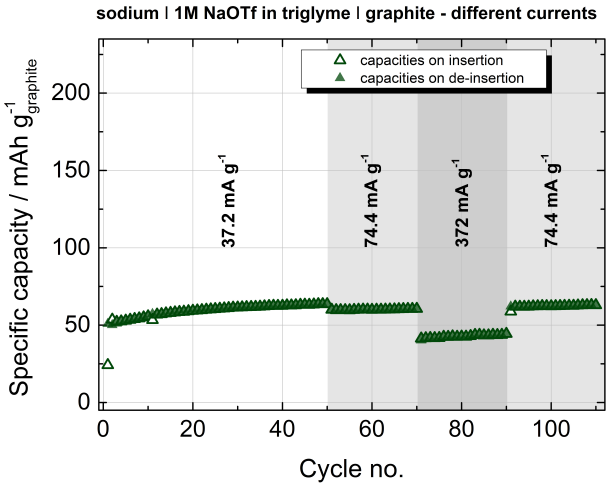

(a) Na/3G

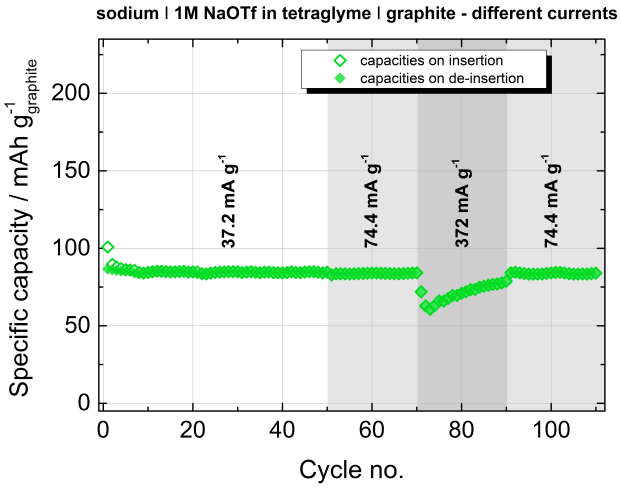

(b) Na/4G

Figure 7.12: Specific capacities per cycle at different constant currents of graphite electrodes in sodium half cells in (a) a triglyme and (b) a tetraglyme based electrolyte.

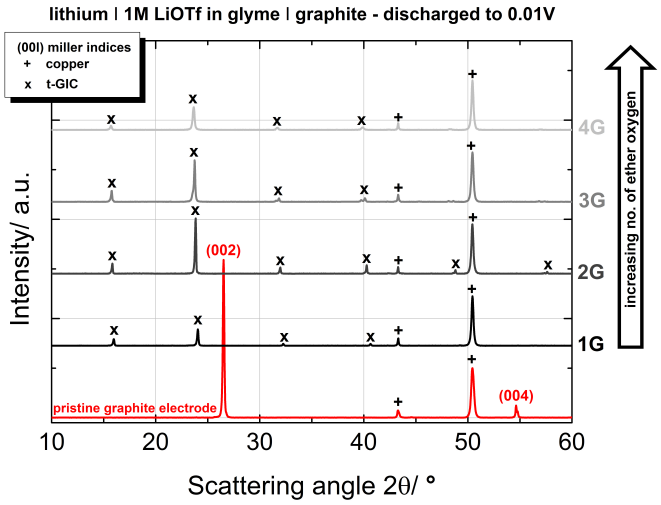

(a) lithium half cells

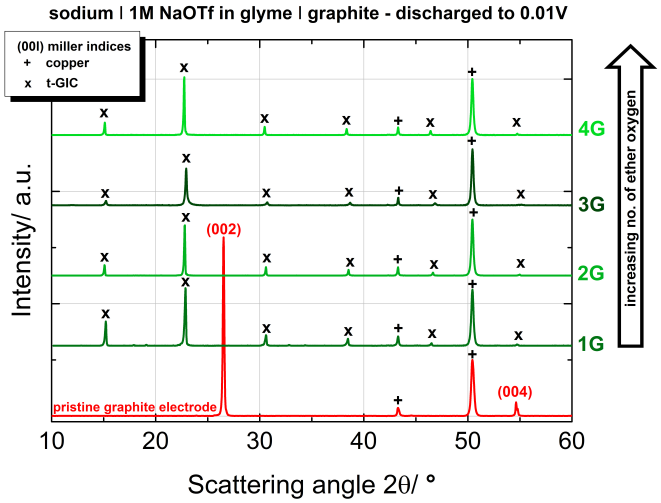

(b) sodium half cells

Figure 7.13: X-ray diffraction patterns of graphite electrodes in (a) lithium and (b) sodium half cells after full lithiation/ sodiation using different glymes.

Table 7.2: Reflex positions and interlayer distances of electrochemically prepared *t*-lithium-glyme-GICs at stage 1 determined with X-ray diffraction (details in the experimental section).

sample	scattering angle / 2θ	repeat distance I_c / Å	intercalant layer thickness Δd / Å
graphite	26.5	3.36 (-)	-
	54.5	3.36 (-)	-
$Li^+(1G)_yC_n$	15.9	11.1 (230 %)	7.7
	24.0	11.1 (230 %)	7.7
	32.2	11.1 (230 %)	7.7
	40.6	11.1 (230 %)	7.7
	49.2	11.1 (230 %)	7.7
$Li^+(2G)_yC_n$	15.8	11.2 (233 %)	7.8
	23.8	11.2 (233 %)	7.8
	31.9	11.2 (233 %)	7.8
	40.2	11.2 (233 %)	7.8
	48.7	11.2 (233 %)	7.8
$Li^+(3G)_yC_n$	15.7	11.3 (236 %)	7.9
	23.7	11.3 (236 %)	7.9
	31.8	11.3 (236 %)	7.9
	40.0	11.3 (236 %)	7.9
	48.5	11.3 (236 %)	7.9
$Li^+(4G)_yC_n$	15.7	11.3 (236 %)	7.9
	23.6	11.3 (236 %)	7.9
	31.7	11.3 (236 %)	7.9
	39.9	11.3 (236 %)	7.9
	48.4	11.3 (236 %)	7.9

Table 7.3: Reflex positions and interlayer distances of electrochemically prepared ***t***-lithium-glyme-GICs at stage 1 determined with X-ray diffraction (details in the experimental section).

sample	scattering angle / 2θ	repeat distance I_c / Å	intercalant layer thickness Δd / Å
graphite	26.5	3.36 (-)	-
	54.5	3.36 (-)	-
$Na^+(1G)_yC_n$	15.2	11.7 (248 %)	8.3
	22.8	11.7 (248 %)	8.3
	30.6	11.7 (248 %)	8.3
	38.4	11.7 (248 %)	8.3
	46.5	11.7 (248 %)	8.3
$Na^+(2G)_yC_n$	15.1	11.7 (248 %)	8.3
	22.9	11.7 (248 %)	8.3
	30.7	11.7 (248 %)	8.3
	38.6	11.7 (248 %)	8.3
	46.7	11.7 (248 %)	8.3
$Na^+(3G)_yC_n$	15.2	11.6 (245 %)	8.2
	22.9	11.6 (245 %)	8.2
	30.7	11.6 (245 %)	8.2
	38.6	11.6 (245 %)	8.2
	46.8	11.6 (245 %)	8.2
$Na^+(4G)_yC_n$	15.1	11.9 (254 %)	8.5
	22.7	11.9 (254 %)	8.5
	30.4	11.9 (254 %)	8.5
	35.3	11.9 (254 %)	8.5
	46.4	11.9 (254 %)	8.5

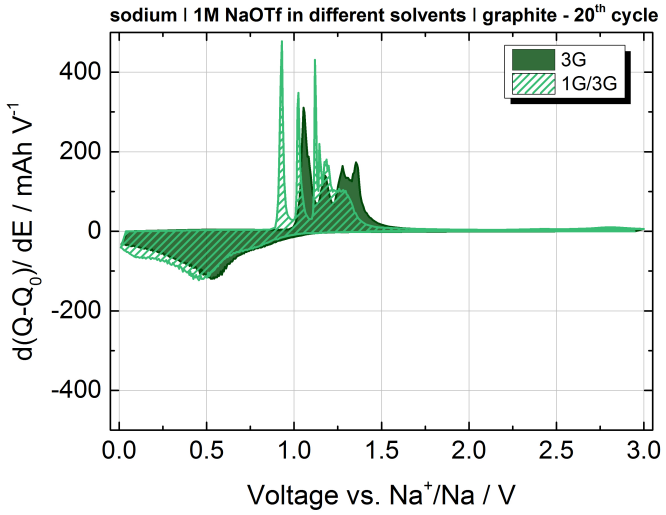

Figure 7.14: Differential capacities in the 20^{th} cycle at a constant current of 37.2 $^{\mathrm{mA}}/_{\mathrm{g}}$ of graphite electrodes in sodium half cells in a in triglyme or a mixture of monoglyme and triglyme ($1:1$) based electrolyte.

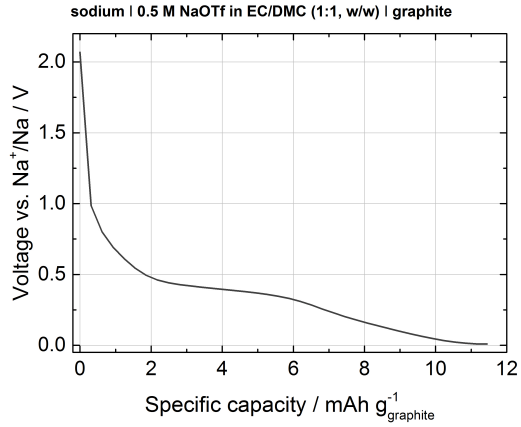

(a) voltage characteristic

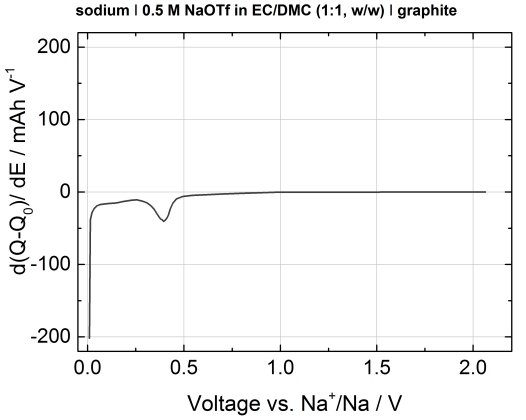

(b) differential capacities

Figure 7.15: (a) Voltage characteristics and (b) differential capacities calculated from galvanostatic cycling measurements of graphite electrodes in sodium half cells with an applied current of 37.2 $^{\mathrm{mA}}/_{\mathrm{g}}$. At first the graphite electrode was discharged (sodiation step) in a carbonate-based electrolyte to form a SEI-layer on its surface. This so prepared graphite electrode is then transferred into a sodium cell with the diglyme-based electrolyte and was cycled as usual (figure 3.19).

Table 7.4: Structure names, abbreviations, CAS-numbers, structures, purity, viscosity, flash points and relative densities of diglyme, DPGDME, Butyl-2G and 1,5-DMP. All data from Sigma Aldrich where the solvents were purchased.

Name	CAS-no.	Purity /%	η $\frac{mm^2}{s}$	b.p. /°C	ρ $\frac{g}{cm^3}$ (25 °)
Bis(2-methoxyethyl) ether (**2G**)	111-96-6	99.5	1.2	162	0.943
Bis(methoxypropyl) ether (**DPGDME**)	111109-77-4	99.0	1.1	74	0.951
Bis(2-butoxyethyl) ether (**Butyl-2G**)	112-73-2	99.0	2.3	118	0.885
1,5-Dimethoxy pentane (**1,5-DMP**)	111-89-7	98.0	No data available	60	0.843

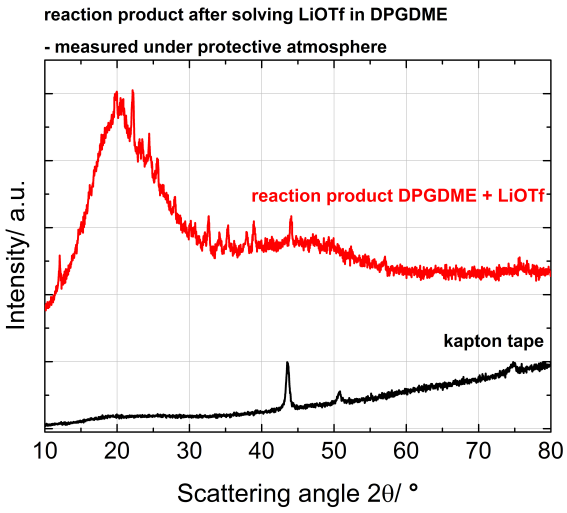

Figure 7.16: Top: X-ray diffraction pattern of the reaction product after dissolving 1 M LiOTf in DPGDME. Bottom: diffraction pattern the Kapton tape that was used to protect the samples from air and water.

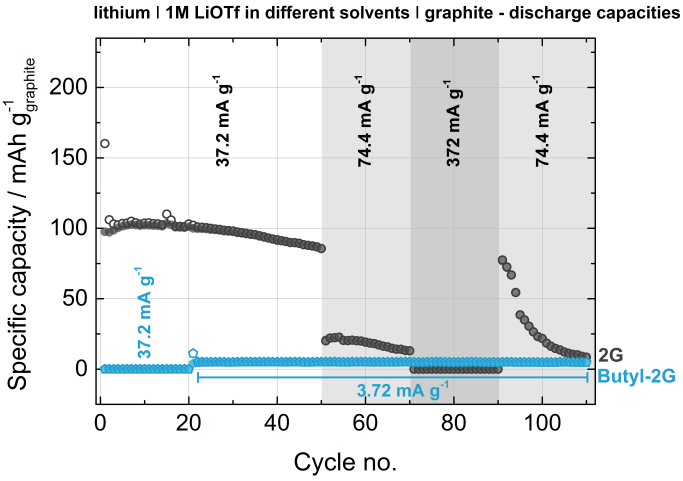

(a) specific capacities

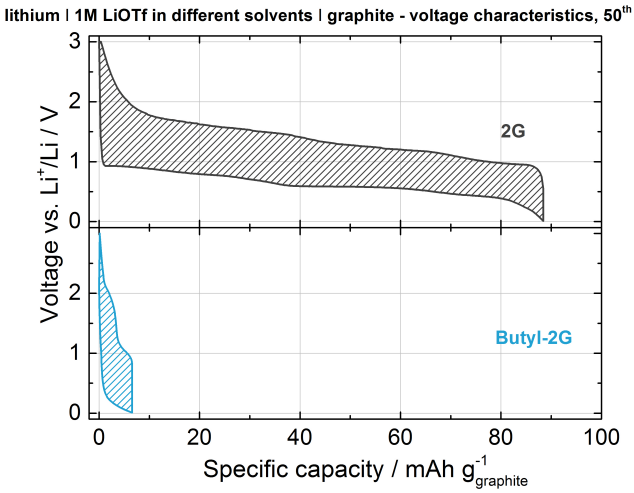

(b) voltage characteristics

Figure 7.17: (a) Specific capacities per cycle at different applied currents and (b) voltage characteristics in the 50^{th} cycle at a constant current of 37.2 $^{\mathrm{mA}}/_{\mathrm{g}}$ of graphite electrodes in sodium half cells in a Butyl-2G based electrolyte.

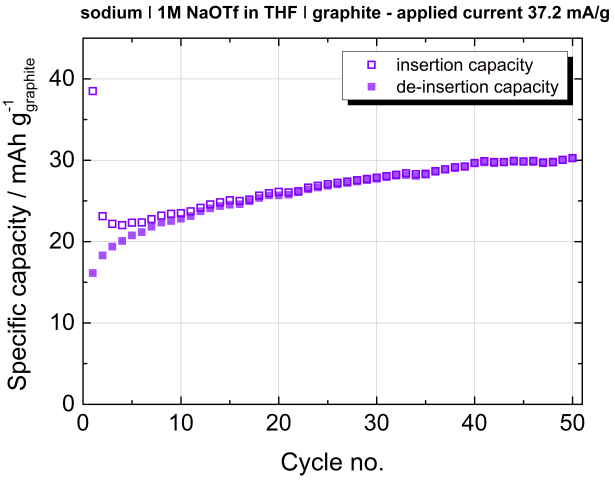

(a) specific capacities

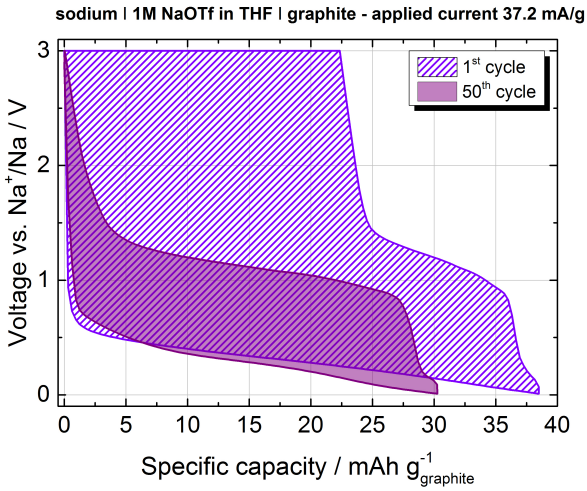

(b) voltage characteristics

Figure 7.18: (a) Specific capacities per cycle and (b) voltage characteristics in the first and 50^{th} cycle at a constant current of 37.2 $^{mA}/_{g}$ of graphite electrodes in sodium half cells in a THF based electrolyte.

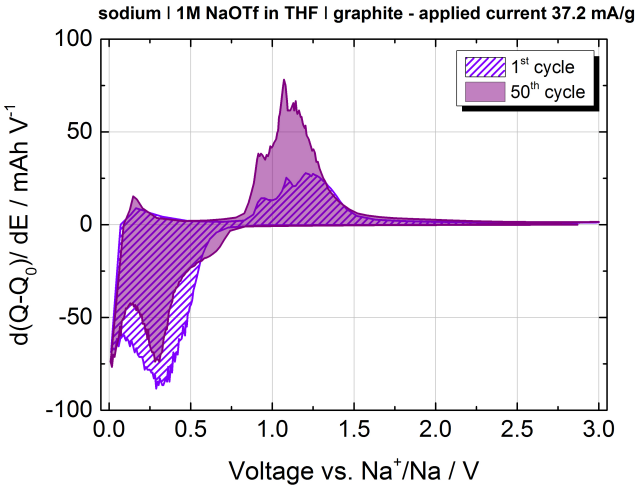

Figure 7.19: Differential capacities in the first and the 50^{th} cycle at a constant current of 37.2 $^{\mathrm{mA}}/_{\mathrm{g}}$ of graphite electrodes in sodium half cells in a in THF based electrolyte.

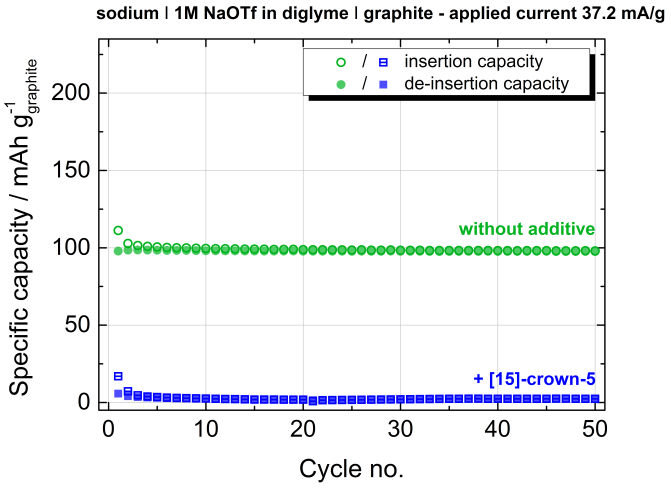

(a) specific capacities

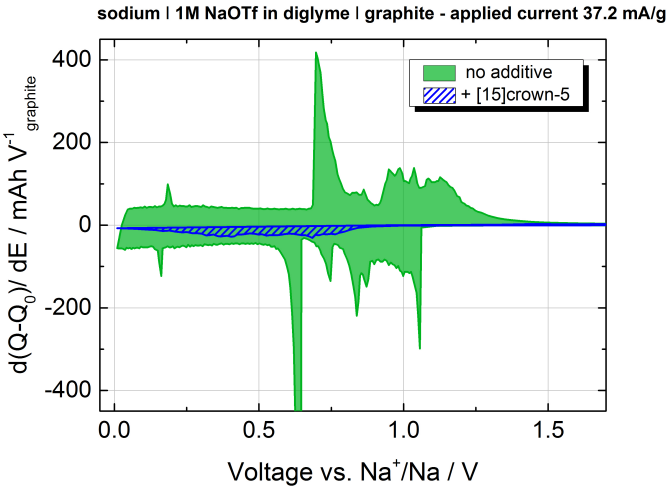

(b) differential capacities

Figure 7.20: (a) Specific capacities per cycle and (b) differential capacities in the first cycle at a constant current of 37.2 $^{\mathrm{mA}}/_{\mathrm{g}}$ of graphite electrodes in sodium half cells in a diglyme or diglyme + 1 M [15]crown-5 based electrolyte.

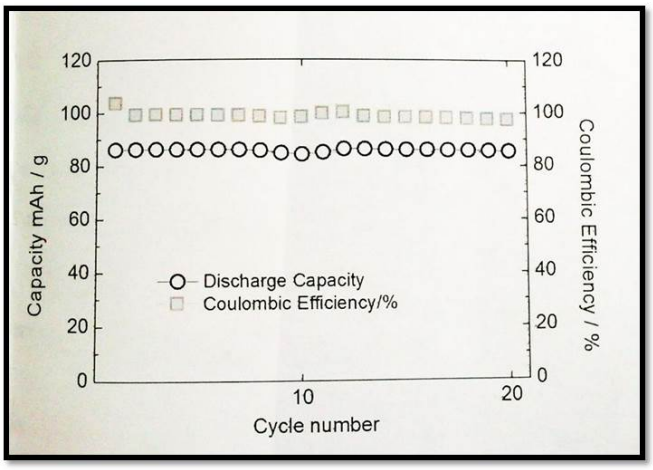

(a) specific capacities and coulombic efficiencies

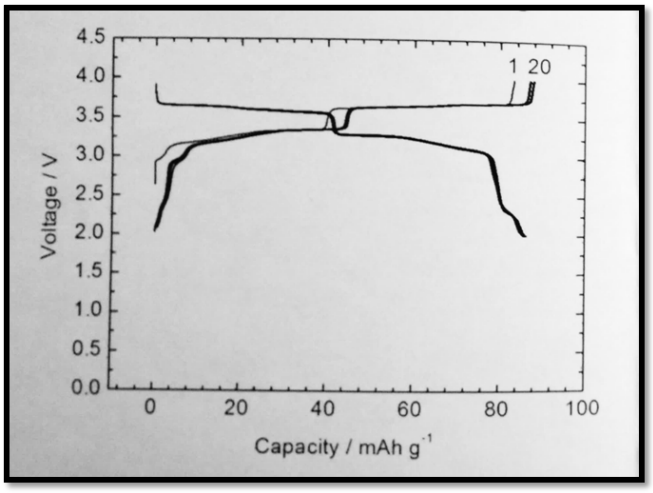

(b) charge/discharge characteristics

Figure 7.21: (a) Specific capacities per cycle and (b) voltage characterisitcs in the first 20 cycles of a NNMO electrode on an aluminium current collector versus sodium metal electrode in a 1 M solution of $NaPF_6$ in PC for 20 cycles at a constant current of 12.05 $^{mA}/_{g}$. Results were recorded and plotted by the group of Prof. Komaba from *Tokyo University of Science*.

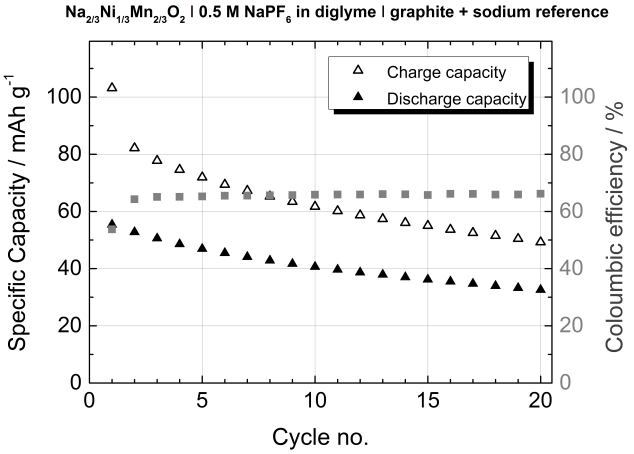

(a) specific capacities and coulombic efficiencies

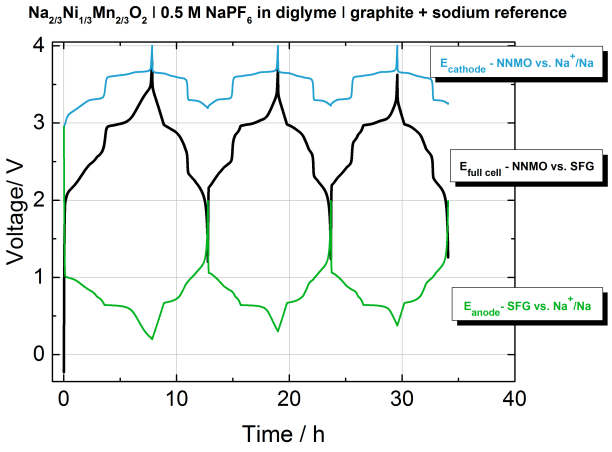

(b) charge/discharge characteristics

Figure 7.22: (a) Specific capacities per cycle and (b) voltage characteristics in the first three cycle at a constant current of 12.04 $^{mA}/_{g}$ (related to NNMO active mass) and additional stop criteria (see corresponding text) of a sodium-ion full cell based on NNMO and graphite in a diglyme based electrolyte.

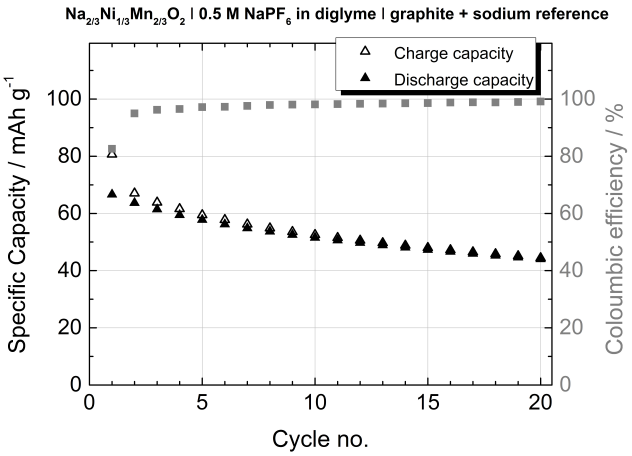

(a) specific capacities and coulombic efficiencies

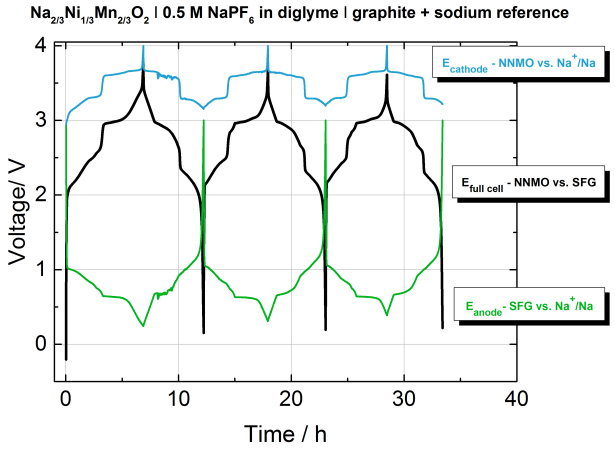

(b) charge/discharge characteristics

Figure 7.23: (a) Specific capacities per cycle and (b) voltage characteristics in the first three cycle at a constant current of 12.04 $^{mA}/_{g}$ (related to NNMO active mass) and additional stop criteria (see corresponding text) of a sodium-ion full cell based on NNMO and graphite with balanced charge storage capacities (see corresponding text) in a diglyme based electrolyte.

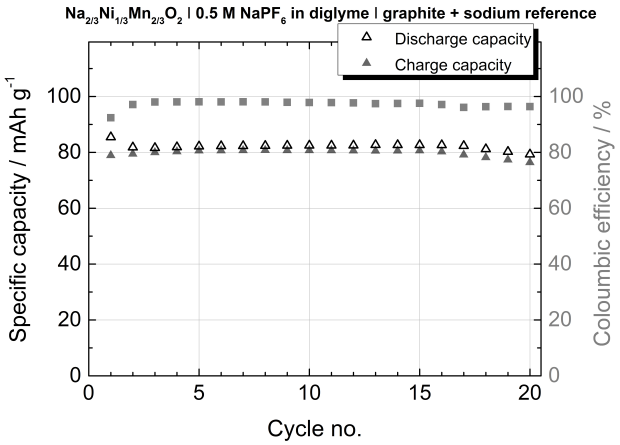

(a) specific capacities and coulombic efficiencies

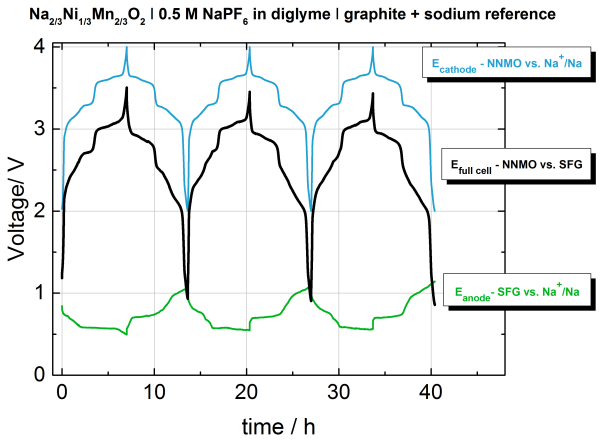

(b) charge/discharge characteristics

Figure 7.24: (a) Specific capacities per cycle and (b) voltage characteristics in the first three cycle at a constant current of 12.04 $^{mA}/_{g}$ (related to NNMO active mass) and additional stop criteria (see corresponding text) of a sodium-ion full cell based on NNMO and graphite with balanced charge storage capacities and a reformed graphite electrode (see corresponding text) in a diglyme based electrolyte.

7.1 Experimental for the Sodium Nickel Manganese Oxide electrodes

The NNMO powder was prepared by the Prof. Komaba group *via* a solid-state reaction. Therefore a stoichiometric mixture of Na_2CO_3, NiO and Mn_2O_3 was ball-milled under wet conditions with acetone addition for 12 hours at 600 rpm. The resulting powder was dried and pressed into pellets which were then heated at 950 °C for 12 hours in air. After this calcination step, the samples were taken out from the still hot furnace, and then immediately transferred into an argon-filled glove box for the cooling process.

Electrode slurries were made from NNMO, acetylene black, polyvinylidenefluoride, and N-methyl-2-pyrrolidone (NMP, *Kanto Chemical Co., Ltd., Japan*). The content of NNMO, acetylene black and binder material was 80:10:10 wt%, respectively. Electrodes were prepared by doctor blading a slurry onto an aluminium foil. Circular electrodes (d=1.2 cm) were punched out and contained 6 mg - 8 mg NNMO as active mass, each. These were further dried at 80 °C under vacuum to evaporate residual NMP and then transferred into an argon-filled glove box, where three-electrode Swagelok type cells or two electrode coin cells (CR2032) for galvanostatic cycling were assembled.

8 Bibliography

[1] B. Jache, P. Adelhelm, "Use of Graphite as a Highly Reversible Electrode with Superior Cycle Life for Sodium-Ion Batteries by Making Use of Co-Intercalation Phenomena", *Angewandte Chemie* **2014**, *53*, 10169–10173.

[2] B. A. Jache, J. O. Binder, T. Abe, P. Adelhelm, "A comparative study on the impact of different glymes and its derivatives as electrolyte solvents for graphite co-intercalation electrodes in lithium-ion and sodium-ion batteries", *Phys. Chem. Chem. Phys.* **2016**, *18*, 14299–14316.

[3] Retrieved October 26th, 2016, from: http://www.energiewende.de/.

[4] Retrieved October 26th, 2016, from: http://www.bmwi.de/DE/Service/gesetze,did=254040.html.

[5] V. L. Chevrier, G. Ceder, "Challenges for Na-ion Negative Electrodes", *Journal of The Electrochemical Society* **2011**, *158*, A1011–A1014.

[6] B. L. Ellis, L. F. Nazar, "Sodium and sodium-ion energy storage batteries", *Current Opinion in Solid State & Materials Science* **2012**, *16*, 168–177.

[7] S.-W. Kim, D.-H. Seo, X. Ma, G. Ceder, K. Kang, "Electrode Materials for Rechargeable Sodium-Ion Batteries: Potential Alternatives to Current Lithium-Ion Batteries", *Advanced Energy Materials* **2012**, *2*, 710–721.

[8] S. Y. Hong, Y. Kim, Y. Park, A. Choi, N.-S. Choi, K. T. Lee, "Charge carriers in rechargeable batteries: Na ions vs. Li ions", *Energy & Environmental Science* **2013**, *6*, 2067–2081.

[9] V. Palomares, M. Casas-Cabanas, E. Castilllo-Martinez, M. H. Han, T. Rojo, "Update on Na-Based Battery Materials. A Growing Research Path", *Energy & Environmental Science* **2013**, *6*, 2312–2337.

[10] H. Pan, Y.-S. Hu, L. Chen, "Room-temperature stationary sodium-ion batteries for large-scale electric energy storage", *Energy & Environmental Science* **2013**, *6*, 2338–2360.

[11] M. D. Slater, D. Kim, E. Lee, C. S. Johnson, "Sodium-Ion Batteries", *Advanced Functional Materials* **2013**, *23*, 947–958.

[12] S. Ha, J.-K. Kim, A. Choi, Y. Kim, K. T. Lee, "Sodium-Metal Halide and Sodium-Air Batteries.", *ChemPhysChem* **2014**, *15*, 1971–1982.

[13] N. Yabuuchi, K. Kubota, M. Dahbi, S. Komaba, "Research Development on Sodium-Ion Batteries", *Chemical Reviews* **2014**, *114*, 11636–11682.

[14] Y. Wang, R. Chen, T. Chen, H. Lv, G. Zhu, L. Ma, C. Wang, Z. Jin, J. Liu, "Emerging non-lithium ion batteries", *Energy Storage Materials* **2016**, *4*, 103–129.

[15] Z. Lu, J. Dahn, "*In Situ* X-Ray Diffraction Study of P2-$Na_{2/3}[Ni_{1/3}Mn_{2/3}]O_2$", *Journal of The Electrochemical Society* **2001**, *148*, A1225–A1229.

[16] R. Berthelot, D. Carlier, C. Delmas, "Electrochemical investigation of the P2-Na_xCoO_2 phase diagram.", *Nature Materials* **2011**, *10*, 74–80.

[17] D. Buchholz, A. Moretti, R. Kloepsch, S. Nowak, V. Siozios, M. Winter, S. Passerini, "Toward Na-ion Batteries –Synthesis and Characterization of a Novel High Capacity Na Ion Intercalation Material", *Chemistry of Materials* **2013**, *25*, 142–148.

[18] H. Yoshida, N. Yabuuchi, K. Kubota, I. Ikeuchi, A. Garsuch, M. Schulz - Dobrick, S. Komaba, "P2-type $Na_{2/3}Ni_{1/3}Mn_{2/3-x}Ti_xO_2$ as a new positive electrode for higher energy Na-ion batteries", *Chemical Communications* **2014**, *50*, 3677–3680.

[19] M. Dahbi, N. Yabuuchi, K. Kubota, K. Tokiwa, S. Komaba, "Negative electrodes for Na-ion batteries.", *Physical Chemistry Chemical Physics* **2014**, *16*, 15007–15028.

[20] C. Bommier, X. Ji, "Recent Development on Anodes for Na-Ion Batteries", *Israel Journal of Chemistry* **2015**, *55*, 486–507.

[21] W. Luo, F. Shen, C. Bommier, H. Zhu, X. Ji, L. Hu, "Na-Ion Battery Anodes: Materials and Electrochemistry", *Accounts of Chemical Research* **2016**, *49*, 231–240.

[22] M.-S. Balogun, Y. Luo, W. Qiu, P. Liu, Y. Tong, "A review of carbon materials and their composites with alloy metals for sodium ion battery anodes", *Carbon* **2016**, *98*, 162–178.

[23] M. S. Whittingham, "Electrical Energy Storage and Intercalation Chemistry", *Science* **1976**, *192*, 1126–1127.

[24] G. H. Newman, L. P. Klemann, "Ambient Temperature Cycling of an Na-TiS_2 Cell", *Journal of The Electrochemical Society* **1980**, *127*, 2097–2099.

[25] K. Mizushima, P. C. Jones, P. J. Wiseman, J. B. Goodenough, "Li_xCoO_2 ($0<x<1$): A new Cathode Material for Batteries of High Energy Density", *Materials Research Bulletin* **1980**, *15*, 783–789.

[26] C. Delmas, C. Foucassier, P. Hagenmuller, "Structural classification and properties of the layered oxides", *Physica B* **1980**, *99*, 81–85.

[27] L. W. Shacklette, T. R. Jow, L. Townsend, "Rechargeable Electrodes from Sodium Cobalt Bronzes", *Journal of The Electrochemical Society* **1988**, *135*, 2669–2674.

[28] K. M. Abraham, "Intercalation Positive Electrodes for Rechargeable Sodium Cells", *Solid State Ionics* **1982**, *7*, 199–212.

[29] E. Peled, "The Electrochemical Behavior of Alkali and Alkaline Earth Metals in Nonaqueous Battery Systems – The Solid Electrolyte Interphase Model", *Journal of The Electrochemical Society* **1979**, *126*, 2047–2051.

[30] Retrieved October 26th, 2016, from: http://www.sony.net.

[31] R. C. Asher, "A lamellar compound of sodium and graphite", *Journal of Inorganic and Nuclear Chemistry* **1959**, *10*, 238–249.

[32] P. Ge, M. Fouletier, "Electrochemical intercalation of sodium in graphite", *Solid State Ionics* **1988**, *28-30*, 1172–1175.

[33] M. M. Doeff, Y. Ma, S. J. Visco, L. C. de Jonghe, "Electrochemical Insertion of Sodium into Carbon", *Journal of The Electrochemical Society* **1993**, *140*, 169–170.

[34] K. Nobuhara, H. Nakayama, M. Nose, S. Nakanishi, H. Iba, "First-principles study of alkali metal-graphite intercalation compounds", *Journal of Power Sources* **2013**, *243*, 585–587.

[35] J. Kummer, N. Weber, "A Sodium-Sulfur Secondary Battery", *Proceedings of the Annual Power Sources Conference* **1967**, *21*.

[36] P. Hartmann, C. L. Bender, M. Vračar, A. K. Dürr, A. Garsuch, J. Janek, P. Adelhelm, "A rechargeable room-temperature sodium superoxide (NaO_2) battery.", *Nature Materials* **2013**, *12*, 228–32.

[37] D. Monti, E. Jónsson, M. R. Palacín, P. Johansson, "Ionic liquid based electrolytes for sodium-ion batteries: Na^+ solvation and ionic conductivity", *Journal of Power Sources* **2014**, *245*, 630–636.

[38] W. R. McKinnon, J. R. Dahn, "Structure and electrochemistry of $Li_xMo_6S_8$", *Physical Review B* **1985**, *31*, 3084–3087.

[39] D. Aurbach, A. Zaban, A. Schechter, Y. Ein-Eli, E. Zinigrad, B. Markovsky, "The Study of Electrolyte Solutions Based on Ethylene and Diethyl Carbonates for Rechargeable Li Batteries", *Journal of The Electrochemical Society* **1995**, *142*, 2873–2882.

[40] D. Aurbach, "Review of selected electrode – solution interactions which determine the performance of Li and Li ion batteries", *Journal of Power Sources* **2000**, *89*, 206–218.

[41] D. Lisbona, T. Snee, "A review of hazards associated with primary lithium and lithium-ion batteries", *Process Safety and Environmental Protection* **2011**, *89*, 434–442.

[42] M. Ishikawa, M. Morita in *Lithium Batteries Science and Technology*, **2009**, Chapter 10, pp. 297 –312.

[43] D. Fauteux, R. Koksbang, "Rechargeable lithium battery anodes: alternatives to metallic lithium", *Journal of Applied Eectrochemistry* **1993**, *23*, 1–10.

[44] P. Adelhelm, P. Hartmann, C. L. Bender, M. Busche, C. Eufinger, J. Janek, "From lithium to sodium: cell chemistry of room temperature sodium-air and sodium-sulfur batteries", *Beilstein Journal of Nanotechnology* **2015**, *6*, 1016–1055.

[45] E. Peled, D. Golodnitsky, H. Mazor, M. Goor, S. Avshalomov, "Parameter analysis of a practical lithium- and sodium-air electric vehicle battery", *Journal of Power Sources* **2011**, *196*, 6835–6840.

[46] Z. W. Seh, J. Sun, Y. Sun, Y. Cui, "A Highly Reversible Room-Temperature Sodium Metal Anode", *ACS Central Science* **2015**, *1*, 449–455.

[47] W. Rüdorff, U. Hofmann, "Über Graphitsalze", *Zeitschrift für anorganische und allgemeine Chemie* **1938**, *238*, 1–50.

[48] W. Rüdorff, E. Schulze, "Über Alkaligraphitverbindungen", *Zeitschrift für anorganische und allgemeine Chemie* **1954**, *277*, 156–171.

[49] W. Rüdorff, "Einlagerungsverbindungen mit Alkali- und Erdalkalimetallen", *Angewandte Chemie* **1959**, *15/16*, 487–491.

[50] D. P. DiVincenzo, E. J. Mele, "Cohesion and structure in stage-1 graphite intercalaction compounds", *Physical Review B* **1985**, *32*, 2538–2553.

[51] M. Winter, J. O. Besenhard, M. E. Spahr, P. Novak, "Insertion electrode materials for rechargeable lithium batteries", *Advanced Materials* **1998**, *10*, 725–763.

[52] M. Yoshio, R. J. Brodd, A. Kozawa, *Lithium-ion batteries: Science and technologies: Carbon Anode materials*, Springer New York, **2009**, pp. 49–73.

[53] M. Winter, J. Besenhard in *Handbook of Battery Materials*, Wiley-VCH Verlag GmbH & Co. KGaA, Weinheim, **2011**, Chapter 15, pp. 433–478.

[54] J. Sangster, "C-Na (Carbon-Sodium) System", *Journal of Phase Equilibria and Diffusion* **2007**, *28*, 571–579.

[55] W. S. Hummers, R. E. Offeman, "Preparation of Graphitic Oxide", *J. Am. Chem. Soc* **1958**, *80*, 1339.

[56] Y. Wen, K. He, Y. Zhu, F. Han, Y. Xu, I. Matsuda, Y. Ishii, J. Cumings, C. Wang, "Expanded graphite as superior anode for sodium-ion batteries.", *Nature Communications* **2014**, *5*, 4033–4042.

[57] D. A. Stevens, J. R. Dahn, "High Capacity Anode Materials for Rechargeable Sodium-Ion Batteries", *Journal of The Electrochemical Society* **2000**, *147*, 1271–1273.

[58] D. A. Stevens, J. R. Dahn, "The Mechanisms of Lithium and Sodium Insertion in Carbon Materials", *Journal of The Electrochemical Society* **2001**, *148*, A803–A811.

[59] P. Thomas, D. Billaud, "Electrochemical insertion of sodium into hard carbons", *Electrochimica Acta* **2002**, *47*, 3303–3307.

[60] S. Komaba, W. Murata, T. Ishikawa, N. Yabuuchi, T. Ozeki, T. Nakayama, A. Ogata, K. Gotoh, K. Fujiwara, "Electrochemical Na Insertion and Solid Electrolyte Interphase for Hard-Carbon Electrodes and Application to Na-Ion Batteries", *Advanced Functional Materials* **2011**, *21*, 3859–3867.

[61] A. Ponrouch, A. R. Goñi, M. R. Palacín, "High capacity hard carbon anodes for sodium ion batteries in additive free electrolyte", *Electrochemistry Communications* **2013**, *27*, 85–88.

[62] J. Zhao, L. Zhao, K. Chihara, S. Okada, J. Yamaki, S. Matsumoto, S. Kuze, K. Nakane, "Electrochemical and thermal properties of hard carbon-type anodes for Na-ion batteries", *Journal of Power Sources* **2013**, *244*, 752–757.

[63] S. Kuze, J. Kageura, S. Matsumoto, T. Nakayama, M. Makidera, M. Saka, T. Yamaguchi, T. Yamamoto, K. Nakane, Development of a Sodium Ion Secondary Battery, tech. rep., Sumitomo Chemical Co., Ltd., Osaka/Tokyo (Japan), **2013**, pp. 1–13.

[64] S. Wenzel, T. Hara, J. Janek, P. Adelhelm, "Room-temperature sodium-ion batteries: Improving the rate capability of carbon anode materials by templating strategies", *Energy & Environmental Science* **2011**, *4*, 3342–3345.

[65] H. Wang, Z. Wu, F. Meng, D. Ma, X. Huang, L. Wang, X. Zhang, "Nitrogen-doped porous carbon nanosheets as low-cost, high-performance anode material for sodium-ion batteries.", *ChemSusChem* **2013**, *6*, 56–60.

[66] K. Tang, L. Fu, R. J. White, L. Yu, M.-M. Titirici, M. Antonietti, J. Maier, "Hollow Carbon Nanospheres with Superior Rate Capability for Sodium-Based Batteries", *Advanced Energy Materials* **2012**, *2*, 873–877.

[67] Y. Cao, L. Xiao, M. L. Sushko, W. Wang, B. Schwenzer, J. Xiao, Z. Nie, L. V. Saraf, Z. Yang, J. Liu, "Sodium ion insertion in hollow carbon nanowires for battery applications.", *Nano Letters* **2012**, *12*, 3783–3787.

[68] F. Klein, B. Jache, A. Bhide, P. Adelhelm, "Conversion reactions for sodium-ion batteries", *Physical Chemistry Chemical Physics* **2013**, *15*, 15876–87.

[69] M. Mortazavi, J. Deng, V. B. Shenoy, N. V. Medhekar, "Elastic softening of alloy negative electrodes for Na-ion batteries", *Journal of Power Sources* **2013**, *225*, 207–214.

[70] M. K. Datta, R. Epur, P. Saha, K. Kadakia, S. K. Park, P. N. Kumta, "Tin and graphite based nanocomposites: Potential anode for sodium ion batteries", *Journal of Power Sources* **2013**, *225*, 316–322.

[71] D. Su, H.-J. Ahn, G. Wang, "SnO_2@graphene nanocomposites as anode materials for Na-ion batteries with superior electrochemical performance.", *Chemical Communications* **2013**, *49*, 3131–3133.

[72] L. Wu, X. Hu, J. Qian, F. Pei, F. Wu, R. Mao, X. Ai, H. Yang, Y. Cao, "A Sn – SnS – C nanocomposite as anode host materials for Na-ion batteries", *Journal of Materials Chemistry A* **2013**, *1*, 7181–7184.

[73] Y. Xu, Y. Zhu, Y. Liu, C. Wang, "Electrochemical Performance of Porous Carbon/Tin Composite Anodes for Sodium-Ion and Lithium-Ion Batteries", *Advanced Energy Materials* **2013**, *3*, 128–133.

[74] A. Darwiche, C. Marino, M. T. Sougrati, B. Fraisse, L. Stievano, L. Monconduit, "Better cycling performances of bulk Sb in Na-ion batteries compared to Li-ion systems: an unexpected electrochemical mechanism.", *Journal of the American Chemical Society* **2012**, *134*, 20805–20811.

[75] M. M. Doeff, J. Cabana, M. Shirpour, "Titanate Anodes for Sodium Ion Batteries", *Journal of Inorganic and Organometallic Polymers and Materials* **2014**, *24*, 5–14.

[76] A. Ponrouch, E. Marchante, M. Courty, J. M. Tarascon, M. R. Palacin, "In search of an optimized electrolyte for Na-ion batteries", *Energy & Environmental Science* **2012**, *5*, 8572–8583.

[77] A. Bhide, J. Hofmann, A. K. Dürr, J. Janek, P. Adelhelm, "Electrochemical stability of non-aqueous electrolytes for sodium-ion batteries and their compatibility with $Na_{0.7}CoO_2$.", *Physical Chemistry Chemical Physics* **2014**, *16*, 1987–1998.

[78] K. Xu, "Electrolytes and Interphases in Li-Ion Batteries and Beyond", *Chemical Reviews* **2014**, *114*, 11503–11618.

[79] A. Ponrouch, D. Monti, A. Boschin, B. Steen, P. Johansson, M. R. Palacín, "Non-aqueous electrolytes for sodium-ion batteries", *J. Mater. Chem. A* **2015**, *3*, 22–42.

[80] J. O. Binder, Master Thesis: Elektrochemische Untersuchungen zum Einfluss der Elektrolytzusammensetzung auf das Interkalationsverhalten von Natriumionen in nichtgraphitische Kohlenstoffmaterialien, tech. rep., Justus-Liebig-University, Gießen, **2015**.

[81] X. Xia, J. R. Dahn, "Study of the Reactivity of Na/Hard Carbon with Different Solvents and Electrolytes", *Journal of The Electrochemical Society* **2012**, *159*, A515–A519.

[82] S. Komaba, T. Ishikawa, N. Yabuuchi, W. Murata, A. Ito, Y. Ohsawa, "Fluorinated Ethylene Carbonate as Electrolyte Additive for Rechchargeable Na Batteries", *Applied Materials and Interfaces* **2011**, *3*, 4165–4168.

[83] A. N. Dey, B. P. Sullivan, "The Electrochemical Decomposition of Propylene Carbonate on Graphite", *Journal of The Electrochemical Society* **1970**, *117*, 222–224.

[84] G. Eichinger, "Graphite electrodes", *Journal of Electroanalytical Chemistry* **1976**, *74*, 183–193.

[85] M. Arakawa, J. Yamaki, "The cathodic decomposition of propylene carbonate in lithium batteries", *Journal of Electroanalytical Chemistry and Interfacial Electrochemistry* **1987**, *219*, 273–280.

[86] S. Tobishima, H. Morimoto, M. Aoki, Y. Saito, T. Inose, T. Fukumoto, T. Kuryu, "Glyme-based nonaqueous electrolytes for rechargeable lithium cells", *Electrochimica Acta* **2004**, *49*, 979–987.

[87] P. G. Bruce, L. J. Hardwick, K. M. Abraham, "Lithium-air and lithium-sulfur batteries", *MRS Bulletin* **2011**, *36*, 506–512.

[88] P. G. Bruce, S. A. Freunberger, L. J. Hardwick, J. M. Tarascon, "Li-O_2 and Li-S batteries with high energy storage", *Nature Materials* **2012**, *11*, 19–29.

[89] D. Aurbach, E. Granot, "The study of electrolyte solutions based on solvents from the 'glyme' family (linear polyethers) for secondary Li battery systems", *Electrochimica acta* **1997**, *42*, 697–718.

[90] T. Matsui, K. Takeyama, "Li^+ adsorption on a metal electrode from glymes", *Electrochimica Acta* **1998**, *43*, 1355–1360.

[91] C. L. Bender, B. Jache, A. Philipp, J. Janek, "Sodiated carbon: A reversible anode for the sodium-oxygen battery and route for the chemical synthesis of sodium superoxide (NaO_2)", *Journal of Materials Chemistry A* **2015**, *3*, 20633–20641.

[92] C. Schafhaeutl, "Ueber die Verbindungen des Kohlenstoffes mit Silicium, Eisen und anderen Metallen, welche die verschiedenen Gattungen von Roheisen, Stahl und Schmiedeeisen bilden.", *Journal für Praktische Chemie* **1840**, *21*, 129–157.

[93] J. Aleman, A. V. Chadwick, J. He, M. Hess, K. Horie, R. G. Jones, P. Kratochvil, I. Meisel, I. Mita, G. Moad, S. Penczek, R. F. T. Stepto, "Definitions of terms relating to the structure and processing of sols, gels, networks, and inorganic-organic hybrid materials", *Pure and Applied Chemistry* **2007**, *79*, 1801–1829.

[94] K. Abraham, "Status of rechargeable positive electrodes for ambient temperature lithium batteries", *Journal of Power Sources* **1982**, *7*, 1–43.

[95] L. B. Ebert, "Intercalation compounds of graphite", *Annual Review of Material Science* **1976**, *6*, 181–211.

[96] M. S. Dresselhaus, G. Dresselhaus, "Intercalation compounds of graphite", *Advances in Physics* **1981**, 139–326.

[97] S. A. Solin, H. Zabel, "The physics of ternary graphite intercalation compounds", *Advances in Physics* **1988**, *37*, 87–254.

[98] H.-P. Boehm, R. Setton, E. Stumpp, "Nomenclature and terminology of graphite intercalation compounds", *Pure and Applied Chemistry* **1994**, *66*, 1893–1901.

[99] S. Flandrois, "Graphite intercalation compounds as electrode materials in batteries", *Synthetic metals* **1982**, *4*, 255–266.

[100] M. Noel, R. Santhanam, "Electrochemistry of graphite intercalation compounds", *Journal of Power Sources* **1998**, *72*, 53–65.

[101] M. S. Dresselhaus, "Intercalation In Layered Materials", *Springer Science + Business Media New York LLC* **1986**, *12*, (Ed.: M. S. Dresselhaus), 24–28.

[102] M. S. Dresselhaus, "Intercalation In Layered Materials", *MRS Bulletin* **1987**, *12*, 24–28.

[103] D. Ginderow, R. Setton, "New graphite lamellar compounds", *Carbon* **1968**, *6*, 81–83.

[104] J. O. Besenhard, H. P. Fritz, "Cathodic reduction of graphite in organic solutions of alkali and NR_4^+ salts", *Electroanalytical Chemistry and Interfacial Electrochemistry* **1974**, *53*, 329–333.

[105] J. O. Besenhard, "The electrochemical preparation and properties of ionic alkali metal-and NR_4-graphite intercalation compounds in organic electrolytes", *Carbon* **1976**, *14*, 111–115.

[106] J. O. Besenhard, H. P. Fritz, "The Electrochemistry of Black Carbons", *Angewandte Chemie International Edition* **1983**, *22*, 950–975.

[107] P. Schoderböck, H. P. Boehm, "Observations of staging in the electrochemical intercalation of lithium into graphite from dimethyl sulfoxide solutions", *Synthetic metals* **1991**, *44*, 239–246.

[108] Y. Mizutani, T. Abe, K. Ikeda, E. Ihara, M. Asano, T. Harada, M. Inaba, Z. Ogumi, "Graphite intercalation compounds prepared in solutions of alkali metals in 2-methyltetrahydrofuran and 2,5-dimethyltetrahydrofuran", *Carbon* **1997**, *35*, 61–65.

[109] J. O. Besenhard, H. P. Fritz, H. Möhwald, J. J. Nickl, "Elektrochemische Intercalation und elektrische Leitfähigkeit von Graphitfasern", *Zeitschrift für Naturforschung* **1978**, *33b*, 737–739.

[110] Y. Hernandez, V. Nicolosi, M. Lotya, F. M. Blighe, Z. Sun, S. De, I. T. McGovern, B. Holland, M. Byrne, Y. Gunko, J. Boland, P. Niraj, G. Duesberg, S. Krishnamurti, R. Goodhue, J. Hutchison, V. Scardaci, A. C. Ferrari, J. N. Coleman, "High yield production of graphene by liquid phase exfoliation of graphite", *Nature Nanotechnology* **2008**, *3*, 563–8.

[111] M. Winter, G. H. Wrodnigg, J. O. Besenhard, W. Biberacher, P. Novák, "Dilatometric Investigations of Graphite Electrodes in Nonaqueous Lithium Battery Electrolytes", *Journal of the Electrochemical Society* **2000**, *147*, 2427–2431.

[112] D. Liu, Z. Yang, W. Li, S. Qiu, Y. Luo, "Electrochemical intercalation of potassium into graphite in KF melt", *Electrochimica Acta* **2010**, *55*, 1013–1018.

[113] Y. Liu, F. Fan, J. Wang, Y. Liu, H. Chen, K. L. Jungjohann, Y. Xu, Y. Zhu, D. Bigio, T. Zhu, C. Wang, "In Situ Transmission Electron Microscopy Study of Electrochemical Sodiation and Potassiation of Carbon Nanofibers", *Nano Letters* **2014**, *14*, 3445–3452.

[114] H. Kim, J. Hong, G. Yoon, H. Kim, K.-Y. Park, M.-S. Park, W.-S. Yoon, K. Kang, "Sodium intercalation chemistry in graphite", *Energy Environ. Sci.* **2015**, *8*, 2963–2969.

[115] D. D. L. Chung, "Structural studies of graphite intercalation compounds", *Journal of Electronic Materials* **1978**, *7*, 189–210.

[116] X. Zhang, N. Sukpirom, M. M. Lerner, "Graphite intercalation of Bis(Trifluoromethanesulfonyl)imide and other anions with perfuoroalkanesulfonyl substituents", *Materials Research Bulletin* **1998**, *34*, 363–372.

[117] A. Hightower, C. C. Ahn, B. Fultz, P. Rez, "Electron energy-loss spectrometry on lithiated graphite", *Applied Physics Letters* **2000**, *77*, 238–240.

[118] M. J. Henderson, J. W. White, "An X-ray Diffraction and Small Angle X-ray Scattering Study of Solvated Li-Graphite Intercalation Compounds", *International Journal of Energy Engineering* **2011**, *1*, 19–26.

[119] G. Schmuelling, T. Placke, R. Kloepsch, O. Fromm, H.-W. Meyer, S. Passerini, M. Winter, "X-ray diffraction studies of the electrochemical intercalation of bis(trifluoromethanesulfonyl)imide anions into graphite for dual-ion cells", *Journal of Power Sources* **2013**, *239*, 563–571.

[120] W. Metz, D. Hohlwein, "Charakterisierung von Graphit-$FeCl_3$-Verbindungen als teilweise geordnete Schichtstrukturen", *Carbon* **1975**, *13*, 87–96.

[121] Y.-C. Su, Z.-M. Ying, Z.-Y. Xu, "Intercalation mechanisms of lithium into graphitized needle cokes", *Trans. Nonferrous Met. Soc. China* **2001**, *11*, 551–554.

[122] N. Daumas, A. Herold, "Relations between phase concept and reaction mechanics in graphite insertion compounds", *Comptes rendus hebdomadaires des seances de l'academie des sciences serie C* **1969**, *268*, 373–382.

[123] M. Heerschap, P. Delavignette, S. Amelinckx, "Electron microscope study of interlamellar compounds of graphite with bromine, iodine monochloride and ferric chloride", *Carbon* **1964**, *1*, 235–238.

[124] C. Sole, N. E. Drewett, L. J. Hardwick, "In situ Raman study of lithium-ion intercalation into microcrystalline graphite", *Faraday Discussions* **2014**, *172*, 223–237.

[125] T. Abe, Y. Mizutani, N. Shinoda, E. Ihara, M. Asano, T. Harada, M. Inaba, Z. Ogumi, "Debye-Waller factors of $FeCl_3$- and ICl-graphite intercalation compounds", *Carbon* **1995**, *33*, 1789–1793.

[126] N. Shinoda, Master Thesis: Structural analysis and determinations of Debye-Waller factors for graphite intercalation compounds, tech. rep., Kyoto University, Kyoto, **1996**.

[127] K. Ikeda, Master Thesis: Alkali-metal-solvent co-intercalation systems, tech. rep., Kyoto University, Kyoto, **1997**.

[128] Y. Mizutani, T. Abe, M. Inaba, Z. Ogumi, "Creation of nanospaces by intercalation of alkali metals into graphite in organic solutions", *Synthetic metals* **2002**, *125*, 153–159.

[129] B. Jache, B. Mogwitz, F. Klein, P. Adelhelm, "Copper sulfides for rechargeable lithium batteries: Linking cycling stability to electrolyte composition", *Journal of Power Sources* **2014**, *247*, 703–711.

[130] J. O. Binder, Research project: XRD-Analyse von chemisch hergestellten ternären Na- bzw. Li-Interkalationsverbindungen, tech. rep., Justus-Liebig-University, Gießen, **2015**.

[131] T. Placke, G. Schmuelling, R. Kloepsch, P. Meister, O. Fromm, P. Hilbig, H.-W. Meyer, M. Winter, "In situ X-ray Diffraction Studies of Cation and Anion Intercalation into Graphitic Carbons for Electrochemical Energy Storage Applications", *Zeitschrift für anorganische und allgemeine Chemie* **2014**, *640*, 1996–2006.

[132] S. Komaba, T. Hasegawa, M. Dahbi, K. Kubota, "Potassium intercalation into graphite to realize high-voltage/high-power potassium-ion batteries and potassium-ion capacitors", *Electrochemistry Communications* **2015**, *60*, 172–175.

[133] Z. Jian, Z. Xing, C. Bommier, Z. Li, X. Ji, "Hard Carbon Microspheres: Potassium-Ion Anode Versus Sodium-Ion Anode", *Advanced Energy Materials* **2016**, *6*, 1–5.

[134] W. Markle, N. Tran, D. Goers, M. E. Spahr, P. Novak, "The influence of electrolyte and graphite type on the PF_6^- intercalation behaviour at high potentials", *Carbon* **2009**, *47*, 2727–2732.

[135] T. Placke, P. Bieker, S. F. Lux, O. Fromm, H.-W. Meyer, S. Passerini, M. Winter, "Dual-ion Cells Based on Anion Intercalation into Graphite from Ionic Liquid-Based Electrolytes", *Zeitschrift für Physikalische Chemie* **2012**, *226*, 391–407.

[136] W.-C. Oh, S.-J. Cho, Y.-S. Ko, "The stability of potassium-graphite deintercalation compounds", *Carbon* **1996**, *34*, 209–215.

[137] K. Xu, "Nonaqueous liquid electrolytes for lithium-based rechargeable batteries.", *Chemical Reviews* **2004**, *104*, 4303–4417.

[138] J. O. Besenhard, M. Winter, J. Yang, W. Biberacher, "Filming mechanism of lithium-carbon anodes in organic and inorganic electrolytes", *Journal of Power Sources* **1995**, *54*, 228–231.

[139] W. Schalkwijk, B. Scrosati in *Advances in Lithium-Ion Batteries*, Kluwer Academic/ Plenum Publishers, New York, **2002**, Chapter 2, pp. 40–47.

[140] Y. Yamada, Y. Takazawa, K. Miyazaki, T. Abe, "Electrochemical Lithium Intercalation into Graphite in Dimethyl Sulfoxide-Based Electrolytes: Effect of Solvation Structure of Lithium Ion", *The Journal of Physical Chemistry C* **2010**, *114*, 11680–11685.

[141] H. Moon, R. Tatara, T. Mandai, K. Ueno, K. Yoshida, N. Tachikawa, T. Yasuda, K. Dokko, M. Watanabe, "Mechanism of Li Ion Desolvation at the Interface of Graphite Electrode and Glyme – Li Salt Solvate Ionic Liquids", *The Journal of Physical Chemistry C* **2014**, *118*, 20246–20256.

[142] J. O. Besenhard, H. Möhwald, J. J. Nickl, "Electronic conductivity and structure of DMSO-solvated A^+ - and NR_4^+-graphite intercalation compounds", *Carbon* **1980**, *18*, 399–405.

[143] T. Abe, H. Fukuda, Y. Iriyama, Z. Ogumi, "Solvated Li-Ion Transfer at Interface Between Graphite and Electrolyte", *Journal of The Electrochemical Society* **2004**, *151*, A1120–A1123.

[144] O. Tanaike, M. Inagaki, "Effect of ether coordination for sodium intercalation into poly(vinylchloride) cokes with different graphitization degree", *Synthetic metals* **1998**, *96*, 109–116.

[145] M. Inagaki, O. Tanaike, "Determining factors for the intercalation into carbon materials from organic solutions", *Carbon* **2001**, *39*, 1083–1090.

[146] T. Maluangnont, W. Sirisaksoontorn, M. M. Lerner, "A comparative structural study of ternary graphite intercalation compounds containing alkali metals and linear or branched amines", *Carbon* **2012**, *50*, 597–602.

[147] T. Abe, N. Kawabata, Y. Mizutani, M. Inaba, Z. Ogumi, "Correlation Between Cointercalation of Solvents and Electrochemical Intercalation of Lithium into Graphite in Propylene Carbonate Solution", *Journal of The Electrochemical Society* **2003**, *150*, A257–A261.

[148] A. F. Holleman, E. Wiberg, N. Wiberg in *Lehrbuch der Anorganischen Chemie*, *Vol. 102*, Walter de Gruyter & Co., Berlin, New York, **2007**, Chapter 20, pp. 1315–1400.

[149] C. J. Pedersen, H. K. Frensdorff, "Macrocyclic polyethers and their complexes.", *Angewandte Chemie International ed.* **1972**, *11*, 16–25.

[150] A. F. Holleman, E. Wiberg, N. Wiberg in *Lehrbuch der Anorganischen Chemie*, Walter de Gruyter & Co., Berlin, New York, **2007**, Chapter 18, pp. 1259–1299.

[151] M. E. Spahr in *Lithium-Ion Batteries: Science and Technologies*, *Vol. 1*, (Eds.: M. Yoshio, R. Brodd, A. Kozawa), Springer New York, New York, **2009**, Chapter 5, pp. 117–154.

[152] J. O. Binder, Research project: XRD-Analyse der Co-Interkalationsprozesse von $Natrium(Diglyme)_2$- und $Lithium(Diglyme)_2$-Komplexen in Graphit-Elektroden, tech. rep., Justus-Liebig-University, Gießen, **2015**.

[153] Z. Ogumi, H. Wang in *Lithium-Ion Batteries: Science and Technologies*, (Eds.: M. Yoshio, R. Brodd, A. Kozawa), Springer New York, New York, **2009**, pp. 49–73.

[154] T. Ohzuku, Y. Iwakoshi, K. Sawai, "Formation of Lithium-Graphite Intercalation Compounds in Nonaqueous Electrolytes and Their Application as a Negative Electrode for a Lithium Ion (Shuttlecock) Cell", *Journal of The Electrochemical Society* **1993**, *140*, 2490–2498.

[155] M. Winter, W. K. Appel, B. Evers, T. Hodal, K.-C. Möller, I. Schneider, M. Wachtler, M. R. Wagner, G. H. Wrodnigg, J. Besenhard, "Studies on the Anode/Electrolyte Interface in Lithium Ion Batteries", *Monatshefte für Chemie* **2001**, *132*, 473–486.

[156] H. Kim, J. Hong, Y.-U. Park, J. Kim, I. Hwang, K. Kang, "Sodium Storage Behavior in Natural Graphite using Ether-based Electrolyte Systems", *Advanced Functional Materials* **2015**, *25*, 534–541.

[157] J. Wang, J. Polleux, J. Lim, B. Dunn, "Pseudocapacitive contributions to electrochemical energy storage in TiO_2 (anatase) nanoparticles", English, *Journal of Physical Chemistry C* **2007**, *111*, 14925–14931.

[158] M. Opitz, J. Yue, J. Wallauer, B. Smarsly, B. Roling, "Mechanisms of charge storage in nanoparticulate TiO_2 and $Li_4Ti_5O_{12}$ anodes: New insights from scan rate-dependent cyclic voltammetry", *Electrochimica Acta* **2015**, *168*, 125–132.

[159] P. Yu, C. Li, X. Guo, "Sodium storage and pseudocapacitive charge in textured $Li_4Ti_5O_{12}$thin films", *Journal of Physical Chemistry C* **2014**, *118*, 10616–10624.

[160] V. Gutmann, "Solvent effects on reactivities of organometallic compounds", *Coordination Chemistry Reviews* **1976**, *18*, 225–255.

[161] S. Tang, H. Zhao, "Glymes as Versatile Solvents for Chemical Reactions and Processes: from the Laboratory to Industry", *RSC Advances* **2013**, *4*, 11251–11287.

[162] W. A. Henderson, "Glyme-lithium salt phase behavior.", *The Journal of Physical Chemistry B* **2006**, *110*, 13177–83.

[163] C. P. Rhodes, M. Khan, R. Frech, "Crystalline Phases of Poly(Ethylene Oxide) Oligomers and Sodium Triflate: Changes in Coordination and Conformation with Chain Length", *The Journal of Physical Chemistry B* **2002**, *106*, 10330–10337.

[164] J. Wahlers, K. D. Fulfer, D. P. Harding, D. G. Kuroda, R. Kumar, R. Jorn, "Solvation Structure and Concentration in Glyme-Based Sodium Electrolytes: A Combined Spectroscopic and Computational Study", *The Journal of Physical Chemistry C*, DOI `10.1021/acs.jpcc.6b06160`.

[165] I. Geoffroy, P. Willmann, K. Mesfar, B. Carre, D. Lemordant, "Electrolytic characteristics of ethylene carbonate-diglyme-based electrolytes for lithium batteries", *Electrochimica Acta* **2000**, *45*, 2019–2027.

[166] E. Peled, D. Golodnitsky, J. Penciner in *Handbook of Battery Materials*, Wiley-VCH Verlag GmbH & Co. KGaA, **2011**, pp. 479–523.

[167] Retrieved October 26th, 2016, from: http://www.clariant.com/en/Business-Units/Industrial-and-Consumer-Specialties/Special-Solvents.

[168] K. Gotoh, C. Sugimoto, R. Morita, T. Miyatou, M. Mizuno, W. Sirisaksoontorn, M. M. Lerner, H. Ishida, "Arrangement and Dynamics of Diamine, Etheric, and Tetraalkylammonium Intercalates within Graphene or Graphite Oxide Galleries by H NMR", *The Journal of Physical Chemistry C* **2015**, *119*, 11763–11770.

[169] Z. Y. Wang, F. Li, N. S. Ergang, A. Stein, "Effects of hierarchical architecture on electronic and mechanical properties of nanocast monolithic porous carbons and carbon-carbon nanocomposites", English, *Chemistry of Materials* **2006**, *18*, 5543–5553.

[170] R. Alcantara, P. Lavela, G. F. Ortiz, J. L. Tirado, "Carbon Microspheres Obtained from Resorcinol-Formaldehyde as High-Capacity Electrodes for Sodium-Ion Batteries", *Electrochemical and Solid-State Letters* **2005**, *8*, A222–A225.

[171] H. Zhang, M. M. Lerner, "Preparation of Graphite Intercalation Compounds Containing Crown Ethers", *Inorganic Chemistry* **2016**, 8281–8284.

[172] H. Kim, G. Yoon, kyungmi Lim, K. Kang, "A comparative study of graphite electrode using co-intercalation phenomenon for rechargeable Li, Na and K batteries", *Chem. Commun.* **2016**, *3*, 1–4.

[173] G. Yoon, H. Kim, I. Park, K. Kang, "Conditions for Reversible Na Intercalation in Graphite: Theoretical Studies on the Interplay Among Guest Ions, Solvent, and Graphite Host", *Advanced Energy Materials* **2016**, DOI 10.1002/aenm.201601519.

[174] Z. Zhu, F. Cheng, Z. Hu, Z. Niu, J. Chen, "Highly stable and ultrafast electrode reaction of graphite for sodium ion batteries", *Journal of Power Sources* **2015**, *293*, 626–634.

[175] I. Hasa, X. Dou, D. Buchholz, Y. Shao-Horn, J. Hassoun, S. Passerini, B. Scrosati, "A sodium-ion battery exploiting layered oxide cathode, graphite anode and glyme-based electrolyte", *Journal of Power Sources* **2016**, *310*, 26–31.

[176] P. Han, X. Han, J. Yao, Z. Liu, X. Cao, G. Cui, "Flexible graphite film with laser drilling pores as novel integrated anode free of metal current collector for sodium ion battery", *Electrochemistry Communications* **2015**, *61*, 84–88.

[177] A. P. Cohn, K. Share, R. Carter, L. Oakes, C. L. Pint, "Ultrafast Solvent-Assisted Sodium Ion Intercalation into Highly Crystalline Few-Layered Graphene", *Nano Letters* **2016**, *16*, 543–548.

[178] Y.-J. Kang, S. C. Jung, J. W. Choi, Y.-K. Han, "Important Role of Functional Groups for Sodium Ion Intercalation in Expanded Graphite", *Chemistry of Materials* **2015**, *27*, 5402–5406.

[179] A. Ramos, I. Cameán, N. Cuesta, C. Antuña, A. B. García, "Expanded graphitic materials prepared from micro- and nanometric precursors as anodes for sodium-ion batteries", *Electrochimica Acta* **2016**, *187*, 496–507.

[180] W. Luo, Z. Jian, Z. Xing, W. Wang, C. Bommier, M. M. Lerner, X. Ji, "Electrochemically Expandable Soft Carbon as Anodes for Na-Ion Batteries", *ACS Central Science* **2015**, *1*, 516–522.

[181] B. Cao, H. Liu, B. Xu, Y. Lei, X. Chen, H. Song, "Mesoporous soft carbon as an anode material for sodium ion batteries with superior rate and cycling performance", *J. Mater. Chem. A* **2016**, *4*, 6472–6478.

[182] Y. Li, M. P. Paranthaman, K. Akato, A. K. Naskar, A. M. Levine, R. J. Lee, S. O. Kim, J. Zhang, S. Dai, A. Manthiram, "Tire-derived carbon composite anodes for sodium-ion batteries", *Journal of Power Sources* **2016**, *316*, 232–238.

[183] P. Han, X. Han, J. Yao, L. Zhang, X. Cao, C. Huang, G. Cui, "High energy density sodium-ion capacitors through co-intercalation mechanism in diglyme-based electrolyte system", *Journal of Power Sources* **2015**, *297*, 457–463.

[184] S. Y. Cho, H. J. Yoon, N. R. Kim, Y. S. Yun, H.-J. Jin, "Sodium-ion supercapacitors based on nanoporous pyroproteins containing redox-active heteroatoms", *Journal of Power Sources* **2016**, *329*, 536–545.

[185] Y. Zhu, L. Suo, T. Gao, X. Fan, F. Han, C. Wang, "Ether-based electrolyte enabled Na/FeS_2 rechargeable batteries", *Electrochemistry Communications* **2015**, *54*, 18–22.

[186] S. K. Das, B. A. Jache, H. Lahon, C. L. Bender, J. Janek, P. Adelhelm, "Graphene mediated improved sodium storage in nanocrystalline anatase for sodium ion batteries with ether electrolyte", *Chem. Commun.* **2016**, *52*, 1428–1431.

[187] A. Darwiche, R. Dugas, B. Fraisse, L. Monconduit, "Reinstating lead for high-loaded efficient negative electrode for rechargeable sodium-ion battery", *Journal of Power Sources* **2016**, *304*, 1–8.

[188] S. Peng, X. Han, L. Li, Z. Zhu, F. Cheng, M. Srinivansan, S. Adams, S. Ramakrishna, "Unique Cobalt Sulfide/Reduced Graphene Oxide Composite as an Anode for Sodium-Ion Batteries with Superior Rate Capability and Long Cycling Stability", *Small* **2016**, *12*, 1359–1368.

[189] A. P. Cohn, N. Muralidharan, R. Carter, K. Share, L. Oakes, C. L. Pint, "Durable potassium ion battery electrodes from high-rate cointercalation into graphitic carbons", *J. Mater. Chem. A* **2016**, DOI 10.1039/C6TA06797B.

[190] B. Zhang, G. Rousse, D. Foix, R. Dugas, D. A. D. Corte, J.-M. Tarascon, "Microsized Sn as Advanced Anodes in Glyme-Based Electrolyte for Na-Ion Batteries", *Advanced Materials* **2016**, DOI 10.1002/adma.201603212.